NASA TECHNICAL REPORT

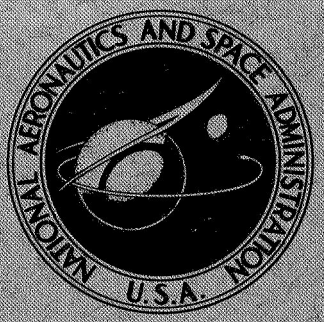

NASA TR R-270

NASA TR R-270

EQUILIBRIUM ANALYSIS AND ITS APPLICATION TO ATTITUDE CONTROL SYSTEMS

by William N. Redisch
Goddard Space Flight Center
Greenbelt, Md.

NATIONAL AERONAUTICS AND SPACE ADMINISTRATION • WASHINGTON, D. C. • AUGUST 1967

NASA TR R-270

EQUILIBRIUM ANALYSIS AND ITS APPLICATION TO ATTITUDE CONTROL SYSTEMS

By William N. Redisch

Goddard Space Flight Center
Greenbelt, Md.

NATIONAL AERONAUTICS AND SPACE ADMINISTRATION

For sale by the Cleoringhouse for Federal Scientific and Technical Informotion
Springfield, Virginia 22151 – CFSTI price $3.00

ABSTRACT

No theoretical technique exists yet that enables the engineer to completely determine the stability of practical complex spacecraft attitude control systems. In this dissertation, a stability approach is developed that utilizes a computer simulation in conjunction with theoretical techniques to locate the potentially troublesome regions of state space and explore their acceptability. It is shown in Part I that for general physical systems, $\dot{\bar{x}} = \bar{f}(\bar{x})$, all limit cycles are associated with equilibrium points that lie "inside" the limit cycles. Thus, if no equilibrium point exists in a region, then no limit cycle is contained in that region. Special properties of limit cycles and equilibrium points are discussed and illustrated. In Part II, equilibrium points are found analytically for spacecraft attitude control systems. A method is devised to determine stability near these equilibrium points. Then, instead of utilizing a uniform or random n-dimensional grid of computer initial conditions, a grid is concentrated around a few calculated points. Several practical examples of actual systems are presented. When control systems are viewed in this light, a high degree of confidence is gained from far fewer computer runs than previously needed.

CONTENTS

EQUILIBRIUM ANALYSIS AND ITS APPLICATION TO ATTITUDE CONTROL SYSTEMS*

by
William N. Redisch
Goddard Space Flight Center

1. INTRODUCTION

No theoretical technique exists yet which enables the engineer to determine the stability of practical complex spacecraft attitude control systems. Linearized models and much simplified nonlinear approximations of a system are studied on paper, but the resulting analyses are nearly always unsatisfactory for describing the stability of the actual system. Hence, the analysis of the complete system relies on the use of detailed computer simulations.

This approach, necessary as it is, leaves much to be desired. Firstly, haw accurate is the simulation? There are oddities in physical hardware which are not known, understood, or sufficiently determinable to generate a mathematical model that can be simulated. Other measurable non-primary characteristics are labeled "higher-order effects" and, to keep the complexity of the simulation reasonable, are not simulated. (For example, secondary emission of x-rays in a radiation belt which causes spurious noise effects on field-effect transistors.) However, the limitations of a computer analysis are acceptable if the engineer takes enough pains to ensure that the differences between real and simulated performances are well below the error tolerances specified for the actual system.

A more important shortcoming of computer analysis for complex high dimensional attitude control systems is that an infinite number of stability runs from an infinite number of initial conditions obviously cannot be made. Hence, it is possible for a limit cycle, which is considered unstable behavior (for the purposes of this dissertation), to exist in state space and never be discovered until after the launching of the spacecraft. That is, the limit cycle-exists in a region never entered by the simulated state vector, because every initial state produced a state-space trajectory that did not pass through the troublesome region. There are many examples of this occurrence, one of which is discussed in Chapter 9.

In this dissertation, a method is developed that employs a complete computer simulation in conjunction with theoretical techniques so as to yield a very high degree of confidence in a stability analysis. That is, after a finite number of runs, the simulated state vector will, with

*Taken from a dissertation submitted to the Faculty of the Polytechnic Institute of Brooklyn in partial fulfillment of the requirements for the degree of Doctor of Philosophy (Electrical Engineering) 1967.

high probability, pass through all troublesome regions in the overall state space of interest. Now, if a system is truly globally unstable or stable, then the response either diverges from or converges to the designed final state (call it the origin) from anywhere in state space, This type of behavior is easily observed on a computer. It is the more nebulous limit cycle or meandering patterns that are difficult even to define from a stability point of view, but are unwanted from an attitude control designer's point of view, that elude the computer analysis. Thus, a theory is needed to indicate the locations of all the potentially troublesome regions. The computer is then used to explore these regions and find out whether they are acceptable. Also, once a method of finding trouble spots is developed, insight into a system is gained, and it is sometimes feasible to design the system so as to eliminate these troubles. Such an approach is illustrated in Chapter 9.

These ideas are not limited to attitude control systems, but apply to systems in general. Hence, this dissertation is divided into two major parts. In Part I, the ideas are put on a mathematical footing applicable to all systems via the linking of system trouble areas to mathematically defined limit cycles. It is shown through general functional relationships that the troublesome regions are always associated with equilibrium points. For second-order systems, it is well known that singular points play an important role in determining the behavior of solutions. Here, it is shown that for general n^{th}-order systems, all limit cycles are associated with equilibrium points which lie "inside" the limit cycles. Thus, if no equilibrium point exists in a region, then no limit cycle is contained in that region and, engineering-wise, the complete physical system does not meander about in this region. The equilibrium points, are found analytically and are usually finite in number. Now, instead of a uniform or random n-dimensional grid of computer initial conditions, a grid concentrated around the calculated points is used.

Part 11presents an engineering application of the equilibrium analysis technique for attitude control systems. Necessary equations are developed, and methods for finding, investigating, and interpreting equilibrium states are discussed with ample illustrations from actual systems. When systems are viewed in this light, a high degree of confidence is gained from several hundred computer runs, where previously the same level of confidence could be obtained only after several hundred thousand runs.

Part I

MATHEMATICAL DEVELOPMENT FOR GENERAL SYSTEMS

2. GROUND RULES AND DEFINITIONS

As a first step, some ground rules and definitions are established. Only systems adequately represented by deterministic models in a physical sense are considered. That is, the system equations have bounded solutions that are unique with respect to any initial conditions. The parameters within the system are time-invariant. The entire system is describable by means of a finite number of finite-order, autonomous, ordinary differential equations, generally non-linear in nature.

A useful theoretical tool often used in the development is the formulation of the mathematical model that represents the system in state-variable form. Thus, if $x_i(t)$ is a state variable ($i = 1, 2, \cdots, n$) for an n-dimensional system, and t represents continuous, non-negative, real time, then the system is described by the following n equations:

$$\begin{aligned}
\frac{dx_1(t)}{dt} &= f_1\left(x_1(t), x_2(t), \cdots, x_n(t)\right) \\
\frac{dx_2(t)}{dt} &= f_2\left(x_1(t), x_2(t), \cdots, x_n(t)\right) \\
&\vdots \\
\frac{dx_n(t)}{dt} &= f_n\left(x_1(t), x_2(t), \cdots, x_n(t)\right),
\end{aligned} \tag{2.1}$$

where n is a finite positive integer. A shorthand derivative notation used is $\dot{x} = dx/dt$, $\ddot{x} = d^2x/dt^2$, etc., or $x^{(i)} = d^ix/dt^i$ where $i = 0, 1, 2, \cdots$, and when $i = 0$ then $x^{(i)} = x$. Thus, Equations (2.1) are equivalent to

$$\dot{x}_i(t) = f_i\left(x_1(t), x_2(t), \cdots, x_n(t)\right) \qquad i = 1, 2, \cdots, n. \tag{2.2}$$

It is also convenient to introduce a vector formalism by defining

$$\bar{x} = \begin{pmatrix} x_1 \\ x_2 \\ \vdots \\ x_n \end{pmatrix} \tag{2.3}$$

and

$$\bar{f}(\bar{x}) = \begin{pmatrix} f_1(\bar{x}) \\ f_2(\bar{x}) \\ \vdots \\ f_n(\bar{x}) \end{pmatrix} , \tag{2.4}$$

such that Equation **(2.1)** can be rewritten as

$$\frac{d\bar{x}(t)}{dt} = \bar{f}\left(\bar{x}(t)\right) . \tag{2.5}$$

Equation **(2.5)** satisfies the imposed uniqueness constraint, that is, it has a unique continuous solution $\bar{x}(t)$ for every initial condition $\%(0) = \mathbf{k}$, , if

$$\left\|\bar{x} - \bar{x}_0\right\| \leq \min(a, bM) , \qquad |t| \leq b ; \tag{2.6}$$

$$\|\bar{f}(\bar{x})\| \leq M ; \tag{2.7}$$

and $f(\bar{x})$ satisfies a Lipschitz condition in the domain $\left\|\bar{x} - \bar{x}_0\right\| \leq a$. (Reference **1,** Chapter 6, and Reference **2,** Chapter **3.)** M, a and **b** are the constants which define the uniqueness domain. The function $\bar{f}(\bar{x})$ satisfies the Lipschitz condition, provided that a constant K is found such that

$$\left\|\bar{f}(\bar{x}_1) - \bar{f}(\bar{x}_2)\right\| \leq K\left\|\bar{x}_1 - \bar{x}_2\right\| , \tag{2.8}$$

where $\|\ \|$ represents the norm of a vector.

Another form in which a system is sometimes represented is

$$x^{(n)}(t) = f\left(x^{(n-1)}(t),\ x^{(n-2)}(t),\ \cdots,\ \dot{x}(t),\ x(t)\right) . \tag{2.9}$$

Neither Equations **(2.1)** nor **(2.9)** contain time explicitly in accordance with the previous ground rules. Equation **(2.1)** is the general state variable form, but form **(2.9)** often has the advantage of facilitating mental visualization of time-trajectories, and can always be changed to form **(2.1)** by letting $x_i = x^{(i-1)}$, where $i = 1, 2, \cdots, n$. However, in general, it is not possible to combine n first-order differential equations to one n^{th}-order differential equation (Reference **1,** Section **2.3** and Reference **2,** Section 6.4). Hence, the state-variable formulation **(2.1)** is more general and encompasses form **(2.9).**

For an n-dimensional system, $n \geq 2$, described in the state-variable form, a limit cycle is a closed, bounded trajectory repeatedly traversed with time in a positive time period τ in n-dimensional state space. Several authors (References 3 and 4) distinguish periodic solutions from limit cycles, calling limit cycles the periodic motion that neighboring solutions tend to as $t \to \infty$. Here, the two are considered as the same. For the proofs in Chapter 3, if a limiting type of limit cycle is the only periodic solution that exists, initial conditions are chosen to lie on the limit cycle such that the solutions are exactly periodic from time equals zero. Thus, each state variable

$$x_i(t) = x_i(t+\tau) \qquad i = 1, 2, \cdots, n \tag{2.10}$$

is a periodic function of time with a common period τ. Each has an average value over the period defined by

$$x_{i\,avg} = \frac{1}{\tau}\int_t^{t+\tau} x_i(A)\, d\lambda \qquad i = 1, 2, \cdots, n\,. \tag{2.11}$$

In n-dimensional state space, the n average values of the n state variables define a point which shall be called the centroid of the limit cycle. For example, in the second-order system

$$\begin{aligned} \dot{x}_1 &= x_2 \\ \dot{x}_2 &= -\omega^2 x_1 + K\,, \end{aligned} \tag{2.12}$$

whose solution is the limit cycle

$$\begin{aligned} x_1(t) &= \left[x_2(0)/\omega\right]\sin wt + \left[x_1(0) - K/\omega^2\right]\cos wt + K/\omega^2 \\ x_2(t) &= x_2(0)\cos wt - \omega\left[x_1(0) - K/\omega^2\right]\sin \omega t\,, \end{aligned} \tag{2.13}$$

the centroid is at

$$x_{1\,avg} = K/\omega^2 \qquad x_{2\,avg} = 0 \tag{2.14}$$

in x_1, x_2 state space, and $\tau = 2\pi/\omega$. This limit cycle and its centroid are shown in Figure 2.1.

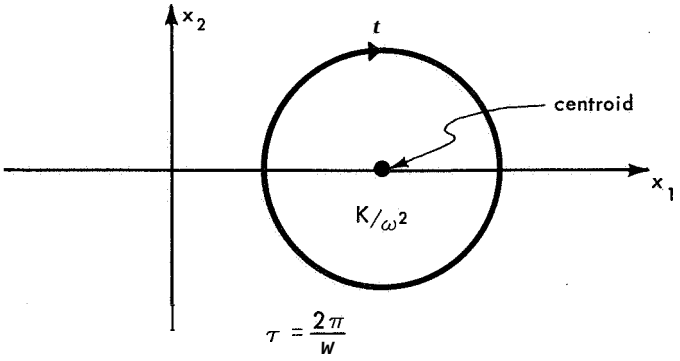

Figure 2.1 — Limit-Cycle Centroid.

Obviously the centroid of a limit cycle lies within the limit cycle where "within" is

defined as follows: If there is a closed bounded curve in n-dimensional state space, then its projection on any of the state variable axes is a finite line segment. A point such as the centroid being within the n-dimensional limit cycle means that

$$x_{im} \leq x_{i\,avg} \leq x_{iM} , \qquad i = 1, 2, \cdots, n , \tag{2.15}$$

where x_{im} and x_{iM} are algebraic quantities representing the end points of the finite line segment projection on the i^{th} axis.

This definition of "within" does not lend itself to the normal conceptual visualization of "inside" a non-simple flat closed curve. For example, suppose that the plane projection of an n^{th}-order limit cycle is a figure-8-type curve as depicted in Figure 2.2 The projection of the centroid on this plane lies anywhere in the shaded region.

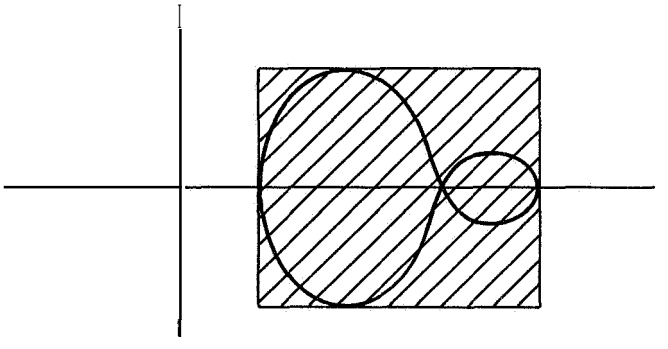

Figure 2.2—Area Within a Limit Cycle.

An equilibrium point in n-dimensional phase space is defined as a point at which the solution to the systems' equations is constant with respect to time. That is, if a set of compatible initial conditions exist such that the left-hand sides of Equations (2.1) remain zero for all time $0 \leq t < \infty$, then these sets of initial state variable values, obtained from the solutions to

$$\begin{aligned} f_1(x_1, x_2, \cdots, x_n) &= 0 \\ f_2(x_1, x_2, \cdots, x_n) &= 0 \\ f_n(x_1, x_2, \cdots, x_n) &= 0 , \end{aligned} \tag{2.16}$$

are equilibrium points. Hence, equilibrium points are trajectories which are the points themselves remaining stationary in state space for all positive time. The points may be stable or unstable equilibriums in the sense that another set of initial conditions, arbitrarily close to an equilibrium point, yields a trajectory that tends toward or away from the equilibrium point with increasing time.

In the next chapter it is shown that all solutions to Equations (2.16) are indeed equilibrium points, and that when limit cycles exist for an n^{th}-order system (2.1), then there is one or more of these equilibrium points within each limit cycle. Hence, a computer simulation of system (2.1) can be used much more effectively by investigating the system around these calculated equilibrium points. It is noted that the solution of Equations (2.16) is a straight-forward algebraic problem that does not involve the dependent variable time. In fact, this straightforward

but tedious task is often automatically performed by the computer simulation itself, whether analog, digital, or hybrid.

Again it is emphasized that this type of procedure, though not 100-percent encompassing, is a powerful one for systems in general. The approach is not tied down to specific (attitude control) systems until Chapter 6. In Chapter 8 it becomes clear that attitude control system equilibrium points do not readily reveal themselves; methodical procedures must be employed to find the more elusive ones.

3. THEOREMS AND PROOFS

In this chapter, preliminary theorems are developed following the ground rules and definitions of Chapter 2. The theorems are then used to prove that at least one equilibrium point lies within a limit cycle when the limit cycle exists in an n^{th}-order system.

Firstly, if $x_i(t)$ and all its derivatives exist for all t, and

$$x_i(t) = x_i(t+\tau) \qquad i = 1, 2, \cdots, n, \tag{3.1}$$

then it immediately follows that

$$x_i^{(k)}(t) = x_i^{(k)}(t+\tau) \qquad k = 0, 1, 2, \cdots \tag{3.2}$$

for all t including $t = 0$. Thus, the relationship in Equation (3.1) adequately defines a limit-cycle behavior for the system (2.2) without the necessity of stating that the derivatives are also periodic.

Since

$$x_i^{(k+1)}(t) = \frac{d}{dt} x_i^{(k)}(t) \tag{3.3}$$

for $k = 0, 1, 2, \cdots$, and $i = 1, 2, \cdots, n$, then

$$x_i^{(k)}(t+\tau) - x_i^{(k)}(t) = \int_t^{t+\tau} x_i^{(k+1)}(\lambda)\, d\lambda , \tag{3.4}$$

assuming $x^{(k+1)}$ has no singularities as dictated by the ground rules. Equation (3.2) implies the vanishing of the left-hand side of (3.4); thus,

$$\int_t^{t+\tau} x_i^{(k+1)}(\lambda)\, d\lambda = \tau x_{i\,avg}^{(k+1)} = 0 . \tag{3.5}$$

Since $\tau > 0$,

$$x_{i\,avg}^{(k+1)} = 0 \quad \text{for} \quad k = 0, 1, 2, \cdots . \tag{3.6}$$

In other words,

$$x_{iavg}^{(k+1)} = \frac{1}{\tau}\int_{t}^{t+\tau} {}^{+1)}(\lambda)\, d\lambda = \frac{1}{\tau}\oint dx_i{}^{k} = 0 \quad , \tag{3.7}$$

that is, the derivatives of a periodic function have zero averages.

It is also clear that

$$\begin{aligned} x_i^{(k)}(t) &= x_i^{(k)}(t+\tau) = x_i^{(k)}\left((t+\tau)+\tau\right) \\ &= x_i^{(k)}\left(((t+\tau)+\tau)+\tau\right) = \cdots \end{aligned} \tag{3.8}$$

or

$$x_i^{(k)}(t) = x^{(k)}(t+j\tau) \tag{3.9}$$

for periodic $x_i(t)$, where $i = 1, 2, \ldots, n$; $j = 0, 1, 2, \ldots$; and $k = 0, 1, 2, \ldots$.

Another useful fact is that no derivative of a non-constant periodic function is identically equal to zero. This is shown by expanding in a Fourier series,

$$\begin{aligned} x(t) = x(t+\tau) &= x_{avg} + \sum_{n=1}^{\infty}\left(a_n \cos \omega n t + b_n \sin wnt\right) \quad , \\ \omega &= \frac{2\pi}{\tau} \neq 0 \quad . \end{aligned} \tag{3.10}$$

Hence,

$$x^{(k)}(t) = x^{(k)}(t\ t7) = \sum_{n=1}^{\infty}\left(A_n \cos \omega n t + B_n \sin \omega n t\right) \quad , \tag{3.11}$$

where

$$\begin{aligned} A_n &= \begin{cases} (-1)^{(k-1)/2}(\omega n)^k\, b_n & k = 1, 3, 5, \cdots \\ (-1)^{k/2}\,(\omega n)^k\, a_n & k = 2, 4, 6, \cdots \end{cases} \\ B_n &= \begin{cases} (-1)^{(k+1)/2}(\omega n)^k\, a_n & k = 1, 3, 5, \cdots \\ (-1)^{k/2}\,(\omega n)^k\, b_n & k = 2, 4, 6, \cdots \end{cases} \quad . \end{aligned} \tag{3.12}$$

Now,

$$A_n = \frac{2}{\tau}\int_0^{\tau} x^{(k)}(t)\cos \omega n t \, dt$$

$$B_n = \frac{2}{\tau}\int_0^{\tau} x^{(k)}(t)\sin \omega n t \, dt \qquad (3.13)$$

Thus, if $x^{(k)} \equiv 0$, then $A_n \equiv B_n \equiv 0$ for all n; hence, $a_n \equiv b_n = 0$ for all n, implying that $x(t) \equiv x_{avg}$ = constant, which is a contradiction.

In Chapter 2, equilibrium points of a system are defined as the points in state space corresponding to constant solutions of the system. Hence, when a system yields a unique solution for any initial conditions, then, if an equilibrium point does exist, choosing it as the initial state of the system ensures that all the derivatives of the system are zero and stay zero. That is, for the n-dimensional system,

$$\frac{d}{dt}\bar{x}(t) = \bar{f}(\bar{x}(t)) \, , \qquad (3.14)$$

if

$$\bar{f}(\bar{x}_e) = 0 \, , \qquad (3.15)$$

then the initial condition

$$\bar{x}(0) = \bar{x}_e \qquad (3.16)$$

implies that

$$\bar{x}^{(k)}(t) \equiv 0 \qquad k = 1, 2, \cdots \qquad (3.17)$$

for all $t \geq 0$, since $x(t) = x_e$ is a unique solution for the system (3.14).

However, there is not necessarily a real $\bar{x}_e$ that satisfies Equation (3.15). For example, consider the simple unique system

$$\frac{d}{dt}\begin{pmatrix} x_1(t) \\ x_2(t) \end{pmatrix} = \begin{pmatrix} x_2(t) \\ 1 \end{pmatrix} , \qquad (3.18)$$

which yields the solution

$$\begin{pmatrix} x_1(t) \\ x_2(t) \end{pmatrix} = \begin{pmatrix} x_1(0) + x_2(0)\,t + \frac{t^2}{2} \\ x_2(0) + t \end{pmatrix} \tag{3.19}$$

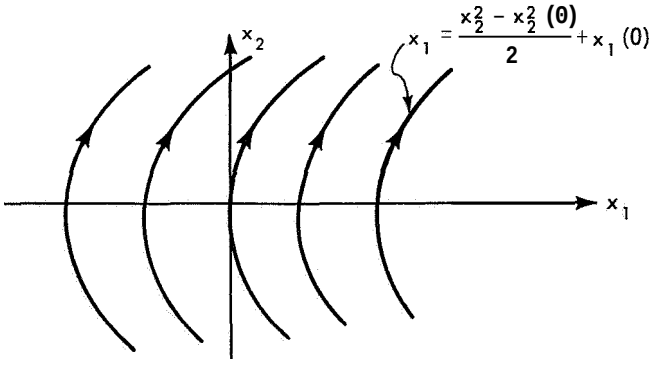

Figure 3.1—Parabolic Trajectories.

as depicted in the state space shown in Figure 3.1.

This system has no equilibrium points, since

$$\begin{pmatrix} x_2(t) \\ 1 \end{pmatrix} = 0 \tag{3.20}$$

has no solution, that is

$$\dot{x}_2 = 1 \neq 0 . \tag{3.21}$$

But, Equation(3.21) also implies that no limit cycle exists, since by Equation (3.6), $\dot{x}_{2avg}$ is zero for limit-cycle behavior, thus requiring $\dot{x}_2(t)$ to be zero at some times $t_1, t_2, \cdots$, which Equation (3.21) does not allow. Thus, the same condition that prevents the existence of an equilibrium point also prevents the existence of a limit cycle.

The previous example is a very special one where $f_2(x_1, x_2)$ is actually independent of the state variable $\bar{x}$. In the next chapter, examples are presented that illustrate systems that have limit cycles and yet have no equilibrium points. With each example is an explanation of those ground rules in Chapter 2 that are being violated. For the systems described in Chapter 2 that have one or more limit cycles as solutions, at least one equilibrium point exists. This is implied by the proofs that follow shortly, which show that at least one equilibrium point lies within a limit cycle whenever the limit cycle exists as a solution to the system equations.

One additional area of interest is noted here. Instead of working in Euclidean state space, it is sometimes more convenient to investigate the topological behavior of solution trajectories in different spaces. For example, if one or more coordinates are cyclic (such as an angle determined by only modulo 2π), then a cylindrical or toroidal rather than a planar representation may be more suitable. Chapter 8 of Reference 5 is devoted to this subject. The main point to note here is that an open curve in a plane can close on itself around the surface of a cylinder, thereby acting as a closed limit cycle in cylindrical space, and yet not encircle any equilibrium or singular points. Hence, it is re-emphasized that this dissertation deals with Euclidean state space only.

By definition, an equilibrium point never lies on the trajectory of a non-trivial limit cycle; if it did, it would mean that the state of the system changes with time (a contradiction). Now, it is demonstrated how at least one equilibrium point lies within a limit cycle. Instead of dealing directly with the general n^{th}-order nonlinear system, the following class of systems is considered in sequence:

A) Linear systems

B) Second-order systems, $\ddot{x} = f(\dot{x}, x)$

C) n^{th}-order systems, $x^{(n)} = f\left(x^{(n-1)}, x^{(n-2)}, \cdots, x\right)$

D) General systems, $\dot{\bar{x}} = \bar{f}(\bar{x})$.

A) Linear Systems.

For linear systems, not only does an equilibrium point lie within a limit cycle, but, also, the centroid of the system is an equilibrium point (which obviously lies within a limit cycle). The centroid of a system is defined in Chapter 2 as the point $x_{i\,avg}$.

Consider first the linear system

$$x^{(n)}(t) = \sum_{j=1}^{n} a_{n-j}\, x^{(n-j)}(t) + c\ , \tag{3.26}$$

where the a's and c are arbitrary constants, and

$$x(t) = x(t+\tau) \qquad \tau > 0 \tag{3.27}$$

is a solution. Now,

$$\begin{aligned} x_{avg}^{(n)} &= \frac{1}{\tau}\int_{t}^{t+\tau} x^{(n)}(\lambda)\, d\lambda \\ &= \frac{1}{\tau}\int_{t}^{t+\tau}\left[\sum_{j=1}^{n} a_{n-j}\, x^{(n-j)}(\lambda) + c\right] d\lambda \\ &= \sum_{j=1}^{n}\frac{1}{\tau}\int_{t}^{t+\tau} a_{n-j}\, x^{(n-j)}(\lambda)\, d\lambda + \frac{1}{\tau}\int_{t}^{t+\tau} c\, d\lambda \\ &= \sum_{j=1}^{n} a_{n-j}\, x_{avg}^{(n-j)} + c\ . \end{aligned} \tag{3.28}$$

But, from Equation (3.6),

$$x_{avg}^{(k)} = 0 , \qquad k = 1, 2, \cdots . \tag{3.29}$$

Hence,

$$0 = a_0 x_{avg} + c . \tag{3.30}$$

But, from Equation (3.26), the equilibrium value of x is

$$0 = a_0 x_e + c . \tag{3.31}$$

Thus, x_{avg} is an equilibrium point.

For the general state variable formulation of the linear system,

$$\dot{x}_i (t) = \sum_{j=1}^{n} a_{ij} x_i + a_{i0} , \qquad i = 1, 2, \cdots , n \tag{3.32}$$

where the a_{ij} are arbitrary constants, let $\bar{x}(t) = \bar{x}(t+\tau)$ be a solution. Then,

$$\begin{aligned} x_{i\,avg} &= \frac{1}{\tau} \int_{t}^{t+\tau} \dot{x}_i (\lambda)\, d\lambda \\ &= \frac{1}{\tau} \int_{t}^{t+\tau} \left[\sum_{j=1}^{n} a_{ij} x_i + a_{i0} \right] d\lambda \\ &= \sum_{j=1}^{n} a_{ij} x_{i\,avg} + a_{i0} \\ &= 0 . \end{aligned} \tag{3.33}$$

But also, by definition,

$$0 = \sum_{j=1}^{n} a_{ij} x_{ie} + a_{i0} , \tag{3.34}$$

and therefore the $x_{i\,avg}$ are the x_{ie}, i.e., the system's centroid which lies within the limit cycle solution is an equilibrium point.

It is noted that the above proofs hold for any system

$$\dot{x}_i(t) = f_i\left(x_1(t), x_2(t), \cdots, x_n(t)\right), \qquad i = 1, 2, \cdots, n \tag{3.35}$$

for which

$$f_i\left(x_{1\,avg}, x_{2\,avg}, \cdots, x_{n\,avg}\right) = \frac{1}{\tau}\int_t^{t+\tau} f_i\left(x_1(\lambda), x_2(\lambda), \cdots, x_n(\lambda)\right) d\lambda \,. \tag{3.36}$$

B) Second-Order Systems.

Consider next the second-order system of the form

$$\ddot{x}(t) = f\left(\dot{x}(t), x(t)\right) \,. \tag{3.37}$$

The Van der Pol plus many other well-studied equations are of this class. Assume that for some initial conditions Equation **(3.37)** has a solution $x(t) = x(t+\tau)$ which corresponds to a closed trajectory in the x, $\dot{x}$ phase plane. The equation of this curve is

$$g(\dot{x}, x, K) = 0 \,. \tag{3.38}$$

Here, as depicted in Figure **3.2,** the constant K is determined by the initial conditions that give rise to the limit cycle. That is,

$$g\left(\dot{x}(0), x(0), K\right) = 0 \,. \tag{3.39}$$

The slope of the trajectory is expressed as

$$sl = \frac{d\dot{x}}{dx} = \frac{\ddot{x}}{\dot{x}} = \frac{f(\dot{x}, x)}{\dot{x}} \,. \tag{3.40}$$

An equilibrium point $\dot{x} = 0$, $x = x_e$ is given by

$$0 = f\left(0, x_e\right) \tag{3.41}$$

and corresponds to a singular point of indeterminate slope. (In engineering parlance, a singular point is a point such that if the system starts there initially, it may mathematically leave that

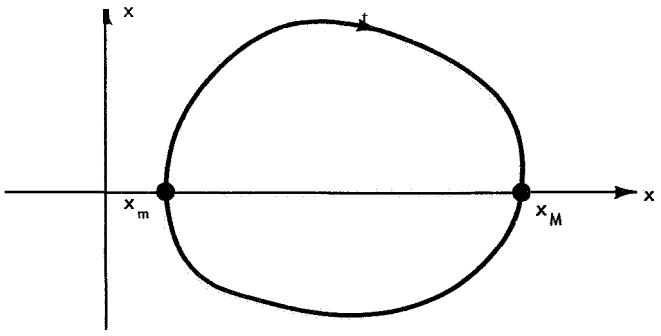

Figure 3.2—Limit-Cycle Trajectory.

point at various angles. But since the solution trajectory is unique, the system remains stationary, in equilibrium, at the singular point.)

The bounded periodic $x(t)$ has minimum and maximum values x_m and x_M, respectively. When $x(t)$ is at one of its extremums, $\dot{x}(t) = 0$. That is,

$$g(0, x_m, K) = 0$$
$$g(0, x_M, K) = 0 \qquad (3.42)$$

Since $\dot{x}_{avg} = 0$ lies between the algebraic extremes of $\dot{x}(t)$, it is only necessary to show that

$$x_m < x_e < x_M \qquad (3.43)$$

in order to demonstrate that an equilibrium point lies within the limit cycle. Obviously $x_e \neq x_m$ and $x_e \neq x_M$ since an equilibrium point is not on the limit cycle except for the trivial case when the limit cycle is a constant solution. Thus, it lies inside or outside the closed trajectory. Along the curve

$$\ddot{x}(\dot{x}, x) = f(\dot{x}, x) = 0 \qquad (3.44)$$

in the phase plane, the slope of a solution trajectory is zero, (that is, the solution trajectory has a horizontal tangent), as evidenced by Equation (3.40), except (possibly) when $\dot{x} = 0$. (The locus of zero slopes $\ddot{x} = 0$ is used in the Lienard construction method, for example, in References 5 and 6). The points where the curve $\ddot{x} = 0$ crosses the x-axis, (i.e. $\dot{x} = 0$), are equilibrium points, since at these points Equations (3.41) and (3.44) become identical. Now, in the upper half of the phase plane where $\dot{x} > 0$, $x(t)$ increases with increasing time; hence the solution trajectories go horizontally from left to right across the zero-slope curve. The opposite is true in the lower half plane, where $\dot{x} < 0$. See Figure 3.3. Since a limit-cycle solution trajectory is a bounded, closed, continuous curve, it has a horizontal tangent (at its crossings of the zero-slope curve) at least twice, that is once for $\dot{x} > 0$ and once for $\dot{x} < 0$. The limit cycle therefore encircles at least one of the x_e points (where the zero-slope curve intersects the $\dot{x} = 0$ axis). That is, at least one equilibrium point lies inside the limit cycle.

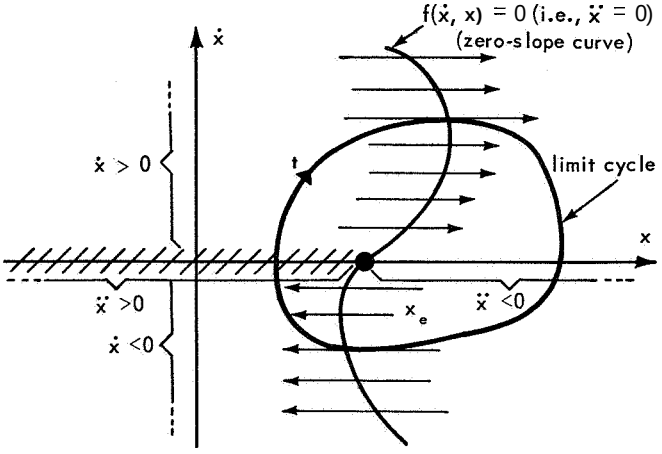

Figure 3.3—Zero-Slope Curve.

The above conclusion (that any general second-order system limit cycle encircles a singular point) is well known. It can be simply developed via Poincaré's theory by showing that at least one singularity lies within a simple closed curve since the total Poincark index is +1 (References 3, 4, and 7). However, the above development lends itself to extension to higher-order systems via the following observations. $x(t)$ reaches a maximum value x_M at instants of time when $\dot{x} = 0$ and $\ddot{x} < 0$, and a minimum value x_m when $\dot{x} = 0$ and $\ddot{x} > 0$. The curve $\ddot{x} = 0$ divides the x, $\dot{x}$ phase plane into two regions, one where $\ddot{x}$ is positive, and the other where $\ddot{x}$ is negative. (One of these regions may be nonexistent when a limit cycle does not exist, such as the example of Equation (3.18), $\ddot{x} = 1$. However, when a limit cycle solution does exist, then $\ddot{x}_{avg} = 0$ as previously proved. Hence, $\ddot{x}$ is positive and negative at different times, implying the existence of phase-plane regions where $\ddot{x}$ is positive and negative.) Furthermore, the x-axis is divided into positive and negative $\ddot{x}$ segments, with the boundary points being equilibrium points. Hence, at least one of these boundary equilibrium points lies between x_m and x_M on the x-axis. That is

$$x_m < x_e < x_M \ . \tag{3.45}$$

C) n^{th}-Order Systems.

For the class of n^{th}-order systems which yield periodic solutions,

$$x^{(n)}(t) = f\left(x^{(n-1)}(t), x^{(n-2)}(t), \cdots, x(t)\right) \ , \tag{3.46}$$

where $n \geq 2$, similiar reasoning as for the second-order case applies. Firstly, since for $k = 1, 2, \cdots, n$,

$$x_m^{(k)} < x_e^{(k)} = 0 = x_{avg}^{(k)} < x_M^{(k)} \ , \tag{3.47}$$

it is only necessary to establish that

$$x_m < x_e < x_M \tag{3.48}$$

in order to state that an equilibrium point lies within a limit cycle. To establish (3.48) for an n^{th}-order system as in (3.46), it is again observed that, even if n is greater than 2, simultaneously $x = x_M$ when $\dot{x} < 0$, and at some other time, $x = x_m$ when $\ddot{x} > 0$. Now, $\ddot{x} = 0$ is an $(n-1)$-dimensional hypersurface which partitions $x, \dot{x}, \ddot{x}, x^{(4)}, \cdots, x^{(n)}$ n-dimensional space into two regions; in one, $\ddot{x}$ is positive; in the other, $\ddot{x}$ is negative. Again, both regions exist if a limit cycle exists. The equilibrium points of the system are where the x-axis intersects the $\ddot{x} = 0$ hypersurface. Thus, the x-axis is segmented by the $\ddot{x} = 0$ hypersurface such that equilibrium points separate the positive and negative $\ddot{x}$ regions. An example is illustrated in Figure 3.4. The projection of a limit cycle on to the x-axis has its extremums separated by at least one $\ddot{x} = 0$ boundary, and thus at least one equilibrium point. That is, the relationship in Equation (3.48) is established.

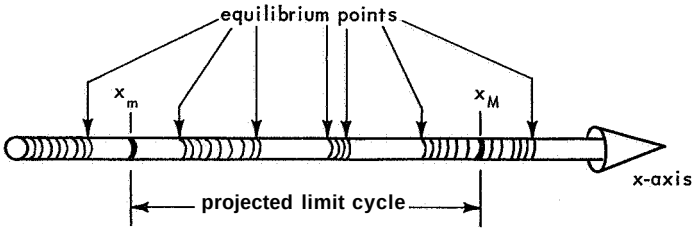

Shaded line segment: $\ddot{x} > 0$
Unshaded line segment: $\ddot{x} < 0$

Figure 3.4—Positive and Negative ;-Segments.

D) General Systems.

The remainder of this chapter is devoted to general systems of the form

$$\dot{\bar{x}} = \bar{f}(\bar{x}) \ . \tag{3.49}$$

The approach to the problem of showing that at least one equilibrium point lies within a limit cycle solution is via level curves and surface gradients, similiar to a geometric interpretation of Liapunov functions (for example, in Reference 8, Section 13). For the general state variable representation of an n^{th}-order system as in Equation (3.49), the state variables x_i are not necessarily time derivatives of each other. Hence, in general,

$$x_{i\,avg} \neq x_{ie} \tag{3.50}$$

for any of the i's, $i = 1, 2, \cdots, n$. Thus, it is imperative here to prove that

$$x_{im} < x_{ie} < x_{iM} \tag{3.51}$$

for all i, $i = 1, 2, \cdots, n$, rather than the previously simpler task where only one variable, x, had to be considered. Here again, expression (3.51) has no equality signs, thus indicating that the trivial static case of $x_{im} = x_{ie} = x_{iM}$ is being ignored.

First, a general second-order case is discussed since its easy visualization tends to make a geometric interpretation significantly clearer. Assume the unique system

$$\begin{aligned} \dot{x}_1(t) &= f_1\left(x_1(t), x_2(t)\right) \\ \dot{x}_2(t) &= f_2\left(x_1(t), x_2(t)\right) \end{aligned} \tag{3.52}$$

that yields a finite limit cycle solution

$$\begin{aligned} x_1(t) &= x_1(t+\tau) \\ x_2(t) &= x_2(t+\tau) \end{aligned} \tag{3.53}$$

for certain initial conditions $x_1(0), x_2(0)$. If time is eliminated in Equations (3.52), then the equivalent system

$$\frac{dx_2}{dx_1} = \frac{f_2\left(x_1, x_2\right)}{f_1\left(x_1, x_2\right)} \tag{3.54}$$

yields an integral solution which is a bounded closed trajectory in the x_1, x_2 plane. This limit cycle is expressed in parametric form with t as the parameter as in (3.53), or more directly by the expression

$$g\left(x_1(t), x_2(t)\right) = K_{L.C.} \quad (3.55)$$

$K_{L.C.}$ is determined by any point (x_1, x_2) on the limit cycle, including the initial conditions $(x_1(0), x_2(0))$. Since the state of the system is confined to the curve (3.55) for all t,

$$\dot{g}\left(x_1(t), x_2(t)\right) = 0 \quad (3.56)$$

for the initial conditions $x_1(0), x_2(0)$. This can be envisioned from a Liapunov point of view by taking as a Liapunov function

$$V\left(x_1, x_2\right) = g\left(x_1, x_2\right), \quad (3.57)$$

such that for the limit cycle case

$$\dot{V}\left(x_1, x_2\right) = \dot{g}\left(x_1, x_2\right) = 0 . \quad (3.58)$$

That is, the system trajectory never leaves the level curve $K_{L.C.}$ of the surface $V = g$. See Figure 3.5.

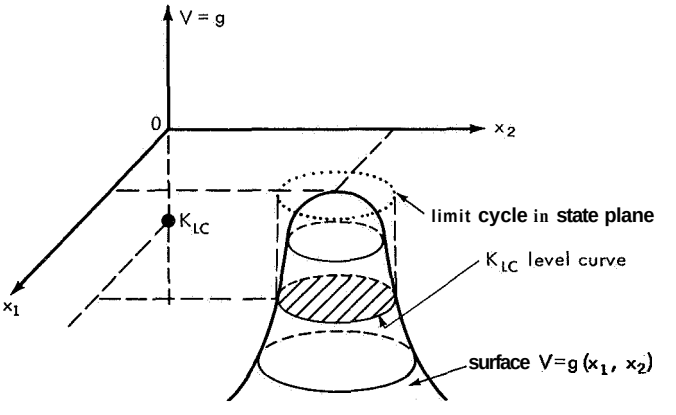

Figure 3.5—Surface Function $g(x_1, x_2)$.

Two vectors are now introduced: a field vector and a gradient vector. The field vector is represented by

$$\bar{S} = \begin{pmatrix} \dot{x}_1 \\ \dot{x}_2 \end{pmatrix} \quad (3.59)$$

or, for geometric purposes,

$$\bar{S} = \dot{x}_1 \hat{x}_1 + \dot{x}_2 \hat{x}_2 , \quad (3.60)$$

where the $\hat{x}_1$ and $\hat{x}_2$ are unit vectors along the positive x_1 and x_2 axes respectively. Hence, for the system (3.52), the field vector

$$\bar{S} = f_1\left(x_1(t), x_2(t)\right) \hat{x}_1 + f_2\left(x_1(t), x_2(t)\right) \hat{x}_2 \quad (3.61)$$

is geometrically tangent to the solution trajectories including the limit cycle in the x_1, x_2 state plane, and points in the direction of increasing time.

The gradient vector of $g(x_1, x_2)$ is represented by

$$\overline{\nabla g} = \begin{pmatrix} \frac{\partial g}{\partial x_1} \\ \frac{\partial g}{\partial x_2} \end{pmatrix} \tag{3.62}$$

or

$$\overline{\nabla g} = \frac{\partial g}{\partial x_1} \hat{x}_1 + \frac{\partial g}{\partial x_2} \hat{x}_2 \ . \tag{3.63}$$

Hence, the time derivative of g is simply the inner or dot product of $\overline{\nabla g}$ and $\overline{S}$. That is,

$$\begin{aligned} \dot{g} &= \left[(\overline{\nabla g}, \overline{S})\right] = \overline{\nabla g} \cdot \overline{S} \\ &= \frac{\partial g}{\partial x_1} \dot{x}_1 + \frac{\partial g}{\partial x_2} \dot{x}_2 \ . \end{aligned} \tag{3.64}$$

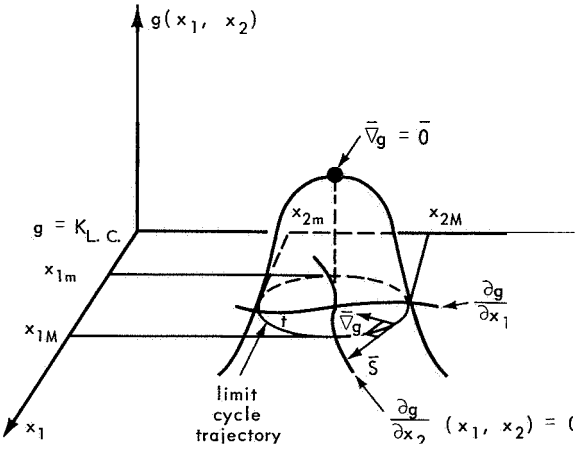

$\overline{\nabla g}$ to outwards) as the limit-cycle trajectory is traversed. Only unique single-valued functions $g(x_1, x_2)$ need be considered. That is,

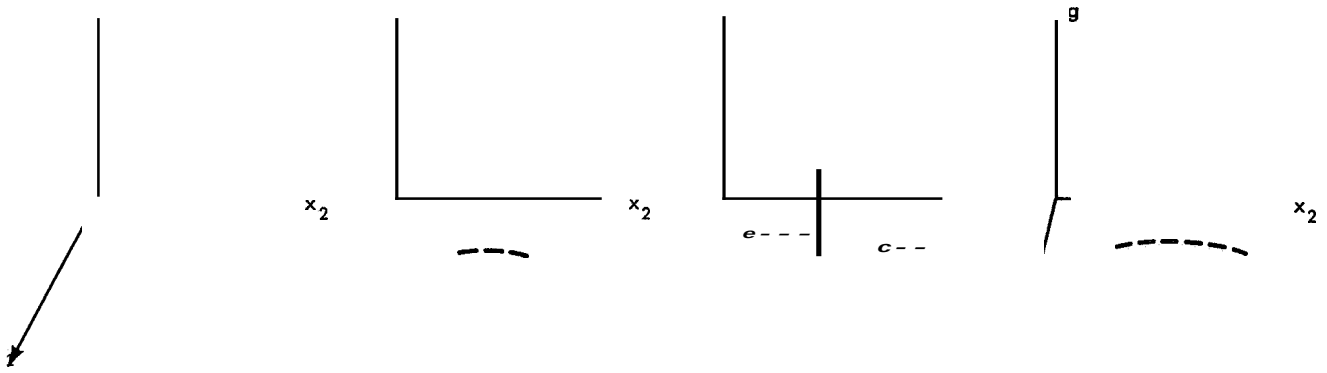

one peak (actually an odd number of extremums) where $\overline{\nabla g} = \overline{0}$ that lies within the limit cycle. This is shown a bit more rigorously by examining $g(x_1, x_2)$ versus x_1 for various values of x_2, that is, scanning across a constant $x_2 = K$. By Rolle's theorem (Reference 10), $\partial g/\partial x_1\big|_{x_2=K} = 0$ occurs at a value x_1 such that $x_{1m} \leq a < x_1 < b \leq x_{1M}$, where $g(a, K) = g(b, K) = K_{L.C.}$. See Figure 3.8. By allowing K to vary from x_{2m} to x_{2M} it is seen that a portion of the curve $\partial g/\partial x_1 (x_1, x_2) = 0$ lies within the limit cycle. Since at the point on the limit cycle where $x_2 = x_{2m}$ or x_{2M}, $\dot{x}_2 = 0$, then $0 = \dot{g} = (\partial g/\partial x_1)\dot{x}_1$ from Equation (3.64). But, except for the trivial case of the limit cycle being an equilibrium point, $\dot{x}_1 \neq 0$ at the x_2 extremum points. Hence, at these points,

$$\left.\frac{\partial g}{\partial x_1}\right|_{\substack{x_2 = x_{2M} \text{ or } x_{2m} \\ g = K_{L.C.}}} = 0 .$$

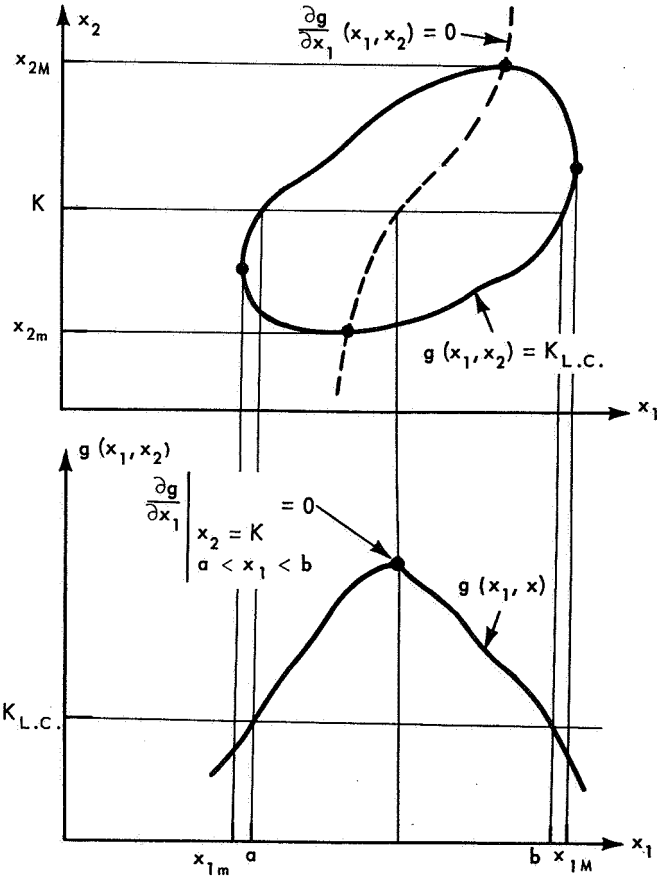

Figure 3.8—Section Views of Surface $g(x_1, x_2)$.

A similiar symmetric argument is presented for g-versus-x_2 curves for constant x_1 values, to show that a portion of the $\partial g/\partial x_2 = 0$ curve lies within the limit cycle, and that

$$\left.\frac{\partial g}{\partial x_2}\right|_{\substack{x_1 = x_{1M} \text{ or } x_{1m} \\ g = K_{L.C.}}} = 0 .$$

Now, $\overline{\nabla g} = \overline{0}$ occurs at the points of intersection of the two continuous curves $\partial g/\partial x_1 = 0$ and $\partial g/\partial x_2 = 0$; at least one such point occurs within the closed limit-cycle trajectory.

Now the question is to determine if this point where $\overline{\nabla g} = \overline{0}$, that lies within the limit cycle, is indeed an equilibrium point. To do this, a new system is defined as

$$\begin{aligned} \dot{x}_1 &= -\frac{\partial g(x_1, x_2)}{\partial x_2} \\ \dot{x}_2 &= \frac{\partial g(x_1, x_2)}{\partial x_1} \end{aligned} \tag{3.65}$$

where the function $g(x_1, x_2)$ is the same solution function to the original system as that given by Equation (3.55). Eliminating time from Equation (3.65) yields the equivalent system

$$\frac{dx_2}{dx_1} = -\frac{\partial g/\partial x_1}{\partial g/\partial x_2}, \tag{3.66}$$

for which the integral solutions are

$$g(x_1, x_2) = K. \tag{3.67}$$

That is, from the definition of the new system (3.65), all the solutions are closed curves in the x_1, x_2 plane, as for example those shown in Figure 3.9.

Along the limit cycle of the original system and at its equilibrium points, $\dot{g} = 0$. Thus, from (3.64),

$$\dot{g} = \frac{\partial g}{\partial x_1} f_1 + \frac{\partial g}{\partial x_2} f_2 = 0 \tag{3.68}$$

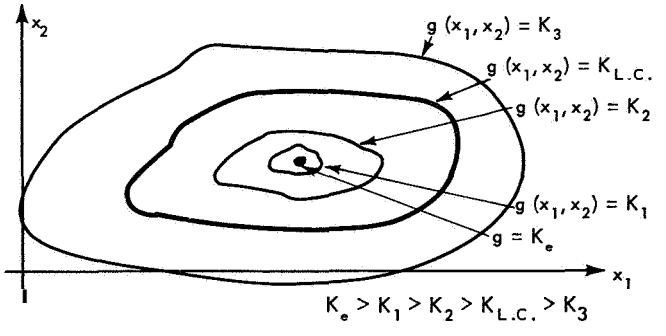

Figure 3.9—Closed-Curve Solutions, $g(x_1, x_2) = K$.

or

$$\frac{f_2}{f_1} = -\frac{\partial g/\partial x_1}{\partial g/\partial x_2}. \tag{3.69}$$

Hence, when $K = K_{L.C.}$, and at all the equilibrium points, the two systems (3.52) and (3.65) are equivalent, that is, they yield the same unique solutions for the same initial conditions. The equilibrium points of the

new system (3.65), by the very definition of that system, are at

$$\frac{\partial g}{\partial x_2} = 0$$

$$\frac{\partial g}{\partial x_1} = 0 \,, \tag{3.70}$$

or in other words,

$$\overline{\nabla g} = \overline{0} \,. \tag{3.71}$$

But at least one point for which $\overline{\nabla g} = \overline{0}$ lies within the limit cycle $g = K_{L.C}$ (for example, the point $g = K_e$ in Figure 3.9), as previously shown. Since the two systems are equivalent at the equilibrium points and on the $K_{L.C}$ limit cycle, it is true that for the original system (3.52), at least one equilibrium point lies within the $K_{L.C.}$ limit-cycle trajectory just as it does for the new system (3.65). Thus, the proof that at least one equilibrium point lies within a limit cycle is established for second-order systems by this gradient technique.

These arguments are now extended to higher-order systems. A third-order system is considered before finally treating an n^{th}-order system.

Consider the unique system

$$\begin{aligned} \dot{x}_1(t) &= f_1\left(x_1(t), x_2(t), x_3(t)\right) \\ \dot{x}_2(t) &= f_2\left(x_1(t), x_2(t), x_3(t)\right) \\ \dot{x}_3(t) &= f_3\left(x_1(t), x_2(t), x_3(t)\right) \,, \end{aligned} \tag{3.72}$$

which yields a finite limit cycle

$$x_i(t) = x_i(t+\tau) \qquad i = 1, 2, 3 \tag{3.73}$$

for certain initial conditions $x_i(0)$. In three-dimensional state space, the bounded closed trajectory is described functionally by the intersection of the two surfaces

$$\begin{aligned} g_1\left(x_1, x_2, x_3\right) &= K_{1L.C.} \\ g_2\left(x_1, x_2, x_3\right) &= K_{2L.C.} \end{aligned} \tag{3.74}$$

This closed curve has projections in the $x_1 x_2$, $x_1 x_3$, and $x_2 x_3$ planes that are described functionally by

$$\begin{aligned} h_3(x_1, x_2) &= c_3 \\ h_2(x_3, x_1) &= c_2 \\ h_1(x_2, x_3) &= c_1 \end{aligned} \tag{3.75}$$

respectively. The c's and K's are constants. It is also true, for the limit-cycle initial conditions, that

$$g = \dot{g}_2 = \dot{h}_1 = \dot{h}_2 = \dot{h}_3 = 0 . \tag{3.76}$$

Introducing the field vector

$$\bar{S} = \begin{pmatrix} \dot{x}_1 \\ \dot{x}_2 \\ \dot{x}_3 \end{pmatrix} \tag{3.77}$$

and the gradient vectors

$$\overline{\nabla h_i} = \begin{pmatrix} \frac{\partial h_i}{\partial x_1} \\ \frac{\partial h_i}{\partial x_2} \\ \frac{\partial h_i}{\partial x_3} \end{pmatrix} , \tag{3.78}$$

then

$$\dot{h}_i = \left[\left(\overline{\nabla h_i}, \bar{S} \right) \right] = 0 , \tag{3.79}$$

where $[(\ )]$ represents the inner product, and $i = 1, 2, 3$. It is noted that

$$\frac{\partial h_i}{\partial x_i}(x_j, x_k) = 0 , \tag{3.80}$$

where the i, j, k are cyclic indices **1, 2, 3.** The slope of the projected limit cycle in the $x_j\ x_k$ plane is

$$\frac{dx_k}{dx_j} = -\frac{\partial h_i/\partial x_j}{\partial h_i/\partial x_k} \cdot \tag{3.81}$$

This is seen from the fact that

$$h_i = \frac{\partial h_i}{\partial x_i}\dot{x}_i + \frac{\partial h_i}{\partial x_j}\dot{x}_j + \frac{\partial h_i}{\partial x_k}\dot{x}_k \tag{3.82}$$

in conjunction with Equation **(3.80).** Equation **(3.81)** corresponds to (3.66), and the second-order case reasoning is applicable. Of course it is true that in this two dimensional projection, the limit-cycle trajectory may cross itself (even though the limit-cycle trajectory in three-dimensional space does not) at points that are not system equilibrium points. That is, $\partial h_i/\partial x_j = \partial h_i/\partial x_k = \mathbf{0}$ implies an indeterminate planar slope at the point, but the system slope in three dimensions is parallel to the x_i axis. The essential idea is that the gradient vector in the $x_j\ x_k$ plane is perpendicular to the projected trajectory, which in turn indicates the necessity for at least one peaking of the surface h_i within the projected limit cycle. See, for example, Figure **3.10.** This $\overline{\nabla h_i} = \overline{0}$ peak corresponds to an $h_i = \mathbf{0}$ equilibrium point as previously shown for the second-order case. Hence, at least one equilibrium point lies within the general limit cycle.

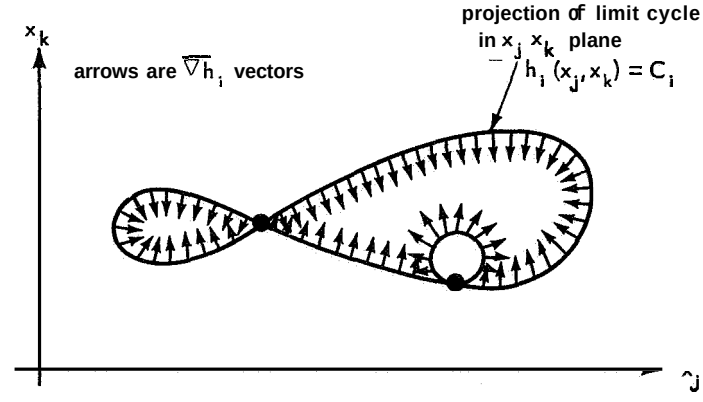

Finally, the transition to the general n^{th}-order system is made, where $n \geq \mathbf{2}$. The general form of the equation is

$$\dot{x}_i = f_i(x_1, x_2, \cdots, x_n) \qquad i = 1, 2, \cdots, n \ . \tag{3.83}$$

Assume some initial conditions $x_i(0)$ yield the limit cycle $x_i(t) = x_i(t+\tau)$ that is a closed bounded curve in n-dimensional state space. The projection of the trajectory in the $x_{i_{n-1}}\ x_{i_n}$ plane is represented by

$$h_{i_1 i_2 \cdots i_{n-2}}(x_{i_{n-1}}, x_{i_n}) = c_{i_1, i_2 \cdots i_{n-2}} \ , \tag{3.84}$$

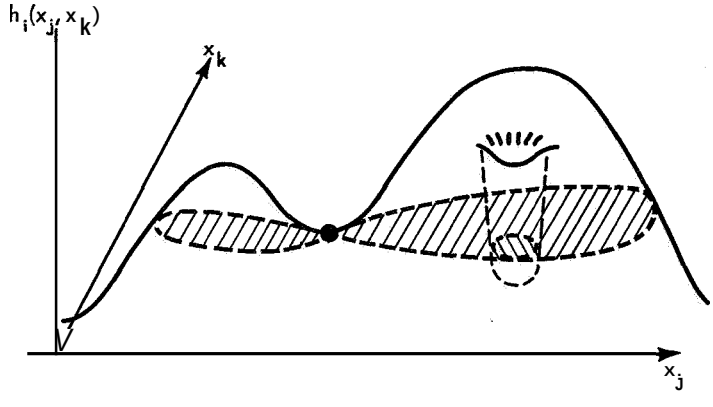

Figure 3.10—$h_i(x_j, x_k) = c_i$ Curves.

where the i's are n cyclic variables **1, 2,** $\cdots$ **,**n**,** and the ***c's*** are constant. There are $n(n-1)/2$ such expressions as in **(3.84).** Defining the field and gradient vectors as

$$\bar{S} = \begin{pmatrix} \dot{x}_1 \\ \dot{x}_2 \\ \vdots \\ \dot{x}_n \end{pmatrix} \tag{3.85}$$

and

$$\overline{\nabla h}_{i_1 i_2 \cdots i_{n-2}} = \begin{pmatrix} \dfrac{\partial h_{i_1 i_2 \cdots i_{n-2}}}{\partial x_1} \\ \dfrac{\partial h_{i_1 i_2 \cdots i_{n-2}}}{\partial x_2} \\ \vdots \\ \dfrac{\partial h_{i_1 i_2 \cdots i_{n-2}}}{\partial x_n} \end{pmatrix}, \tag{3.86}$$

then

$$h_{i_1 i_2 \cdots i_{n-2}} = \left[\left(\overline{\nabla h}_{i_1 i_2 \cdots i_{n-2}}, \bar{S} \right) \right] = 0 \tag{3.87}$$

along the projected limit cycles. All of the previous arguments hold true such that at least one $\overline{\nabla h} = 0$ point lies within all **of** the projected limit cycles. These points are equilibrium points the same as previously shown, since

$$\frac{dx_{i_n}}{dx_{i_{n-1}}} = \frac{f_{i_n}}{f_{i_{n-1}}} = - \frac{\partial h_{i_1 i_2 \cdots i_{n-2}} / \partial x_{i_{n-1}}}{\partial h_{i_1 i_2 \cdots i_{n-2}} / \partial x_{i_n}} . \tag{3.88}$$

Equation **(3.88)** is derived from **(3.83)** and the following two equations:

$$\dot{h}_{i_1 i_2 \cdots i_{n-2}} = \frac{\partial h_{i_1 i_2 \cdots i_{n-2}}}{\partial x_{i_1}} \dot{x}_{i_1} + \frac{\partial h_{i_1 i_2 \cdots i_{n-2}}}{\partial x_{i_2}} \dot{x}_{i_2} + \cdots + \frac{\partial h_{i_1 i_2 \cdots i_{n-2}}}{\partial x_{i_n}} \dot{x}_{i_n} = 0 \tag{3.89}$$

and

$$\frac{\partial h_{i_1 i_2 \cdots i_{n-2}}}{\partial x_j} \left(x_{i_{n-1}}, x_{i_n} \right) = 0 \tag{3.90}$$

for $j = i_1, i_2, \cdots, i_{n-2}$. Hence, the previous arguments from the second- and third-order cases still apply to the general n^{th}-order case.

It is therefore concluded that, for a general n^{th}-order system that follows the ground rules of Chapter 2, if a limit cycle exists, then there is at least one equilibrium point that lies within the limit cycle. That is,

$$x_{im} < x_{i\,equib} < x_{iM} \qquad i = 1, 2, \cdots n \; . \tag{3.91}$$

4. EXAMPLES

In this chapter, several examples are presented that illustrate the ideas of the previous chapters. Included also are "counter-examples" that apparently violate some of the theorems of Chapter 3. With each counter-example is an explanation of those ground rules in Chapter 2 that are broken.

Example 1. First, a linear system is considered. The fourth-order differential equation is

$$\dddot{x}(t) = -5\omega^2 \ddot{x}(t) - 4\omega^4 \left(x(t) - x_a\right) , \tag{4.1}$$

where ω and x_a are arbitrary real constants. Assume that initial conditions

$$\begin{aligned} x(0) &= x_a + K^2/4 \\ \dot{x}(0) &= 0 \\ \ddot{x}(0) &= 0 \\ \dddot{x}(0) &= 0 , \end{aligned} \tag{4.2}$$

where K is an arbitrary real constant. The solution is

$$x(t) = x_a + \frac{K^2}{3} \cos \omega t - \frac{K^2}{12} \cos 2\omega t , \tag{4.3}$$

which is a limit cycle with period $\tau = 2\pi/\omega$. The periodic derivative functions are

$$\begin{aligned} \dot{x}(t) &= \frac{-K^2 \omega}{3} \sin \omega t + \frac{K^2 \omega}{6} \sin 2\omega t \\ \ddot{x}(t) &= \frac{-K^2 \omega^2}{3} \cos \omega t + \frac{K^2 \omega^2}{3} \cos 2\omega t \\ \dddot{x}(t) &= \frac{K^2 \omega^3}{3} \sin \omega t - \frac{2K^2 \omega^3}{3} \sin 2\omega t \\ \ddddot{x}(t) &= \frac{K^2 \omega^4}{3} \cos \omega t - \frac{4K^2 \omega^4}{3} \cos 2\omega t . \end{aligned} \tag{4.4}$$

Taking the averages of all these functions yields

$$x_{avg} = \frac{\omega}{2\pi}\int_{t}^{t+2\pi/\omega} x(\lambda)\,d\lambda = x_a$$

$$x_{avg}^{(i)} = \frac{\omega}{2\pi}\int_{t}^{t+2\pi/\omega} x^{(i)}(\lambda)\,d\lambda = 0\ , \qquad (4.5)$$

where $i = 1, 2, 3, 4$. From Equation (4.1), the equilibrium point is at

$$x_e = x_a$$

$$x_e = \ddot{x}_e = \dddot{x}_e = \ddddot{x}_e = 0\ . \qquad (4.6)$$

That is, the centroid or average point (which lies within the limit cycle) is the equilibrium point as proved in Chapter 3. Note that the projection of the limit cycle on the x-axis, shown in Figure 4.1, illustrates how the equilibrium point separates the positive and negative $\ddot{x}$ regions of the x-axis.

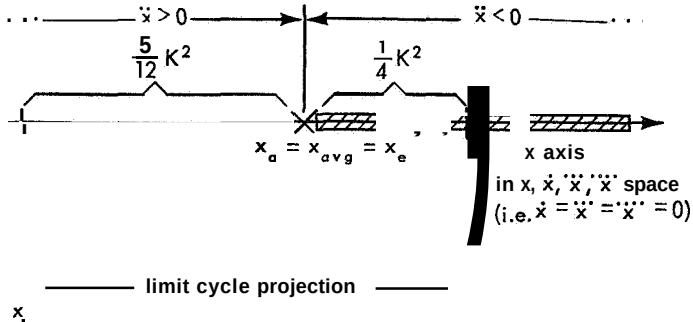

Figure 4.1—Linear-System Centroid.

Example 2. The second example illustrates how one may easily be misled when solving for equilibrium points. Consider the periodic function

$$x(t) = \sin t\ . \qquad (4.7)$$

This is the solution to the differential equation

$$\dot{x}^2(t) + x^2(t) = 1\ , \qquad (4.8)$$

with the initial condition $x(0) = 0$. Now, $x_{avg} = 0$, but it appears from Equation (4.8) that $x_{equib} = \pm 1$, by setting $\dot{x}(t) = 0$. If this is so, then these two equilibrium points lie on the limit cycle. See Figure 4.2. This contradicts the definition of an equilibrium point. Furthermore, $x(t)$ is also the solution to the linear second-order differential equation

$$\ddot{x}(t) = -x(t)\ , \qquad (4.9)$$

and it is shown in Chapter 2 that, for linear systems, $x_{avg} = x_{equib}$ (as well as the fact that only one equilibrium point exists for a linear system). This is not the case when the equilibriums are calculated from Equation (4.8) which is the integral of the linear Equation (4.9). (Of course,

all is proper when Equation **(4.9)** is used to calculate the equilibrium points.) A ground rule of Chapter **2** is violated by Equation **(4.8).** Equilibrium points are defined as $0 = f(0, 0, \cdots, x_e)$ for the system

$$x^{(n)} = f\left(x^{(n-1)}, x^{(n-2)}, \cdots, \dot{x}, x\right) , \quad (4.10)$$

where n is a positive integer. But Equation **(4.8)** cannot be put into this form, such that every initial x yields a unique $\dot{x}$. Either time is involved explicitly, or the system contains memory such that

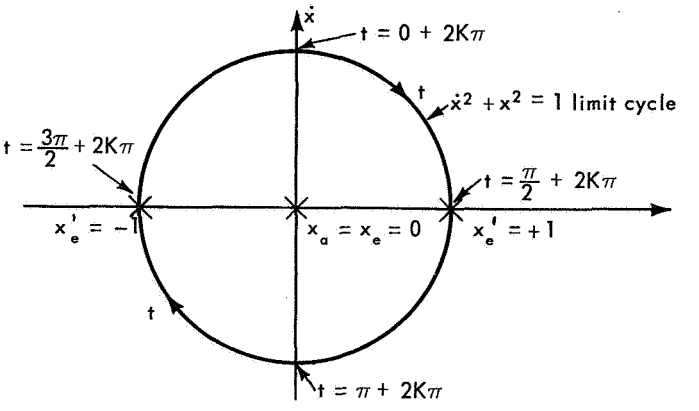

Figure 4.2—Limit-Cycle Circle.

$$\dot{x} = \begin{cases} +\sqrt{1 - x^2} & \text{for } 0 \le t < \frac{\pi}{2}, \quad \frac{(3+4k)\pi}{2} \le t < \frac{(5+4k)\pi}{2} \\ -\sqrt{1 - x^2} & \text{for } \frac{(1+4k)\pi}{2} \le t < \frac{(3+4k)\pi}{2}, \end{cases} \quad (4.11)$$

where $k = 0, 1, 2, \cdots$. Misuse of relationships such as Equation **(4.8)** must be avoided.

Example **3.** The well-studied nonlinear Van der Pol equation,

$$\ddot{x} = \epsilon\left(1 - x^2\right)\dot{x} - x , \qquad \epsilon > 0 \quad (4.12)$$

has as a solution a limit cycle that encircles the origin in the $x - \dot{x}$ phase plane (Reference **11).** See Figure **4.3(a).** Substituting $y = -\dot{x} + \epsilon\left(x - x^3/3\right)$ in **(4.12)** yields the equivalent system

$$\ddot{y} = \epsilon\left(\dot{y} - \frac{\dot{y}^3}{3}\right) - y , \quad (4.13)$$

where $x = \dot{y}$. Equation **(4.13)** likewise has a limit-cycle solution encircling the origin (see Figure **4.3b).** In both cases the origin is an equilibrium point of the system. In the next chapter some further properties of Equations **(4.12)** and **(4.13)** are investigated.

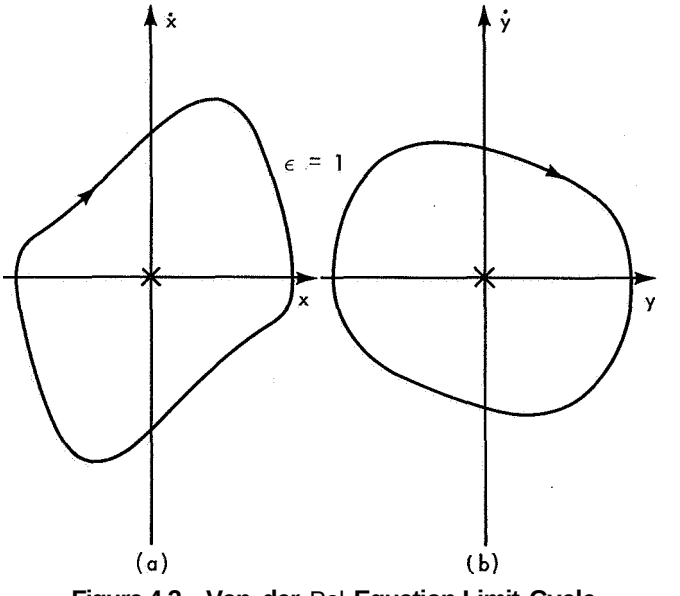

Figure 4.3—Van der Pol Equation Limit Cycle.

Example **4.** This example illustrates two things: **(1)** equilibrium points may be difficult to find, and **(2)** an average point (centroid) is not necessarily an equilibrium

point for nonlinear systems. Consider the system

$$\ddot{x} = \begin{cases} -\omega^2 (x + B) & x < -X \\ 6\left(K^2 x\right)^{1/3} & |x| \leq X \\ -\omega^2 (x - B) & x > X \end{cases} \qquad (4.14)$$

where ω and K are arbitrary positive real constants, and $B = 20K/\omega^3 > X > 0$. **Assume** the initial conditions

$$\begin{aligned} x(0) &= B + A/\omega \\ \dot{x}(0) &= 0 , \end{aligned} \qquad (4.15)$$

where $A = 12\sqrt{2}K/\omega^2$. This yields a limit cycle of period $\tau = (3\pi + 8)/\omega$, of which one cycle from $0 \leq t \leq \tau$ is described by

$$x(t) = \begin{cases} B + \frac{A}{\omega} \cos \omega t & 0 \leq t < \Delta \\ -K\left(t - \frac{\tau}{4}\right)^3 & \Delta \leq t < \frac{\tau}{2} - \Delta \\ -B - \frac{A}{\omega} \cos \omega \left(t - \frac{\tau}{2}\right) & \frac{\tau}{2} - \Delta \leq t < \frac{\tau}{2} + \Delta \\ K\left(t - \frac{3\tau}{4}\right)^3 & \frac{\tau}{2} + \Delta \leq t < \tau - \Delta \\ B + \frac{A}{\omega} \cos \omega (t - \tau) & \tau - \Delta \leq t \leq \tau \end{cases} \qquad (4.16)$$

$$\dot{x}(t) = \begin{cases} -A \sin wt & 0 \leq t < \Delta \\ -3K\left(t - \frac{\tau}{4}\right)^2 & \Delta \leq t < \frac{\tau}{2} - \Delta \\ A \sin \omega \left(t - \frac{\tau}{2}\right) & \frac{\tau}{2} - \Delta \leq t < \frac{\tau}{2} + \Delta \\ 3K\left(t - \frac{3\tau}{4}\right)^2 & \frac{\tau}{2} + \Delta \leq t < \tau - \Delta \\ -A \sin \omega (t - \tau) & \tau - \Delta \leq t \leq \tau \end{cases} \qquad (4.17)$$

$$x(t) = \begin{cases} -A\omega \cos \omega t & 0 \le t < \Delta \\ -6K\left(t - \frac{\tau}{4}\right) & \Delta \le t < \frac{\tau}{2} - \Delta \\ A\omega \cos \omega\left(t - \frac{\tau}{2}\right) & \frac{\tau}{2} - \Delta \le t < \frac{\tau}{2} + \Delta \\ 6K\left(t - \frac{3\tau}{4}\right) & \frac{\tau}{2} + \Delta \le t < \tau - \Delta \\ -A\omega \cos \omega(t - \tau) & \tau - \Delta \le t \le \tau \end{cases} \quad (4.18)$$

where $x(\Delta) = X$, and $\Delta = 3\pi/4\omega$. These functions are plotted in Figure 4.4 Note that $x(t)$, and its first two derivatives are continuous for all t. This is forced to be true by constraining x,

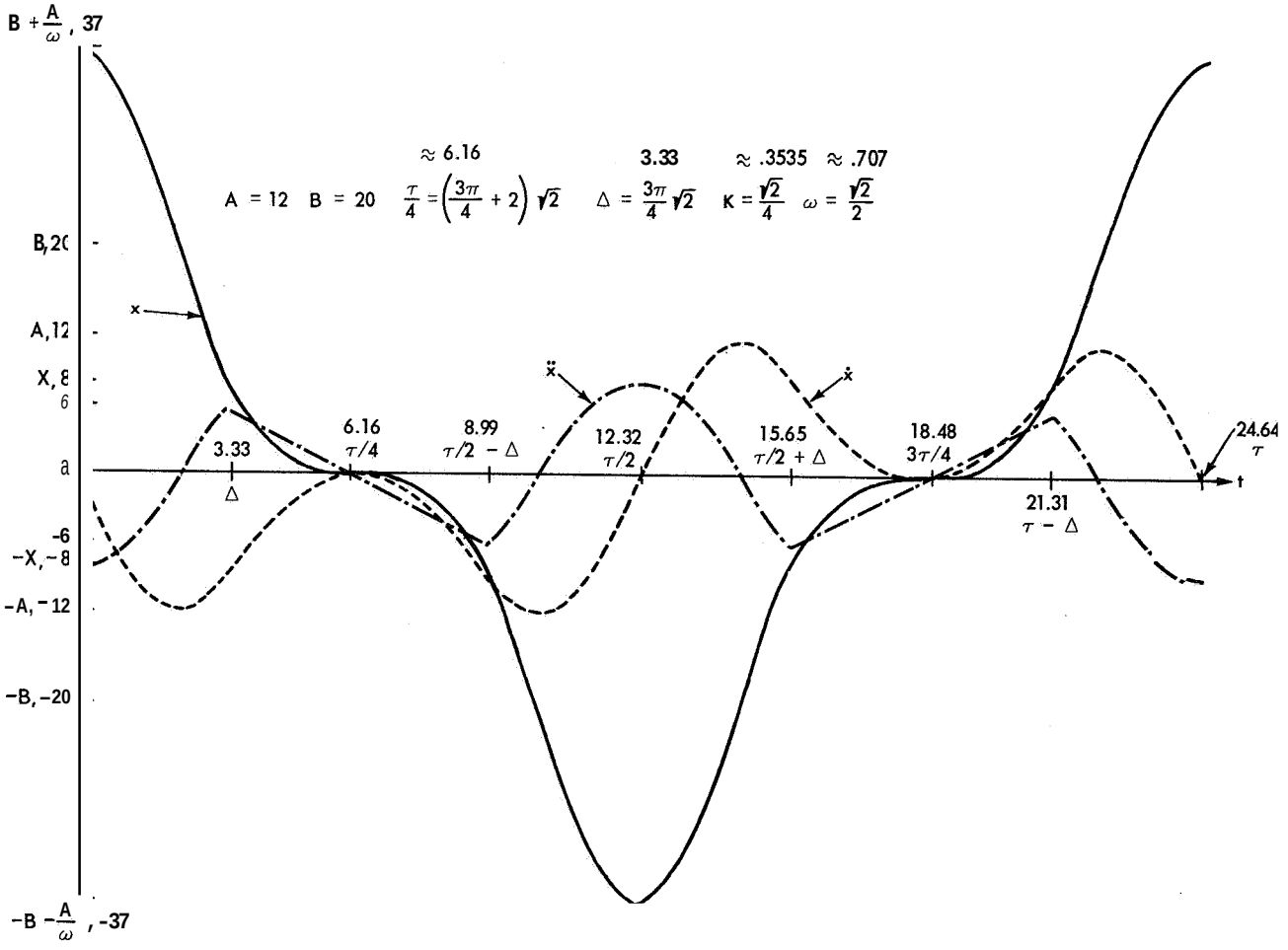

Figure 4.4—Example4 Functions Versus Time.

$\dot{x}$, and $\ddot{x}$ at $t = 0$, A, $\tau/2-\Delta$, $\tau/2+\Delta$, $\tau - A$, and τ by the equations

$$
\begin{aligned}
B + \frac{A}{\omega}\cos\omega\Delta &= -K\left(\Delta - \frac{\tau}{4}\right)^3 \\
A\sin\omega\Delta &= 3K\left(\Delta - \frac{\tau}{4}\right)^2 \\
A\omega\cos\omega\Delta &= 6K\left(A - \frac{\tau}{4}\right),
\end{aligned}
\tag{4.19}
$$

respectively. To simplify the algebra, $\omega\Delta$ is arbitrarily chosen as $\omega\Delta = 3\pi/4$, and A, B, and τ are solved as functions of ω and K.

Equation (4.14) apparently has three equilibrium points:

$$
x_{equib} = 0, \pm B \; . \tag{4.20}
$$

Also, from Equation (4.16), one calculates the average of x(t) and finds

$$
_{avg} = \frac{1}{\tau}\int_0^{\tau} x(t)\,dt = 0 \; . \tag{4.21}
$$

(It is also true that $\dot{x}_e = \ddot{x}_e = \dot{x}_a = \ddot{x}_a = 0$, as expected.) Thus it appears that the origin is the centroid of the system, and is an equilibrium point. But this point lies on the limit cycle. The phase-plane trajectory is plotted in Figure 4.5. Its equations are,

$$
\begin{aligned}
&(x+B)^2\omega^2 + \dot{x}^2 = A^2 \quad \text{for} \quad x \le -X \\
&\left.\begin{aligned}
\dot{x}^3 &= 27Kx^2 \quad \text{for} \quad \dot{x} \ge 0 \\
\dot{x}^3 &= -27Kx^2 \quad \text{for} \quad \dot{x} < 0
\end{aligned}\right\} \text{for} \quad |x| < X \\
&(x-B)^2\omega^2 + \dot{x}^2 = A^2 \quad \text{for} \quad x \ge X \; .
\end{aligned}
\tag{4.22}
$$

A defect in this example is that Equation (4.14) fails the uniqueness test of Chapter 2. That is, Equation (2.6) and (2.7) are satisfied, but the Lipschitz condition of Equation (2.8) is violated at the origin, since a Lipschitz constant must be greater than $(x)^{-1/3}$. In fact, $\ddot{x} = 6(K^2 x)^{1/3}$ has three possible solutions from initial conditions at the origin. They are

$$
x = 0, \pm Kt^3 \; , \tag{4.23}
$$

of which only the first is an equilibrium solution. The last two are part of the limit cycle of Equation **(4.16).**

The system is made unique if initial conditions that lie on the limit cycle shown in Figure **4.5** (which includes the origin) are not considered. By varying A in the initial conditions of Equation **(4.15),** a family of limit cycles is obtained (see Figure **4.6).** The heavy figure-8 curve is the forbidden limit cycle where $A = 12\sqrt{2}\,K/\omega^2$. However, it is not a separatrix (Reference **6)** that separates regions and passes through equilibrium points so that it takes an infinite time to traverse. (A separatrix exists in the nonlinear pendulum example 8, and also example **11,** both of which are discussed later in this chapter.)

If the initial conditions of Equation **(4.15)** are

$$x(0) = \pm B \pm A/\omega$$
$$\dot{x}(0) = 0\,, \qquad \textbf{(4.24)}$$

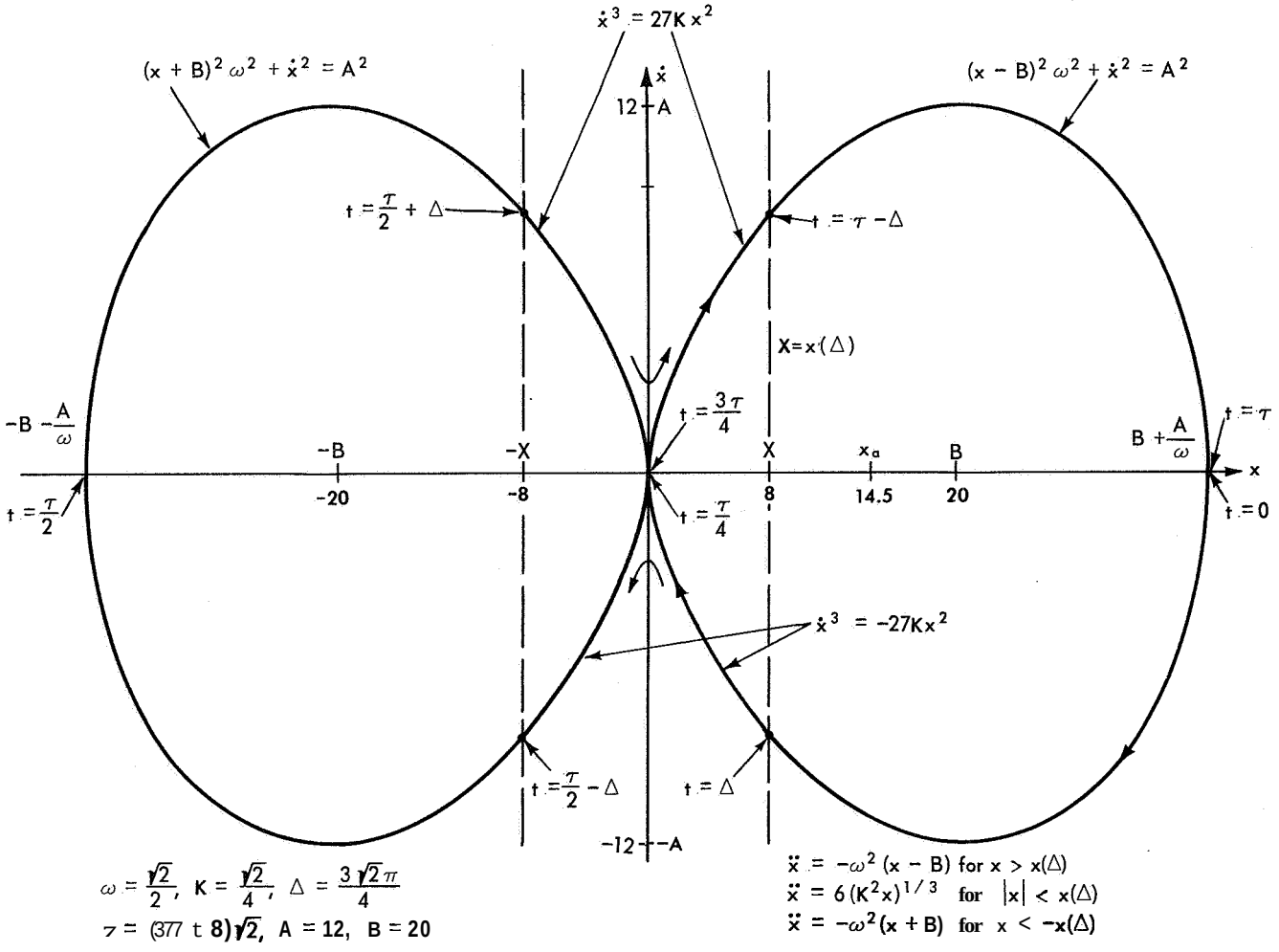

Figure 4.5—Phase-Plane Plot for Example 4.

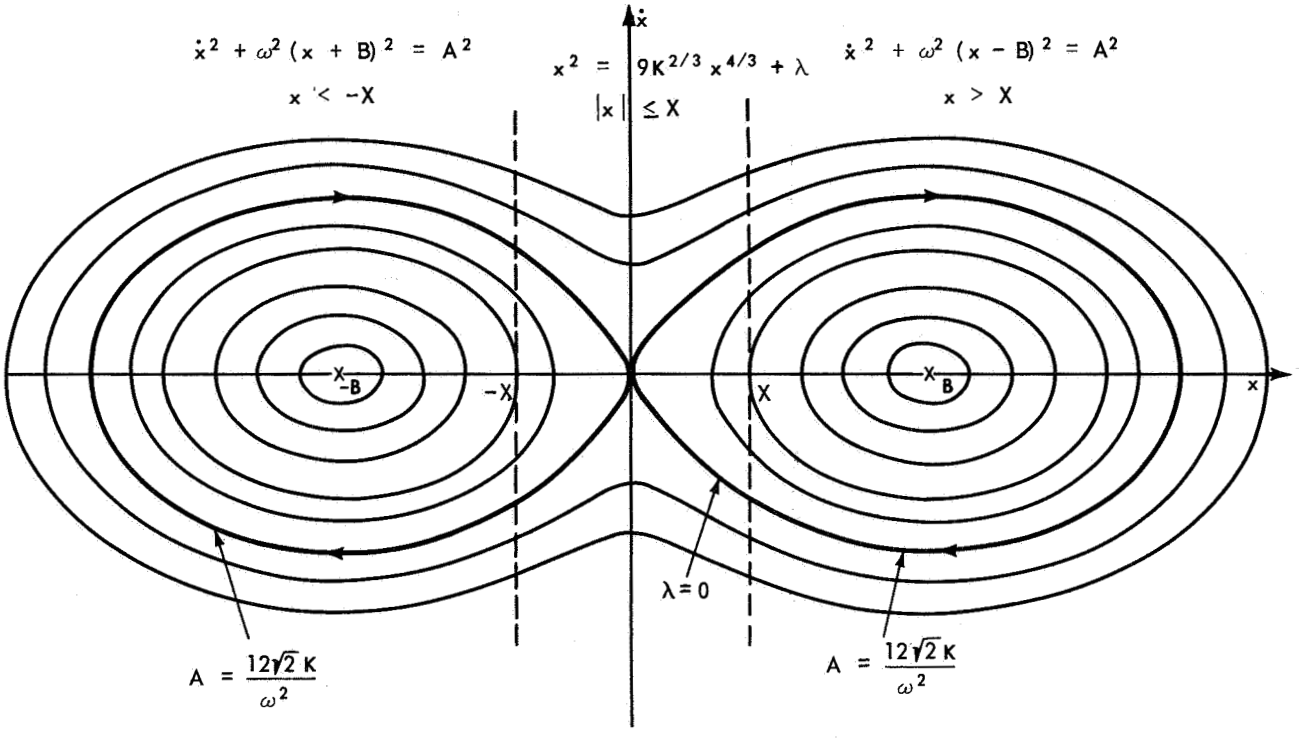

Figure 4.6—Phase-Plane Portrait for Example 4.

such that $A/\omega \leq B - X$, then linear harmonic motion exists such that $x(t) = \pm B + (A/\omega) \cos \omega t$. The limit cycles encircle the $\pm B$ equilibrium points, which are also the centroids of the limit cycles. However, for the same initial conditions of **(4.24)** but $B - X < A/\omega < 12\sqrt{2}K/\omega^2$, the resulting limit cycles are still contained within the forbidden figure-8 limit cycle and still encircle the $\pm B$ equilibrium points; but these points are no longer their centroids. The centroids actually occur on the x-axis, but closer to the origin than $\pm B$. For example, consider the $\lambda = 0$ limiting limit cycle in the right-half plane. (The $\lambda = 0$ curve is chosen even though it is part of the forbidden limit cycle, to avoid elliptic integrals.) x_{avg} is calculated as

$$\left| \int_0^{\Delta} \left(B + \frac{A}{\omega} \cos \omega t \right) dt + 2 \int_{\Delta}^{\tau'/2} \qquad \left(\frac{\tau'}{2} \right)^3 dt \right| , \tag{4.25}$$

where

$$\begin{aligned} A &= \frac{12K\sqrt{2}}{\omega^2} \\ B &= \frac{20K}{\omega^3} \\ \Delta &= \frac{3\pi}{4\omega} \\ \tau' &= \frac{3\pi + 8}{2w} , \end{aligned} \tag{4.26}$$

such that τ' is half of the original forbidden limit cycle period τ. Performing the integration yields

$$x_{avg} = B\left[1 - \frac{24}{5(3\pi + 8)}\right] = 0.725B \quad , \quad (4.27)$$

which is not the equilibrium point, $x_e = B$, inside the limit cycle. (When $\dot{x}_{avg}$ and $\ddot{x}_{avg}$ are calculated, they of course are zero.) This limiting limit cycle is shown in Figure 4.7.

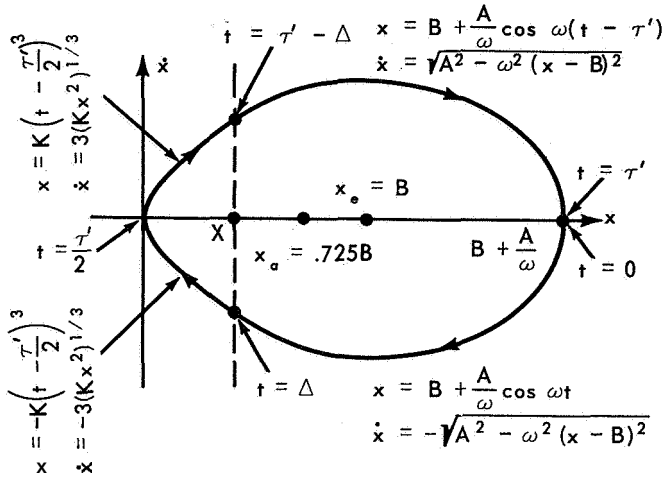

Figure 4.7—Limiting Limit Cycle for Example 4.

Example 5. In Chapter 8, a mathematical on-off controller (of the sgn(x) type) is modified to match physical characteristics that have no jump discontinuities (see Figure 8.4). This example illustrates how a non-physical system may raise difficulties. Consider the system defined by

$$\begin{aligned} \ddot{x} &= K \qquad \text{for} \quad \dot{x} \geq 0 \ , \ 0 \leq x < K \\ \ddot{x} &= -K \qquad \text{for} \quad \dot{x} \geq 0 \ , \ -K < x < 0 \\ \ddot{x} &= -x \qquad \text{elsewhere} \ , \end{aligned} \quad (4.28)$$

where K is a positive real constant. No equilibrium point exists, since $\dot{x}$ and $\ddot{x}$ are never both zero simultaneously. However, many limit cycles exist, as shown in the phase-plane plot of Figure 4.8. This contradicts the theorem in Chapter 2, which states that if a limit cycle exists then an equilibrium point exists. The theorem is violated because the Lipschitz condition in Equation (2.8) is violated by the discontinuous jump of $\ddot{x}$. One cycle of $\ddot{x}$ versus time is plotted in Figure 4.9 for the heavily drawn limit cycle going through the origin in Figure 4.8. The jump discontinuity is re'medied by allowing $\ddot{x}$ to vary anywhere between ±K (including zero) along the boundaries of Equation (4.28), that is, $\dot{x} = 0$ and $x = 0$. Thus, there are an infinite number of equilibrium points for $\dot{x} = 0$ when $|x| < K$. (The origin lies inside all the limit cycles.)

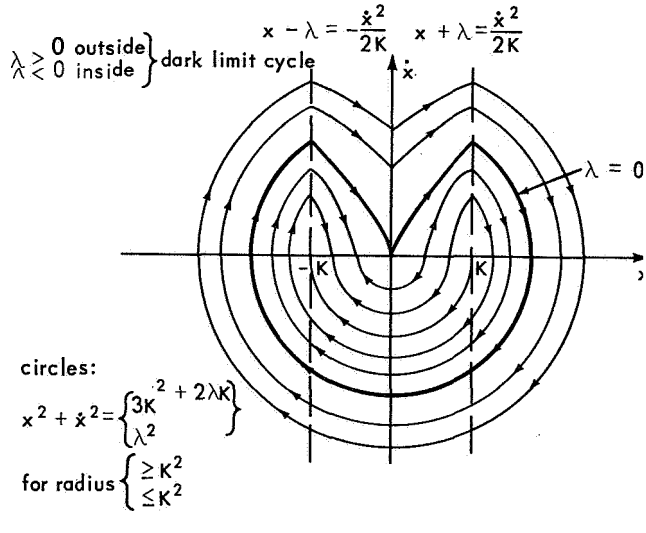

Figure 4.8—Phase Portrait for Example 5.

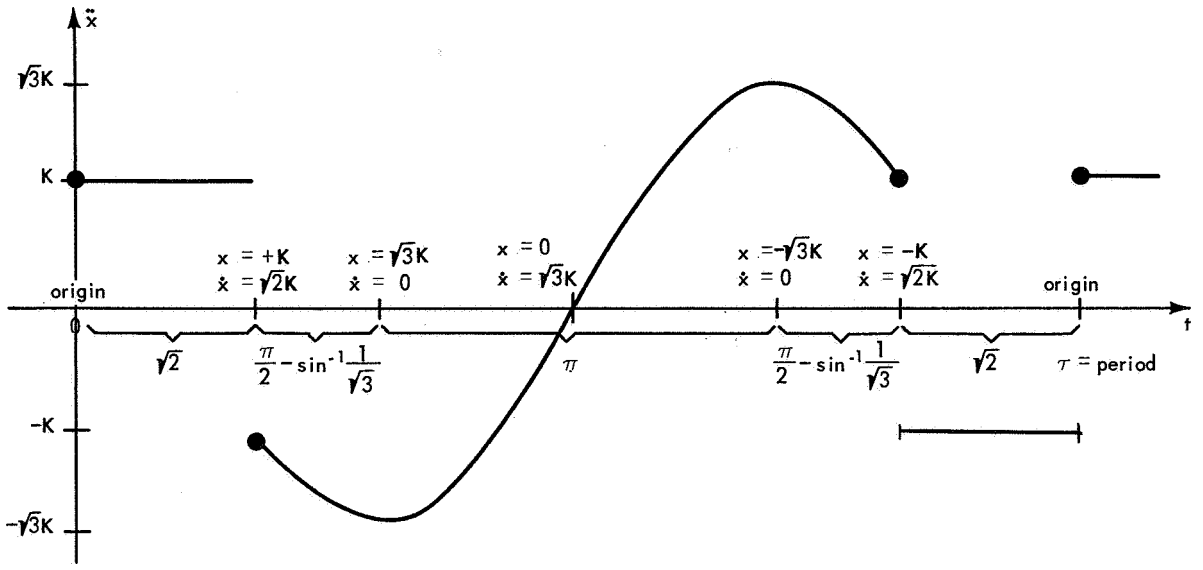

Figure 4.9—$\ddot{x}(t)$ for Example 5.

Example 6. This interesting example yields finite closed solution curves in the phase plane, but they are not limit cycles. The one point common to all the curves is the only equilibrium point of the system. The defining equations are:

$$\begin{aligned} \dot{x} &= x^2 - y^2 \\ \dot{y} &= 2xy \ . \end{aligned} \tag{4.29}$$

The solution trajectories satisfy the relationship

$$x^2 + (y-c)^2 = c^2 \ . \tag{4.30}$$

Equation (4.30) represents a family of circles of radius c and with center on the y axis at $y = c$. From Equation (4.30)

$$c = \frac{x^2 + y^2}{2y}$$

Substituting this expression for c in the derivative of (4.30),

$$2x\dot{x} + 2(y-c)\dot{y} = 0 \ ,$$

yields

$$\frac{\dot{y}}{\dot{x}} = \frac{2xy}{x^2 - y^2} \ ; \tag{4.31}$$

thus proving that Equation **(4.30)** represents the integral solutions to **(4.29).** The phase-plane curves of **(4.30)** are shown in Figure **4.10.** From Equation (4.29), the origin is the only equilibrium point. It takes an infinite time **to** traverse any of the closed circles. This example appears on page **10** of Reference **8,** in Hahn's discussion of unstable equilibrium points.

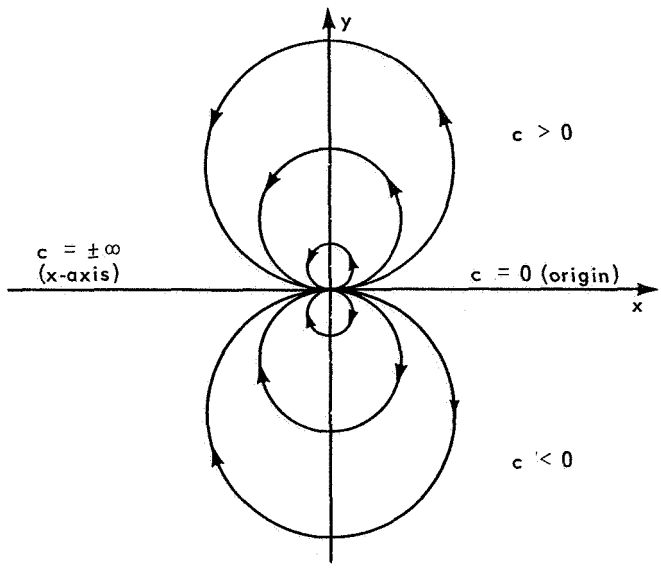

Figure 4.10—Non-Periodic Closed Curves.

Example 7. Example 5 presents a system with a limit cycle but no equilibrium point. Example 6 presents a system with an equilibrium point but no limit cycle. Example 1 presents a system with both an equilibrium point and a limit cycle, and this example presents a system with neither. (Equation **(3.18)** in the previous chapter is also such an example.) The system under consideration is:

$$\ddot{x} = x\dot{x} - 2 . \qquad (4.32)$$

Obviously, no finite real **x** exists such that $\ddot{x} = \dot{x} = 0$. It is seen from Figure **4.11** that any phase-plane trajectory crosses the $\ddot{x} = 0$ curve only once, and the curve itself does not ever cross the x-axis. Hence a limit cycle does not exist.

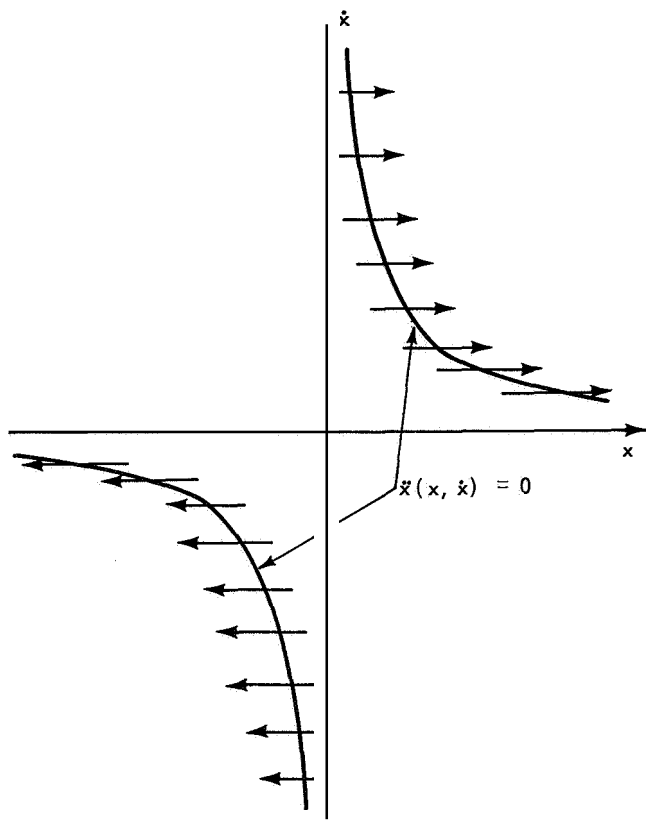

Figure 4.11—Zero-Slope Curve for Example 6.

Example **8.** This example is the classic system of the simple pendulum,

$$\ddot{x} = -\lambda^2 \sin x . \qquad (4.33)$$

The second-order nonlinear system **(4.33)** yields an infinite number of isolated equilibrium points along the **x**-axis, i.e. $x_e = \pm n\pi$, where $n = 1, 2, \cdots$. Equation **(4.33)** can be integrated once, since

$$\ddot{x} = \dot{x}\frac{d\dot{x}}{dx} = -\lambda^2 \sin x \qquad (4.34)$$

Thus,

$$\dot{x}^2 = 2\lambda^2 \cos x + K \ . \tag{4.35}$$

These solution trajectories are plotted in Figure **4.12.** For initial conditions such that $|K| < 2\lambda^2$, limit cycles exist. $K = -2\lambda^2$ are the equilibrium points, and $K = 2\lambda^2$ is the darkened separatrix curve which is the boundary between periodic and non-periodic solution curves. The limit cycles encircle a stable equilibrium point in between two unstable ones. Another interesting property of this nonlinear system is that the period of a limit cycle depends on the initial conditions (as opposed to the constant period in the linear Example 1). That is,

$$\tau = 4 \int_{x(t_0)}^{x(t_0+\tau/4)} \frac{dx}{\sqrt{2\lambda^2 \cos x + K}} \tag{4.36}$$

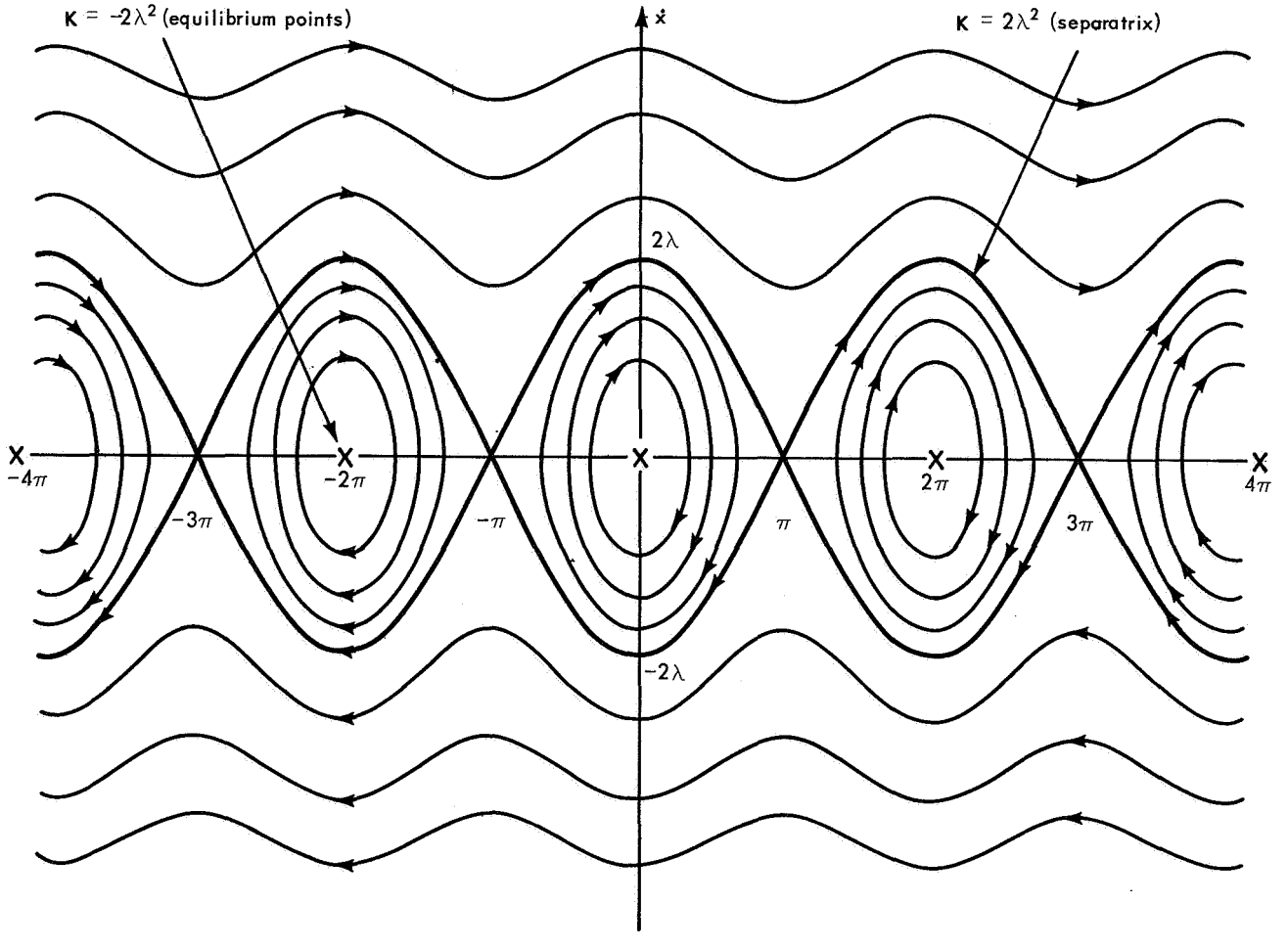

Figure 4.12—Phase-Plane Portrait for Simple Pendulum.

Letting $x(t_0) = 0$, $x(t_0 + \tau/4) = a$, $\dot{x}(t_0 + \tau/4) = 0$ $(\therefore 0 = 2\lambda^2 \cos a + K)$, and $\sin(x/2) = \sin(a/2)\sin\theta$, yields

$$\tau = 4/\lambda \int_0^{\pi/2} \frac{d\theta}{\sqrt{1 - \sin^2 \frac{a}{2} \sin^2 \theta}} , \tag{4.37}$$

which is a complete elliptic integral of the first kind, and is a function of a, which in turn is a function of K or the initial conditions.

Example 9. Example 8 contains an infinite number of isolated equilibrium points and limit cycles; Example 9 contains an infinite number of non-isolated equilibrium points, but no limit cycle. Consider the system,

$$\begin{aligned} \dot{x} &= (x - y)\left(1 - x^2 - y^2\right) \\ \dot{y} &= (x + y)\left(1 - x^2 - y^2\right) . \end{aligned} \tag{4.38}$$

Choosing a Liapunov function (Reference 8, p. 18),

$$V = r^2 = x^2 + y^2 , \tag{4.39}$$

yields

$$\dot{V} = 2\left(1 - r^2\right) r^2 \tag{4.40}$$

Therefore, if $0 < r^2 < 1$, then $\dot{V} > 0$ and $r^2 \to 1$, and if $1 < r^2$, then $\dot{V} < 0$ and $r^2 \to 1$ as time increases. That is, the origin is an unstable equilibrium point, and anywhere on the unit circle in the x, y state plane are stable equilibrium points for the system (4.38). The solutions to (4.38) in polar coordinates are

$$\begin{aligned} r(t) &= \left[\frac{1}{1 + K_1 e^{-2t}}\right]^{1/2} \\ \theta(t) &= \ln\left[\frac{K_2}{\left(1 + K_1 e^{-2t}\right)^{1/2}}\right] , \end{aligned} \tag{4.41}$$

where

$$\begin{aligned} r &= +\sqrt{x^2 + y^2} \\ \theta &= \tan^{-1}\frac{y}{x} \end{aligned} \tag{4.42}$$

and

$$K_1 = \frac{1}{r_0^2} - 1$$
$$K_2 = \frac{1}{r_0} e^{\theta_0} \quad , \tag{4.43}$$

where r_0 and θ_0 are the values of r and θ at $t = 0$. Note that from Equation (4.41),

$$\lim_{t \to \infty} r(t)\Big|_{r_0 \neq 0} = 1 \ ,$$

and

$$\lim_{t \to \infty} \theta(t) = \ln K_2$$

There are no non-constant limit cycles in this system. Initial conditions on the unit circle give rise to constant solutions. A few trajectories are plotted in Figure 4.13. (Note that this system does not violate Chapter 2 ground rules, since every initial condition gives rise to a unique solution.)

Example 10. When an n^{th}-order system is described by one n^{th}-order equation such as Equation (2.9), then the equilibrium points are found by setting all the derivative terms equal to zero. When describing the system in the more general state variable form of n first-order equations such as Equation (2.1), the n first-derivative terms are set equal to zero in order to find the equilibriums. It is not in general true that setting n arbitrary derivative terms to zero (including second and higher derivatives of any one of the variables) for the state variable formulation, yields equilibriums. This example is an illustration of this fact for a second-order system.

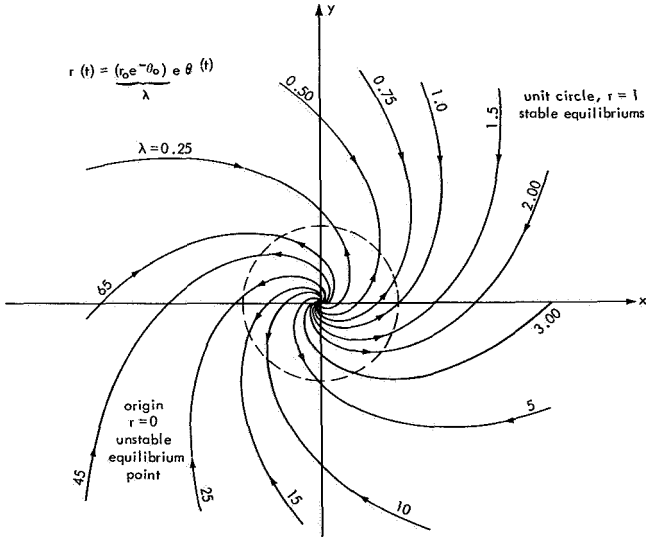

Figure 4.13—State-Space Portrait for Example 9.

Consider the system described by

$$\dot{x}_1 = -x_2 + \frac{x_1}{2}\left(1 - x_1^2 - x_2^2\right)$$
$$\tag{4.44}$$
$$\dot{x}_2 = x_1 + \frac{x_2}{2}\left(1 - x_1^2 - x_2^2\right) \ .$$

This system has a limit cycle which is a circle of unit radius centered at the origin in the x_1, x_2 state plane. That is, if

$$x_1^2(0) + x_2^2(0) = 1 , \tag{4.45}$$

then

$$\begin{aligned} x_1(t) &= x_2(0)\sin t + x_1(0)\cos t \\ x_2(t) &= x_2(0)\cos t - x_1(0)\sin t , \end{aligned} \tag{4.46}$$

which is the unity-circle limit cycle with period $\tau = 2\pi$. From Equation (4.44), there is only one equilibrium point, and it is at the origin (which of course, lies within the limit cycle). It is found by setting $\dot{x}_1 = \dot{x}_2 = 0$, which yields only one solution, $x_1 = x_2 = 0$. In fact, for any initial conditions other than at the origin, the system approaches the stable unity limit cycle with increasing time. That is,

$$\begin{aligned} r(t) &= \left[\frac{1}{1 + \left(\frac{1}{r^2(0)} - 1 \right) e^{-t}} \right]^{1/2} \\ \theta(t) &= \theta(0) - t , \end{aligned} \tag{4.47}$$

where $r = \left[x_1^2 + x_2^2\right]^{1/2}$ and $\theta = \tan^{-1}\left(x_2/x_1\right)$, and

$$\lim_{t\to\infty} r(t)\Big|_{r(0)\neq 0} = 1 \tag{4.48}$$

That the unity circle is a stable limit cycle is also shown by choosing a Liapunov function

$$\begin{aligned} V &= r^2 = x_1^2 + x_2^2 \\ \dot{V} &= r^2\left(1 - r^2\right) , \end{aligned} \tag{4.49}$$

so that

$$\begin{aligned} &\dot{V} > 0 \quad \text{for} \quad r^2 < 1 (r \neq 0) , \qquad \therefore r^2 \to 1 \ \text{as} \ t \to \infty \\ &\dot{V} < 0 \quad \text{for} \quad r^2 > 1 , \qquad \therefore 1 \leftarrow r^2 \ \text{as} \ t \to \infty \\ &V = 0 \quad \text{for} \quad r^2 = 1 \ \text{or} \ 0, \qquad \therefore r \ \text{remains} \ 1, 0 \ \text{for all} \ t \geq 0 . \end{aligned} \tag{4.50}$$

However, what happens if an "equilibrium" point is defined by $\dot{x}_1 = \ddot{x}_1 = 0$ or $\dot{x}_2 = \ddot{x}_2 = 0$ for the second-order system (4.44)? That is,

$$\begin{aligned} \dot{x}_1 &= f_1(x_1, x_2) \\ \dot{x}_2 &= f_2(x_1, x_2) \end{aligned} \tag{4.51}$$

and therefore,

$$\begin{aligned} \ddot{x}_1 &= \frac{\partial f_1}{\partial x_1} f_1 + \frac{\partial f_1}{\partial x_2} f_2 = g_1(x_1, x_2) \\ \ddot{x}_2 &= \frac{\partial f_2}{\partial x_1} f_1 + \frac{\partial f_2}{\partial x_2} f_2 = g_2(x_1, x_2) \end{aligned} \tag{4.52}$$

Hence, for $\dot{x}_1 = \ddot{x}_1 = 0$,

$$\begin{aligned} f_1(x_1, x_2) &= 0 \\ g_1(x_1, x_2) &= 0 \end{aligned} \tag{4.53}$$

is satisfied. Thus, from Equation (4.52), if $f_1 \neq 0$ (since then $f_1 = f_2 = 0$, which is the equilibrium point already defined), then

$$\begin{aligned} f_1(x_1, x_2) &= 0 \\ \frac{\partial f_1}{\partial x_2}(x_1, x_2) &= 0 \end{aligned} \tag{4.54}$$

For the system (4.44), the above equations (4.54) are

$$\begin{aligned} 0 &= x_2 + \frac{x_1}{2}\left(1 - x_1^2 - x_2^2\right) \\ 0 &= 1 - x_1 x_2 \end{aligned} \tag{4.55}$$

Solving (4.55) yields

$$\begin{aligned} x_1 &= \pm\sqrt{\frac{1 + \sqrt{5}}{2}} \\ x_2 &= 1/x_1 \end{aligned} \tag{4.56}$$

However, the points given by Equation **(4.56)** yield non-zero $\dot{x}_2$ and $\ddot{x}_2$, that is,

$$\dot{x}_2 = -\frac{\sqrt{5}}{x_1}$$

$$\ddot{x}_2 = \frac{2\sqrt{5}}{\quad}. \qquad (4.57)$$

Hence, the points of **(4.56)** which satisfy $\dot{x}_1 = \ddot{x}_1 = 0$, for the system **(4.44)** are not equilibrium points. (A similar situation occurs when $\dot{x}_2 = \ddot{x}_2 = 0$.) That is, setting $\dot{x}_1 = \ddot{x}_1 = 0$ in a system **(4.51)**, does *not* necessarily yield an equilibrium point.

In Figure **4.14**, several curves are plotted in the x_1, x_2 phase plane. $f_1(x_1, x_2) = 0$ and $f_2(x_1, x_2) = 0$ are the two S-shaped dashed curves. Note that they intersect only at the origin, which is the only true equilibrium state of the system. The S-shaped solid curve is $\ddot{x}_1 = g_1(x_1, x_2) = 0$. It intersects the $f_1(x_1, x_2) = 0$ curve at two mirror-image points, $x_1 = \pm 1.27$, $x_2 = \pm 0.786$. To demonstrate that these two points are not equilibrium points, a system trajectory of **(4.44)** is shown with initial conditions

$$x_1(0) = \sqrt{\frac{1+\sqrt{5}}{1+2\sqrt{5}}} = 1.27$$

$$x_2(0) = 1/x_1(0) = 0.786 \qquad (4.58)$$

as the heavily drawn curve. The arrowheads are in the direction of increasing time, and in several units of time the system has settled into its limit-cycle behavior.

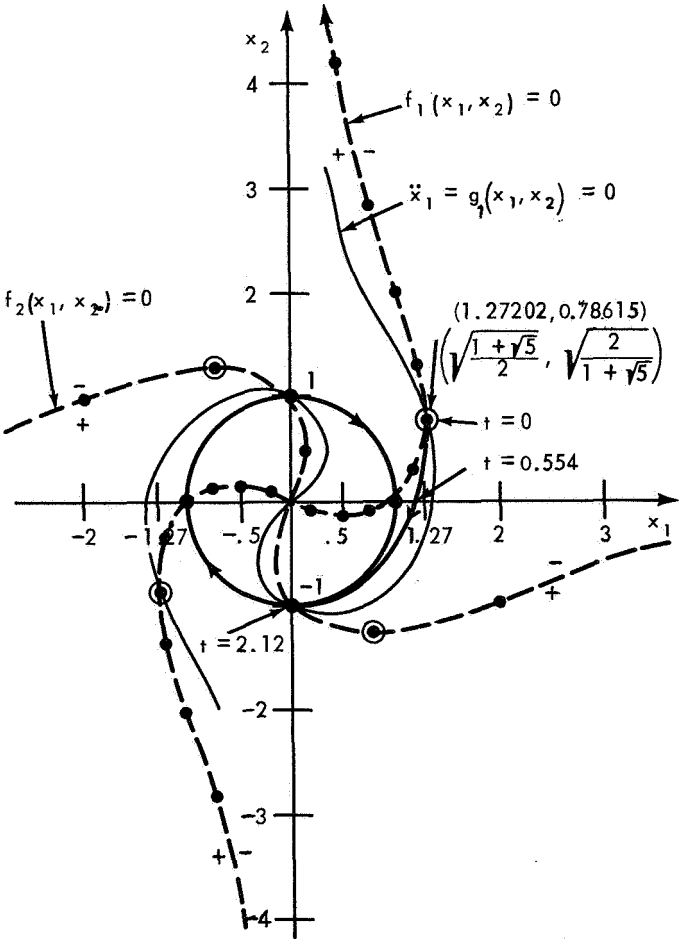

Figure 4.14—State-Space Curves for Example 10.

Example **11.** This last example illustrates two things. One is the argument in Chapter 3 that the point where the gradient of the surface $g(\bar{x})$ vanishes is an equilibrium point, and the other, like Example **4**, is that the centroid of a limit cycle is not necessarily an equilibrium point for general nonlinear systems.

In the xy plane, consider the locus of a point P(x, y) such that the product of the distances from P(x, y) to two points on the

x-axis at $x = \pm a$, is constant, say b^2. In polar coordinates, the curve is expressed by (Reference **12,** Section **7.3)**

$$g(r, \theta) = a^4 - b^4 + r^4 - 2a^2 r^2 \cos 2\theta = 0 , \qquad (4.59)$$

or, in x, Y coordinates,

$$g(x, y) = a^4 - b^4 + (x^2 + y^2)^2 - 2a^2(x^2 - y^2) = 0 . \qquad (4.60)$$

The graphs of the curves represented by Equations **(4.59)** and **(4.60)** for different values of the ratio **b/a** are shown in Figure **4.15.** The curves in both (a) and (b) are called lemniscates, and the curve in (c) consists of two separate closed portions known as "ovals of Cassini." In Figure **4.16,** $g(x, y) + b^4$ is shown as a surface. The gradient vector as introduced in Chapter **3,** is

$$\nabla g = \frac{\partial g}{\partial x}\hat{x} + \frac{\partial g}{\partial y}\hat{y}$$

$$= 4x(x^2 + y^2 - a^2)\hat{x} + 4y(x^2 + y^2 + a^2)\hat{y} . \qquad (4.61)$$

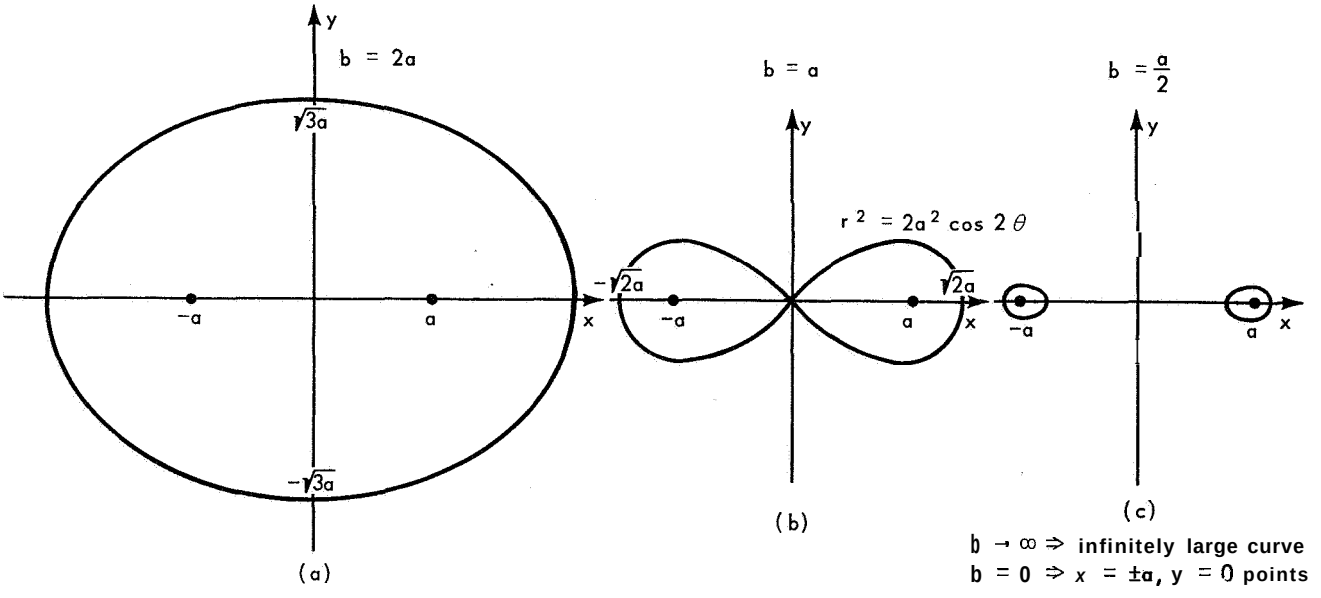

Figure 4.15—Lemniscates and Ovals of Cassini.

Thus the gradient vanishes at three points,

$$x = 0, \pm a$$
$$y = 0 \qquad (4.62) ,$$

which correspondto the saddle point, and two minimum points of the surface shown in Figure **4.16.**

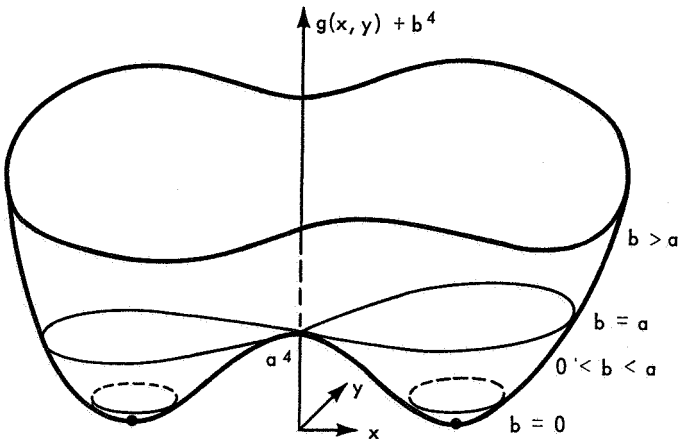

Figure 4.16—Surface of Example 11.

The differential equations that uniquely gives rise to these curves are

$$\dot{x}(t) = y(t)\left(x^2(t)+y^2(t)+a^2\right)$$
$$\dot{y}(t) = -x(t)\left(x^2(t)+y^2(t)-a^2\right), \qquad (4.63)$$

since the solution curves are the limit-cycle trajectories

$$\left(x^2+y^2\right)^2 - 2a^2\left(x^2-y^2\right) = \lambda \qquad (4.64)$$

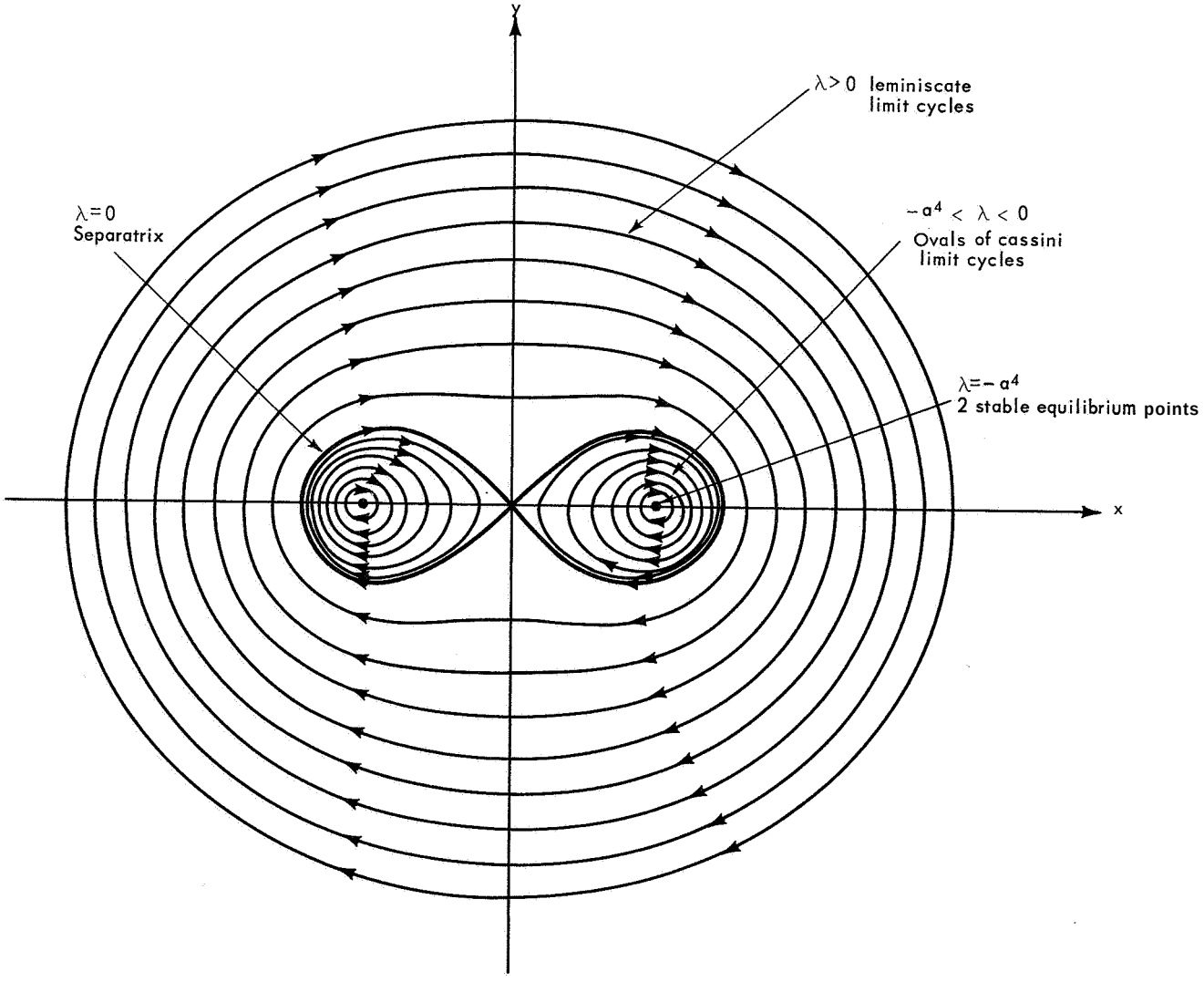

Figure 4.17—State-Space Portrait for Example 11.

(The A = 0 curve is a separatrix for the different types of limit cycles; it is not in itself a limit cycle since it passes through the equilibrium point at the origin.) The equilibrium points for Equations **(4.63)** are the same three points as given in Equations **(4.62)**, that is, where $\bar{\nabla}g = \bar{0}$ there is an equilibrium point. The trajectories are plotted in Figure **4.17.** Note that there is always an odd number, one or three, equilibrium points **(i.e.** surface peaks) within each limit cycle.

Equations **(4.63)** were programmed on a digital computer, with **a** = 1, for a family of initial conditions. For each **run,**

$$x_{avg} = \frac{1}{\tau}\int_0^{\tau} x(t)\,dt \tag{4.65}$$

and τ was computed, where τ is the limit-cycle period. These values are listed in the Table in Figure **4.18.** Note that both x_{avg} and τ are different for each limit cycle, and that

$$x_{avg} \neq x_{equib} \tag{4.66}$$

x(0)	τ	xavg
0	∞	**0**
±0.1	6.72	k0.468
±0.2	5.38	±0.584
±0.3	4.66	±0.675
±0.4	4.17	k0.754
±0.5	3.82	±0.822
k0.6	3.57	±0.880
±0.7	3.38	±0.929
±0.8	3.25	k0.966
±0.9	3.17	±0.991
±1.0	m	±1.000
±1.1	3.18	±0.989
k1.2	3.31	±0.948
±1.3	3.67	±0.856
k1.4	5.38	±0.582
± √2	∞	—

$\bar{a} = 1$
$y(0) = 0$
$y_{avg} = 0$
$\dot{x}_{avg} = 0$
$\dot{y}_{avg} = 0$
for **all cases**

x(0)	τ	xavg
±1.5	6.38	**0**
±1.6	4.58	**0**
k1.7	3.60	**0**
±1.8	2.96	**0**
±1.9	2.50	**0**
±2.0	2.16	**0**
±2.1	1.89	**0**
±2.2	1.67	**0**
±2.3	1.49	**0**
±2.4	1.34	**0**
±2.5	1.21	**0**
±2.6	1.10	**0**
k2.7	1.01	**0**
±2.8	0.92	**0**
±2.9	0.85	**0**
±3.0	0.79	**0**

Figure 4.18—Table of Computed Values for Example 11.

5. MISCELLANEOUS RELATED PROPERTIES

This chapter is devoted to some miscellaneous discussions and concepts of ordinary differential equations and limit cycles that do not fit into the mainstream of the previous chapters. These discussions are included for their interesting properties, as an aid toward a better understanding of the overall topic, and possibly, to generate future ideas in this area.

(1) For a second-order system,

$$\ddot{x}(t) = f\left(\dot{x}(t), x(t)\right) , \tag{5.1}$$

a solution trajectory in the x-versus-$\dot{x}$ phase plane that linearly (i.e., as a straight line) crosses the x-axis (i.e., $\dot{x} = 0$) at a non-infinite slope, signifies that the crossing point is an equilibrium point. Such a crossing is illustrated in Figure 5.1.

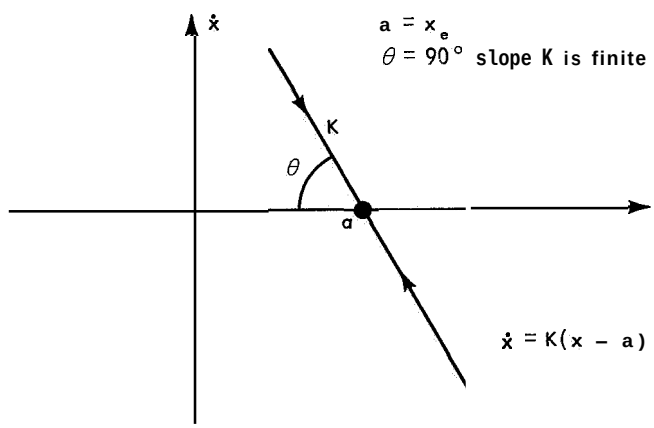

finite K,

$$\Delta t = t - t_0 = \int_{x(t_0)}^{a} \frac{dx}{\dot{x}} = \int_{x(t_0)}^{a} \frac{dx}{K(x - a)}$$

$$= \frac{1}{K} \ln(x - a) \Big|_{x=x(t_0)}^{x=a} = \infty . \tag{5.2}$$

The straight-line constraint is not neces-

$$\text{slope } K = \frac{d\dot{x}}{dx} = \frac{\ddot{x}}{\dot{x}} = \frac{f(\dot{x}, x)}{x} , \tag{5.3}$$

then for K finite at $\dot{x} = 0$, $f(0, x)$ is zero. Thus, this point is an equilibrium point.

(2) For systems (obeying the ground rules of Chapter 2) of the form

$$x^{(n)} = f\left(x^{(n-1)}, x^{(n-2)}, \cdots, x\right) , \tag{5.4}$$

only $n = 2$ yields non-trivial limit cycles. That is when $n = 0$, Equation (5.4) is the algebraic equation $\dot{x} = f(x)$, which yields a constant solution with respect to time.

If $n = 1$, then

$$\dot{x} = f(x) . \tag{5.5}$$

Hence, when a solution $x(t)$ is at a relative maximum or minimum value, $\dot{x}(t)$ is zero. But Equation (5.5) yields only unique solutions for any initial condition. Thus, $x_{min} = x_{Max} = x_e$ is an equilibrium point. That is, Equation (5.5) does not yield a time-varying solution with finite extremum values; hence, no finite limit cycle exists.

(3) In general, it is very difficult to find limit-cycle solutions for nonlinear differential equations. This is true for even a second-order system, although the well-known Bendixson criterion (Reference **14)** sometimes indicates where a limit cycle cannot exist. That is, if

$$\frac{\partial f_1}{\partial x_1}(x_1, x_2) + \frac{\partial f_2}{\partial x_2}(x_1, x_2) \tag{5.6}$$

does not change its sign within a domain D of the x_1, x_2 state plane, then no closed trajectories exist in that domain. A proof by contradiction is simple, since if a closed curve Γ exists in D, then by Gauss's theorem, for D' the domain bounded by Γ,

$$\iint_{D'} \left(\frac{\partial f_1}{\partial x_1} + \frac{\partial f_2}{\partial x_2}\right) dx_1\, dx_2 = \oint_{\Gamma} (f_1\, dx_2 - f_2\, dx_1) \neq 0 . \tag{5.7}$$

But, along the path Γ,

$$\begin{aligned} \dot{x}_1 &= f_1(x_1, x_2) \\ \dot{x}_2 &= f_2(x_1, x_2) . \end{aligned} \tag{5.8}$$

Thus, $f_1\, dx_2 - f_2\, dx_1 = 0$, which contradicts (5.7).

For higher-order systems, Hahn refers to "rotating Liapunov functions" (Reference 8) of the form

$$u(\bar{x}) = f(\bar{x})/g(\bar{x}) . \tag{5.9}$$

$u(x)$ is interpreted as an angle-coordinate in a suitably chosen cylindrical coordinate system under certain assumptions about the pencil of surfaces determined by $f(\bar{x}) - cg(\bar{x}) = 0$,

i.e., by $u = c$ = constant. As an example, for a third-order system, $u = x_1/x_2$ yields a pencil of surfaces which are planes in three-dimensional state space. If $\dot{u} > 0$, the corresponding motion rotates about the axis of the pencil of surfaces always in the same rotational sense. Motions always remaining within a torus-like domain infer the existence of almost periodic motion. The precise analytical formulation of rotating Liapunov functions is given in Reference 13. This concept is not necessary for two-dimensional phase-plane considerations, since the existence of periodic solutions is guaranteed if the phase trajectories remain in an annular domain. For second-order systems, the concept of "contact curves," as introduced by Poincaré, is appealing.

For the system (5.8), an arc A (open or closed at one or the other end) is said to be "without contact" wherever λ contains no equilibrium points and the (unique) solution trajectory path through any point of λ is never tangent to λ at that point (Reference 11). Assuming these properties hold for every point of a simple closed curve L, then L is called a "cycle without contact." This implies that once a solution trajectory enters (leaves) the region bounded by L, it cannot leave (enter) it. Furthermore, a structurally stable system has only a finite number of limit cycles in the region bounded by L (Reference 15).

If a cycle (or arc) without contact is expressed by

$$L(x_1, x_2) = \text{constant} , \tag{5.10}$$

then the tangent to L at any point is

$$-\frac{\partial L/\partial x}{\partial L/\partial x_2} . \tag{5.11}$$

For L to be without contact, the field vector

$$\bar{S} = f_1 \hat{x}_1 + f_2 \hat{x}_2 \tag{5.12}$$

(see Chapter 3) is not tangent to L (and $\bar{S}$ is not equal to zero on L). However, contact curves $C'(x_1, x_2)$ that are tangent to $\bar{S}$ are found by equating the slope of Equation (5.12) with that of $C(x_1, x_2)$ given by (5.11) with L = C. That is,

$$f_1 (x_1, x_2) \frac{\partial C}{\partial x_1} (x_1, x_2) + f_2 (x_1, x_2) \frac{\partial C}{\partial x_2} (x_1, x_2) = 0 . \tag{5.13}$$

To illustrate this method of contact curves, a family of concentric circles centered at an equilibrium point, assumed to be at the origin, is considered. Thus,

$$C = .xp + x_2^2 , \tag{5.14}$$

and Equation (5.13) yields the locus of points, i.e., the contact curve, where the circles are tangent to the integral curves of (5.8). If a limit cycle exists at all, it lies in a ring domain, with center at the equilibrium point, whose boundaries are the innermost and outermost circles of radii r_{min} and r_{MAX} respectively, which touch the contact curve. (See Reference 6, Figure 2.2 for a numerical example.) Note that the equilibrium point, $f_1 = f_2 = 0$, is a solution to (5.13). Thus, if it is considered part of the contact curve, $r_{min} = 0$, and the limit cycle encircles the equilibrium point as previously proved. The r_{MAX}-radius contact circle curve is a measure of how large a region confines the limit cycle. If this contact-surface concept is extended to higher than second-order systems, then limit cycles are contained in the hypervolumes within the largest norm hypercontact-surface. That is, this dissertation proves that limit cycles encircle equilibrium points so that only regions with equilibrium points need be considered. For practical systems, one expects the regions to be small. Contact surfaces mathematically define the boundaries of these regions.

Instead of the above topological approach, another viewpoint of circular contact curves is obtained dynamically by defining

$$R(t) = \sqrt{x_1^2(t) + x_2^2(t)} \tag{5.15}$$

Then $\dot{R} = 0$ when $R(t)$ equals R_{min} and R_{MAX} (the minimum and maximum radii of the contact curve, respectively) and $R_{min} \leq R \leq R_{MAX}$. (A question that arises is: "Can any information about an 'average limit cycle', R_{avg}, be obtained without knowing $x_1(t)$ or $x_2(t)$?") This approach sometimes aids in plotting limit cycles.

For example, consider a second-order system of the form

$$\ddot{x} = f(\dot{x}, x) \quad , \tag{5.16}$$

where $R = \sqrt{x^2 + \dot{x}^2}$. Then $\dot{R} = \dot{x}(x + \ddot{x})/R = 0$ when

$$\dot{x} = 0 \quad \text{or} \quad x + \ddot{x} = 0 \quad . \tag{5.17}$$

For the Van der Pol equation in the previous chapter (Equations (4.12) and (4.13) with $y = x$), $\dot{x} = 0$ yields $\ddot{R} = 0$. That is, the x-axis crossings of the limit cycle are inflection points of $R(t)$. For Equation (4.12), with $\varepsilon = 1$, $\ddot{x} = (1 - x^2)\dot{x} - x$, and

$$\left.\dot{R}\right|_{x=\pm 1} = 0$$

$$\left.\ddot{R}\right|_{x=\pm 1} = \mp \frac{2\varepsilon \dot{x}^3}{R} \tag{5.18}$$

give the four alternating extremums of R(t) as shown in Figure 5.2(a). For Equation (4.13), with $y = x$, $\epsilon = 1$, $\ddot{x} = \dot{x} - \dot{x}^3/3 - x$, and

$$\dot{R}\Big|_{\dot{x}=\pm\sqrt{3}} = 0$$

$$\ddot{R}\Big|_{\dot{x}=\pm\sqrt{3}} = \pm\frac{2\epsilon\sqrt{3}\,x}{R} \qquad (5.19)$$

give the four alternating extremums of R(t) as shown in Figure 5.2(b). Also plotted in Figure 5.2 are the circles of radius R_{avg}.

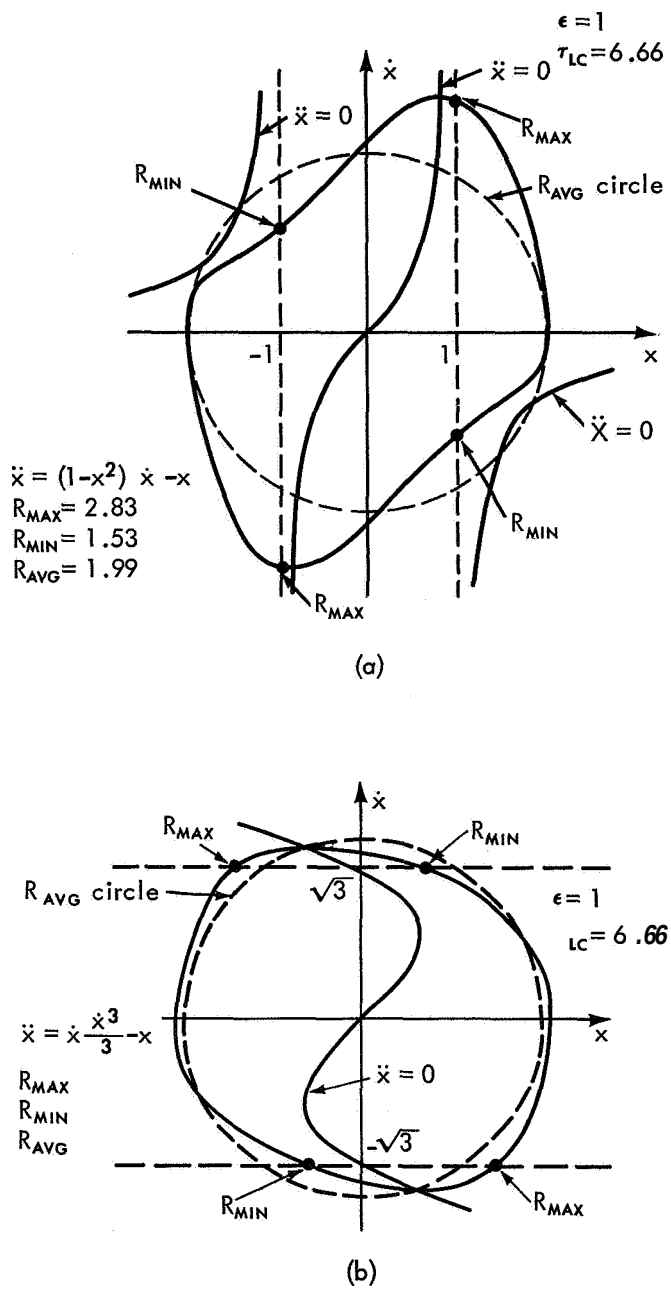

Figure 5.2— Properties of Van der Pol Limit Cycle.

(4) A great deal is known about the behavior of phase portraits around singular points for second-order systems. (See Reference 16, for example.) For higher-order systems very little is known. Among others, Poincaré (Reference 17) studied third-order singularities, Mendelson (Reference 18) investigated special higher-order systems, and Haas (Reference 19) discusses complex singular points. However, for most practical, complicated, high-order systems a computer is needed; also, engineering ingenuity plays an important role. (For example, time is run backwards and forwards to determine stability of equilibrium points, limit cycles, and alternating stable–unstable limit cycles.) This dissertation is intended to bridge part of the gap that exists between mathematical theory and engineering applications. Much more knowledge is needed. For example, what are the necessary conditions for equilibrium points and limit cycles to exist? (Chapter 3 showed that the system equations must allow $\dot{x}_i$ to take on values of both polarities, since $\dot{x}_{i_{avg}} = 0$ for periodic x.) Another interesting question is: When is a centroid an equilibrium point? (That is, when does $\bar{f}(\bar{x}_{avg}) = \bar{0}$, as proven for linear systems?) What about non-autonomous systems, and systems with time-varying parameters? How can equilibrium points be moved around in state space, that is, what are the sensitivity functions $\partial x_{i_{equib}}/\theta$ (parameter)? These, and many more questions remain to be answered.

Part II

APPLICATION TO ATTITUDE CONTROL SYSTEMS

6. INTRODUCTION TO ATTITUDE CONTROL SYSTEMS

Attention is now focused on spacecraft attitude control systems. Of special interest are three-axis stabilized, either vertically earth-oriented or inertially oriented, earth-orbiting satellites. Normally, six positional degrees of freedom are associated with rigid-body motion; three translational and three rotational. The guidance and control requirements for navigating the center of gravity of a spacecraft with respect to a desired trajectory or orbit (or midcourse maneuvering or orbital station keeping) is not discussed here, although the techniques of this dissertation are definitely applicable. Instead, attention is restricted to the control of the rotational motion of a rigid body, or system of coupled rigid bodies, by means of devices that store or change the momentum of the bodies. Only the three rotational-position degrees of freedom per rigid body need then be considered, and since the rigid bodies may have sources of torque acting upon them, there are three rotational-rate degrees of freedom yielding a six-dimensional system per rigid body, with constraints relating the bodies. (If a torque applied to a single rigid body is not a pure couple, then the trajectory of the center of mass changes and, in general, one must consider a 12-dimensional system. However, the torques and forces associated with attitude control are usually extremely small compared to any that significantly change the trajectory of a spacecraft. As a matter of fact, one is often forced to cope with the small components of huge orbit stationkeeping thrust vectors (such as to keep a synchronous 24-hour orbital period earth satellite in a proper orbit) which do not pass through the spacecraft center of gravity, as attitude disturbance torques).

It is emphasized at this point that the intention is to present not an all-encompassing development of attitude control and related background areas, but rather a broad framework that leads to system equations to which the equilibrium technique is applicable. The development is kept fairly general and practical, in order to understand the equations in a physical sense. A complete general attitude control system is shown in Figure 6.1. The system is divided into a designable spacecraft and its governing laws of motion. The first step taken by the attitude control engineer is to develop the system equations in a mathematically convenient form. This first step is discussed in the next chapter. In this chapter, the philosophy of a design-analysis-redesign-reanalysis-etc. approach is presented, for the sake of a physical understanding of the equations. Ideally, a paper design is desired that results in an optimum or near-optimum control system that satisfies all the various spacecraft requirements. Once the paper design is completed, a synthesis-type problem would exist. Unfortunately however, owing to practical limitations and the lack of analytical tools for highly nonlinear systems, practical designs are based on engineering intuition and experience. The effectiveness of these designs demands the solution of an analysis-type problem for which a computer serves as the main nonlinear tool. This important role of the computer is pursued further after a brief discussion of the nonlinear dynamics and kinematics of the system shown in Figure 6.1.

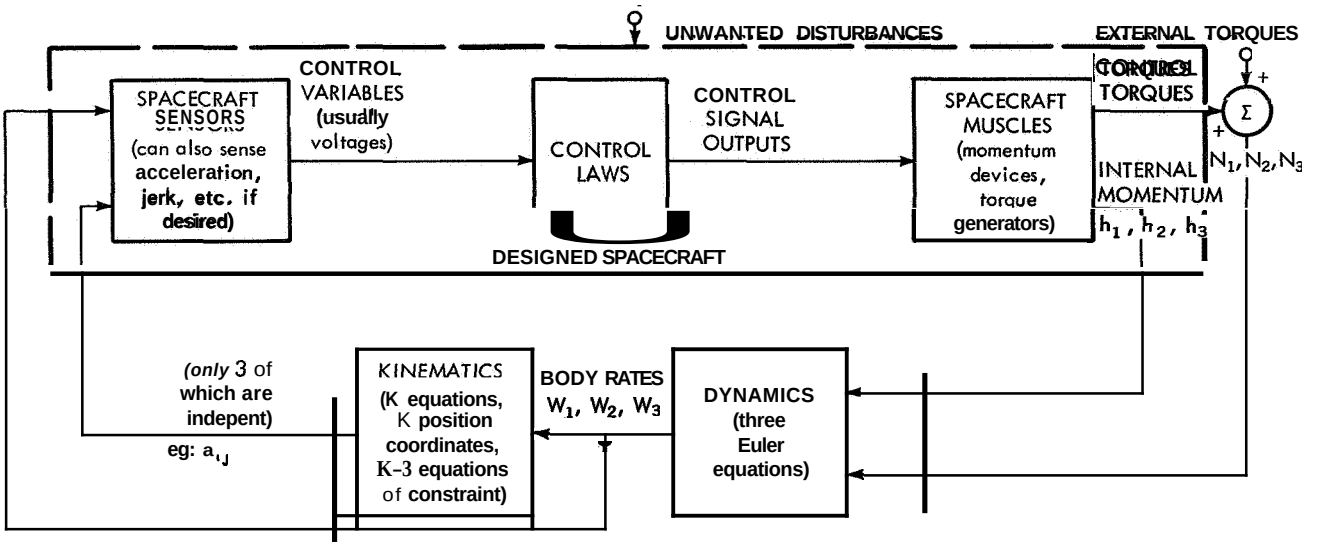

Figure 6.1 — Attitude Control System

The dynamic behavior of a system is determined by the equations which relate the external torques and the angular momentum of the system. The momentum consists of two components: the momentum of the rigid body due to its angular rate $\overline{W}$ with respect to inertial space, and the stored momentum from internal rotating members. The dynamic behavior of attitude-controlled systems is determined by three scalar nonlinear, first-order, time-invariant, ordinary differential equations. These equations are derived in Chapter 7, and their scalar form, Equation (7.45) is

$$
\begin{aligned}
I_1 \dot{W}_1 &= (I_2 - I_3) W_2 W_3 + N_1 - \dot{h}_1 + h_2 W_3 - h_3 W_2 \\
I_2 \dot{W}_2 &= (I_3 - I_1) W_3 W_1 + N_2 - \dot{h}_2 + h_3 W_1 - h_1 W_3 \\
I_3 \dot{W}_3 &= (I_1 - I_2) W_1 W_2 + N_3 - \dot{h}_3 + h_1 W_2 - h_2 W_1 ,
\end{aligned}
\qquad (6.1)
$$

where the symbols and assumptions are given in Chapter 7. These equations are sometimes referred to as the Euler equations of motion and are heavily crosscoupled with nonlinear terms.

As opposed to the well-defined dynamics equations, the formulation of the kinematics of a system is more arbitrary in that there are many sets of position variables to choose from in order to describe the attitude of a rigid body. The kinematics are relationships between the rates and one of these sets. In translational motion, the kinematics are simply

$$\dot{x}_i = v_i \qquad i = 1, 2, 3 ,$$

where the set is a 3-parameter rectilinear coordinate system, For rotational motion, the kinematics become much more complex nonlinear coupled relationships, but still, only three independent coordinates are necessary to specify the attitude. The three most commonly used sets of coordinates are now discussed.

The first set is the three Euler angles taken in any advantageous (but independent) sequence, such as azimuth, elevation, and "spin" of a gun mount. See Reference 20 for example. The main advantage of this set is that there are only three first-order differential equations relating the angles and the angular rates. They are very easy to visualize for reasonably limited angular motion (such as the roll, pitch, and yaw of a ship), and for sufficiently small angles become linearly decoupled, thus facilitating small-angle fine-pointing control analysis. The main disadvantages are the non-uniqueness of the formulation, and the existence of singular points for large angles (90 degrees). Since computers cannot maintain accuracy for infinite quantities, Euler angles are not in general suitable for all-attitude simulations. As an example, taking a yaw, roll, pitch, (i.e., Ψ, ϕ, θ) sequence yields:

$$\begin{aligned} \dot{\Psi} &= (W_1 \cos\theta - W_3 \sin\theta)/\cos\phi \\ \dot{\theta} &= W_2 + W_1 \tan\phi \sin\theta - W_3 \tan\phi \cos\theta \\ \dot{\phi} &= W_1 \cos\theta + W_3 \sin\theta \end{aligned} \tag{6.2}$$

The second set of coordinates is the nine direction cosines, a_{ij} (i, j = 1, 2, 3). The formulation contains nine defining first order differential equations which relate the positional direction cosines to angular rates, plus six algebraic equations of constraint, thus yielding the three necessary independent position variables. Hence, there, are many equations and many variables, but they are all well-defined and well-behaved for all attitudes. It is easy to mentally visualize the physical meaning of the direction cosine which enhances intuitive-type manipulation of the equations, and lends itself to the functional developments used later in this dissertation. See for example Reference 21. However, the direction cosine formulation requires unnecessary computer equipment for direct simulation. The nine differential equations take the matrix form,

$$\frac{d}{dt}[A] = \frac{d}{dt}\begin{bmatrix} a_{11} & a_{12} & a_{13} \\ a_{21} & a_{22} & a_{23} \\ a_{31} & a_{32} & a_{33} \end{bmatrix} = \begin{bmatrix} 0 & W_3 & -W_2 \\ -W_3 & 0 & W_1 \\ W_2 & -W_1 & 0 \end{bmatrix} [A] \tag{6.3}$$

where the a_{ij} are the nine coordinates. The 6 constraint equations are

$$[A]\,[A]^T = \begin{bmatrix} 1 & 0 & 0 \\ 0 & 1 & 0 \\ 0 & 0 & 1 \end{bmatrix}, \tag{6.4}$$

where $[A]^T$ is the transpose of $[A]$.

The third set of coordinates is the four Euler symmetric parameters (Reference 22) whose formulation is a good compromise between the efficient but ill-behaved Euler angles, and the non-efficient but easy to use direction cosines. With only four defining first-order differential equations and one algebraic equation of constraint, the four variables and their derivatives are

conveniently bounded and uniquely defined for all attitudes. They also lend themselves to a simple physical interpretation. This formulation is usually the most efficient to use in all attitude analog simulations and then, if desired, the direction cosines are formed algebraically from the four symmetric parameters (Reference 23). This is usually done to facilitate the sensors' simulation since the mathematical models of attitude sensors are most simply described via direction cosines. The four differential equations take the form

$$\frac{d}{dt}\begin{pmatrix}\lambda_1\\ \lambda_2\\ \lambda_3\\ \lambda_4\end{pmatrix} = \frac{1}{2}\begin{bmatrix}-\lambda_2 & -\lambda_3 & -\lambda_4\\ \lambda_1 & -\lambda_4 & \lambda_3\\ \lambda_4 & \lambda_1 & -\lambda_2\\ -\lambda_3 & \lambda_2 & \lambda_1\end{bmatrix}\begin{pmatrix}W_1\\ W_2\\ W_3\end{pmatrix} \tag{6.5}$$

where the equation of constraint is

$$\sum_{i=1}^{4}\lambda_i^2 = 1 \ , \tag{6.6}$$

and $A_{,,}\ \lambda_2, \lambda_3, \lambda_4$, are the four position coordinates. (See Reference 23 for relationships between all three sets of position coordinates.)

There are additional sets of position coordinates which are used less frequently for describing the kinematics, such as the Gibbs vector, Quarternions, and the Caley-Klein parameters (Reference 24). They are sometimes used to advantage in specialized formulation of the control laws for paper-and-pencil analysis techniques.

Thus the dynamics and kinematics are determined by well-defined mathematical relationships which close the loop around any rigid body as shown in Figure 6.1. It is the spacecraft hardware which is designed by the attitude control engineer to make the overall system work properly. The sensors (such as gyros, star trackers, sun sensors, earth horizon scanners, etc.) and the muscles (such as torque-generating pneumatic subsystems, momentum-storing flywheels, etc.) are usually selected very early in the design since they are the long-lead items. In fact, it is usually not until after the sensing and torquing components are being developed that the overall simulation becomes more realistic, since then the hardware characteristics are measured. Hence, upon analyzing the system, the only functional design change which is comparatively easy and not too time-consuming is in the control laws. Modification of the sensors and muscles is possible to an extent, but the really flexible part of the system is the control logic. Therefore, after a system goes through its basic design, its performance is analyzed and redesign initiated in the event that specifications are not met. This cycle is continued until a satisfactory design is achieved. The computer simulation is essential to this type of design-analysis cycle, since, once the dynamics, kinematics, and sensors are simulated

(the most difficult and component-consuming aspects of the simulation), it is not difficult to change the simulation of the control laws. It is demonstrated in this dissertation how the computer can be intelligently and fruitfully used to find the potential trouble areas via system-equilibrium points, and further indicate how they can be remedied.

7. DEVELOPMENT OF ATTITUDE CONTROL EQUATIONS

In this chapter, the necessary dynamic and kinematic equations are developed using the direction cosines which relate a body-fixed spacecraft reference coordinate system to an inertially-fixed reference coordinate system. The more general case of an "in-between" non-inertial orbital reference frame (for example an earth-oriented orbital frame which rotates one revolution per orbit in inertial space) is considered first. That is, for perfect attitude, the control system aligns the spacecraft reference frame to the orbital reference frame. The assumption is made that the plane of the satellite's orbit is inertially fixed. This is usually a good approximation since, during the time interval in which an attitude control system responds, the orbit precesses a negligible amount. Also, the 0.04 degree/hr earth rate around the sun and similar motions are ignored. If it is necessary to take long-term disturbance effects into account, a fourth reference frame is fixed (for example to the sun) and considered to move in inertial space (for instance with respect to a star).

Since this dissertation is not intended as an all-encompassing text on attitude control and related areas, several additional assumptions are made, any of which can be readily removed by generalizing-type modifications to the equations. Orbits are taken as circular about perfectly homogeneous spherical earths. No translational, but only rotational, motions are considered with all reference-frame origins continuously coincident. The spacecraft is a single rigid body, and all inertial momentum storage devices have negligible inertias. Cross product of inertia terms, and sensor-actuator misalignment terms are omitted.

For present purposes, the following three orthogonal right-hand Euclidean reference frames are defined. (See Figure 7.1). As previously stated, the only interest is rotational behavior; thus all frames are assumed to have origins at the spacecraft's center of mass. The symbol ^ represents a spacial unit vector.

The first reference frame is the inertial frame, $\hat{z}_1$, $\hat{z}_2$, $\hat{z}_3$, such that the $\hat{z}_1$, $\hat{z}_3$ plane defines the spacecraft orbital plane which was assumed inertially fixed. At some point in the orbit the positive $\hat{z}_1$ axis points in the same direction as the velocity vector of the spacecraft's center of gravity, and the positive $\hat{z}_3$ axis points to the center of the earth (local vertical). A quarter of an orbital period later, $\hat{z}_1$ points away from the center of the earth and $\hat{z}_3$ is along the spacecraft velocity vector since the inertial frame does not rotate as the spacecraft goes around the earth. The $\hat{z}_2$ axis is always perpendicular to the orbital plane throughout the orbital period and is to the right as one looks down the positive $\hat{z}_2$ axis, i.e., $\hat{z}_2 = \hat{z}_3 \times \hat{z}_1$. Hence the momentum of the spacecraft due to its center of mass being in orbit around the earth is along the negative $\hat{z}_2$ axis.

The second reference frame is the orbital reference frame, $\hat{y}_1$, $\hat{y}_2$, $\hat{y}_3$, such that: the positive $\hat{y}_1$ *axis* always points along the spacecraft velocity vector in the direction of forward

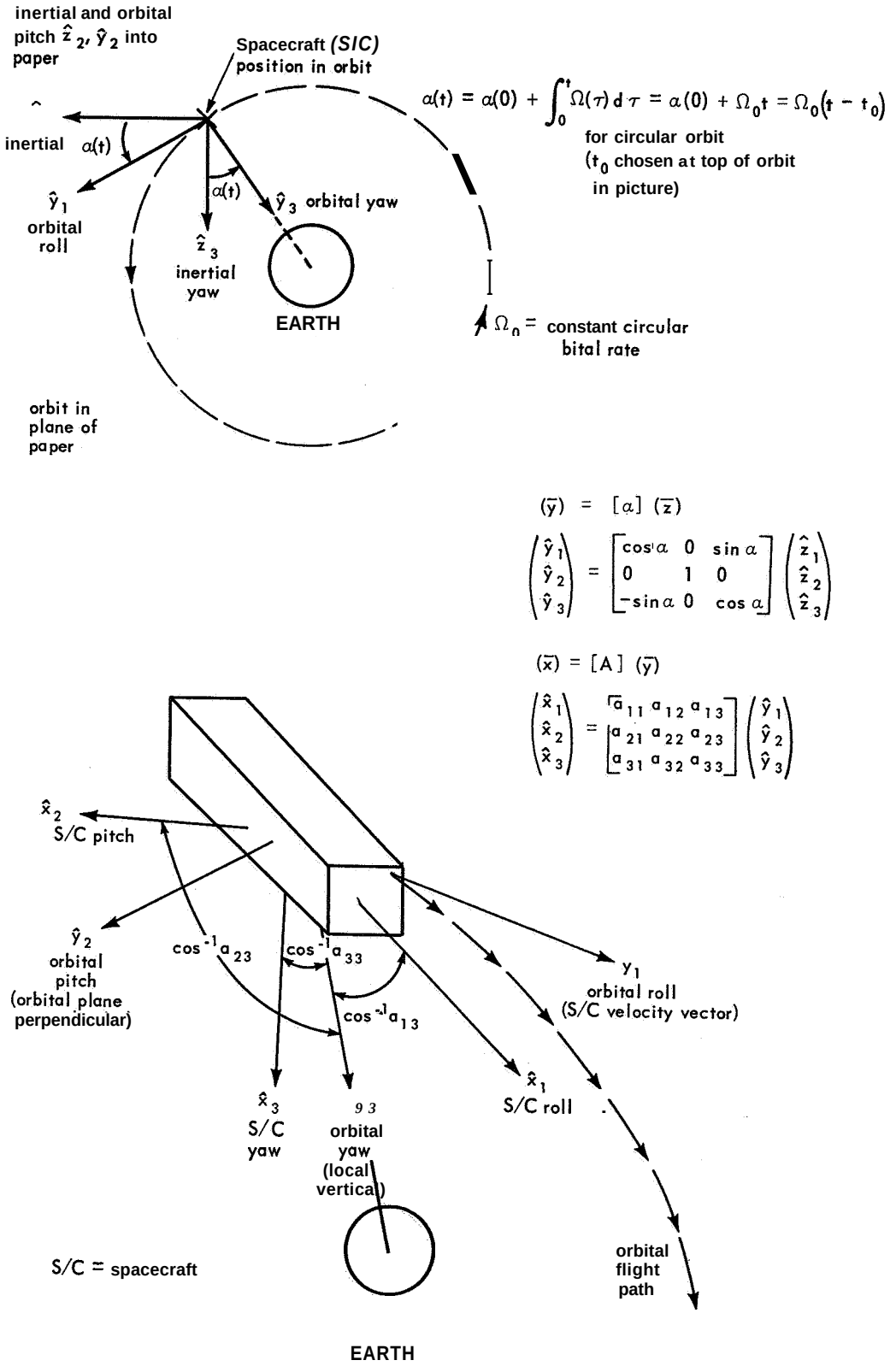

Figure 7.1—Coordinate Reference Frames.

motion; the positive $\hat{y}_3$ axis points along the local vertical towards the center of the earth; and the $\hat{y}_2$ axis is coincident with the inertial $\hat{z}_2$ axis. Thus, if $\alpha(t) = \Omega_0 t$, where Ω_0 is the constant orbital rate in rad/sec, then α is the orbital angle defining the position of the spacecraft in its orbit. When the orbital reference and inertial frames are coincident, $\alpha = 0$. The inertial and orbital reference frames rotate with respect to each other about the colinear $\hat{y}_2$ and $\hat{z}_2$ axes at a rate Ω_0. They are related by the matrix equation

$$\begin{pmatrix} \hat{y}_1 \\ \hat{y}_2 \\ \hat{y}_3 \end{pmatrix} = \begin{bmatrix} \cos\alpha & 0 & \sin\alpha \\ 0 & 1 & 0 \\ -\sin\alpha & 0 & \cos\alpha \end{bmatrix} \begin{pmatrix} \hat{z}_1 \\ \hat{z}_2 \\ \hat{z}_3 \end{pmatrix} \tag{7.1}$$

or, in shorthand notation,

$$(\bar{y}) = [\alpha](\bar{z}) \ . \tag{7.2}$$

The third reference frame is the spacecraft frame $\hat{x}_1$, $\hat{x}_2$, $\hat{x}_3$. It is coincident with the principal axes of the spacecraft. When the spacecraft is perfectly controlled, the principal axes are aligned with the orbital reference frame. $\hat{x}_1$, $\hat{x}_2$, $\hat{x}_3$ are the roll, pitch, and yaw axes, respectively. Because they are along the principal axes of the spacecraft (which is considered a rigid body), the cross product of inertia terms vanish. Therefore, the inertial matrix associated with the inertia tensor (Reference 21) becomes diagonalized with only three non-vanishing terms: I_1, I_2, I_3. These are the roll, pitch, and yaw principal moments of inertia and are positive quantities. At any time, each of the body-fixed unit vectors may be resolved into components along the orbital reference directions. This fundamental concept allows one to express mathematically each of the spacecraft fixed unit vectors as a linear combination of the orbitally fixed unit vectors as

$$\hat{x}_i = \sum_{j=1}^{3} a_{ij} \hat{y}_j \ , \qquad i = 1, 2, 3 \ , \tag{7.3}$$

where the coefficients a_{ij} are time-varying if the spacecraft rotates with respect to the orbital frame. In matrix notation

$$\begin{pmatrix} \hat{x}_1 \\ \hat{x}_2 \\ \hat{x}_3 \end{pmatrix} = \begin{bmatrix} a_{11} & a_{12} & a_{13} \\ a_{21} & a_{22} & a_{23} \\ a_{31} & a_{32} & a_{33} \end{bmatrix} \begin{pmatrix} \hat{y}_1 \\ \hat{y}_2 \\ \hat{y}_3 \end{pmatrix} \ , \tag{7.4}$$

or, in shorthand notation,

$$(\bar{x}) = [A](\bar{y}) \ . \tag{7.5}$$

Since the $\bar{x}$, $\bar{y}$, and $\bar{z}$ coordinate systems are orthogonal,

$$\begin{aligned} \hat{x}_i \cdot \hat{x}_i &= \delta_{ij} \\ \hat{y}_i \cdot \hat{y}_j &= \delta_{ij} \qquad i, j = 1, 2, 3 \ , \\ \hat{z}_i \cdot \hat{z}_j &= \delta_{ij} \end{aligned} \tag{7.6}$$

where the Kronecker delta is defined as

$$\delta_{ij} = \begin{cases} 1 & \text{for } i = j \\ 0 & \text{for } i \neq j \end{cases} \tag{7.7}$$

Hence, multiplying both sides of Equation 7.3 by $\hat{y}_k$, yields

$$\hat{x}_i \cdot \hat{y}_k = \sum_{j=1}^{3} a_{ij} (\hat{y}_j \cdot \hat{y}_k) = \sum_{j=1}^{3} a_{ij} \delta_{jk} = a_{ik} . \tag{7.8}$$

Since the geometric definition of the inner product of two vectors is

$$\hat{x}_i \cdot \hat{y}_k = |\hat{x}_i| \cdot |\hat{y}_k| \cos \}_i^k = cos,; \tag{7.9}$$

where $| \; |$ represents the magnitude of the vector, and where $\}_i^k$ is the plane angle between the two vectors, then

$$a_{ik} = \cos \}_i^k \quad (i, k = 1, 2, 3) . \tag{7.10}$$

The a_{ik} are the so-called direction cosines. This geometric interpretation is shown graphically in Figure 7.1 for $k = 3$.

The transformation matrix [A] has many interesting properties from the point of view of manipulation and computation. Forming the inner product $(\hat{x}_i \cdot \hat{x}_k)$ from Equation (7.3), one obtains

$$\begin{aligned} \hat{x}_i \cdot \hat{x}_k &= \sum_{j=1}^{3} a_{ij} \hat{y}_j \sum_{m=1}^{3} a_{km} \hat{y}_m \\ &= \sum_{j=1}^{3} \sum_{m=1}^{3} a_{ij} a_{km} \hat{y}_j \cdot \hat{y}_m \\ &= \sum_{j=1}^{3} \sum_{m=1}^{3} a_{ij} a_{km} \delta_{jm} \\ &= \sum_{j=1}^{3} a_{ij} a_{kj} \end{aligned} \tag{7.11}$$

But from Equation (7.6), $\hat{x}_i \cdot \hat{x}_k = \delta_{ik}$. Hence,

$$\sum_{j=1}^{3} a_{ij} a_{kj} = \delta_{ik} , \tag{7.12}$$

where $i, k = 1, 2, 3$.

Equation (7.12) represents six properties of [A] which will later be referred to as six equations of constant. Equation (7.12) establishes that the sum of the squares of the elements of each row of [A] is unity, and the sum of products of the respective elements of each pair of

rows of [A] vanishes identically. When the six equations, (7.12), are written out, they are

$$\begin{aligned} a_{11}^2 + a_{12}^2 + a_{13}^2 &= 1 \\ a_{21}^2 + a_{22}^2 + a_{23}^2 &= 1 \end{aligned} \tag{7.13a}$$

$$\begin{aligned} a_{31}^2 + a_{32}^2 + a_{33}^2 &= 1 \\ a_{21} + a_{12}a_{22} + a_{13}a_{23} &= \\ a_{11}a_{31} + a_{12}a_{32} + a_{13}a_{33} &= \\ a_{21}a_{31} + a_{22}a_{32} + a_{23}a_{33} &= \end{aligned} \tag{7.13b}$$

The transpose of the matrix [A] is

$$[A]^T = \begin{bmatrix} a_{11} & a_{21} & a_{31} \\ a_{12} & a_{22} & a_{32} \\ a_{13} & a_{23} & a_{33} \end{bmatrix} . \tag{7.14}$$

Clearly, the element in the i^{th} row and j^{th} column of the product matrix [A] $[A]^T$ is

$$\sum_{j=1}^{3} a_{ij}\, a_{kj} = \delta_{ik}$$

Therefore,

$$[A]\,[A]^T = \begin{bmatrix} a_{11} & a_{12} & a_{13} \\ a_{21} & a22 & a_{23} \\ a_{31} & a_{32} & a_{33} \end{bmatrix} \begin{bmatrix} a_{11} & a_{21} & a_{31} \\ a_{12} & a_{22} & a_{32} \\ a_{13} & a_{23} & a_{33} \end{bmatrix}$$

$$= \begin{bmatrix} 1 & 0 & 0 \\ 0 & 1 & 0 \\ 0 & 0 & 1 \end{bmatrix}$$

$$= [U] , \tag{7.15}$$

where [U] is the three-by-three identity matrix. Thus, [A] is a unitary or orthogonal matrix. That is,

$$[A]^{-1} = [A]^T \tag{7.16}$$

where $[A]^{-1}$ is the inverse matrix of [A]. Also,

$$\text{Det}[A] = |A| = +1 \tag{7.17}$$

since all reference frames are right-handed sets.

Another useful property of [A] is that

$$a_{ij} = \text{cof}(a_{ij}) \quad , \tag{7.18}$$

where $\text{cof}(a_{ij})$ denotes the cofactor of element a_{ij} and is defined as the product of $(-1)^{i+j}$ and the determinant of the square array formed by removing the row and column in which a_{ij} appears from [A]. This is readily shown from

$$[A]^{-1} = \frac{\text{Adj}[A]}{\text{Det}[A]} \quad , \tag{7.19}$$

where Adj[A] is the adjoint matrix of [A] formed by replacing each element a_{ij} of [A] by its cofactor and transposing. Substituting Equations (7.16) and (7.17) in Equation (7.19) yields

$$[A]^T = \text{Adj}[A] \quad , \tag{7.20}$$

which is the same as Equation (7.18). Writing out these nine relationships leads to

$$\begin{aligned}
a_{11} &= a_{22}a_{33} - a_{23}a_{32} \\
a_{12} &= a_{23}a_{31} - a_{21}a_{33} \\
a_{13} &= a_{21}a_{32} - a_{22}a_{31} \\
a_{21} &= a_{13}a_{32} - a_{12}a_{33} \\
a_{22} &= a_{11}a_{33} - a_{13}a_{31} \\
a_{23} &= a_{12}a_{31} - a_{11}a_{32} \\
a_{31} &= a_{12}a_{23} - a_{13}a_{22} \\
a_{32} &= a_{13}a_{21} - a_{11}a_{23} \\
a_{33} &= a_{11}a_{22} - a_{12}a_{21}
\end{aligned} \tag{7.21}$$

The last useful property noted is another form of the six constraint Equations, (7.13). These follow directly from equating the elements of

$$[A]^T[A] = [U] \quad , \tag{7.22}$$

which yields

$$\sum_{i=1}^{3} a_{ij}\, a_{ik} = \delta_{jk} \tag{7.23}$$

or,

$$a_{11}^2 + a_{21}^2 + a_{31}^2 = 1$$
$$a_{12}^2 + a_{22}^2 + a_{32}^2 = 1 \qquad (7.24a)$$
$$a_{13}^2 + a_{23}^2 + a_{33}^2 = 1$$

$$a_{11}a_{12} + a_{21}a_{22} + a_{31}a_{32} = 0$$
$$a_{11}a_{13} + a_{21}a_{23} + a_{31}a_{33} = 0 \qquad (7.24b)$$
$$a_{12}a_{13} + a_{22}a_{23} + a_{32}a_{33} = 0 .$$

Many more interesting relationships can be derived (Reference 24), but for present purposes, the above suffices.

It is often useful to have available differential equations, rather than algebraic equations of constraint, for manipulative purposes. From Equations (7.12) and (7.15), the following are obtained:

$$\sum_{j=1}^{3} \left(\dot{a}_{ij}\, a_{kj} + a_{ij}\, \dot{a}_{kj}\right) = 0 \qquad (7.21')$$
$$i, k = 1, 2, 3$$

or its equivalent

$$[A]\,\frac{d}{dt}[A]^T + \frac{d}{dt}[A]\cdot[A]^T = 0 . \qquad (7.15')$$

From Equation (7.17), $|A|$ is constant. Therefore

$$\frac{d}{dt}|A| = 0 \qquad (7.17')$$

and $[\dot{A}]$ is singular, possessing no inverse.* From Equation (7.18),

$$\dot{a}_{ij} = \frac{d}{dt}\left[\text{cof } a_{ij}\right] , \qquad i, j = 1, 2, 3 . \qquad (7.18')$$

*In general, Det $d/dt[A] \neq d/dt$ Det $[A]$, but for $[A]$ orthogonal, $[A]\,[A]^T = [U]$, $[A]\,[\dot{A}]^T + [\dot{A}]\,[A]^T = 0$, $\therefore [\dot{A}] = -[\dot{A}]^T[A]$. Thus, $|\dot{A}| = (-1)^n |A|\,|\dot{A}^T|\,|A| = -|d/dt\, A^T|$, since the determinant of the product of two square matrices is the product of the determinants (Reference 25), $n = 3$, and $|A| = 1$. But, the determinant of a matrix is equal to the determinant of its transpose, hence $|\dot{A}| = |\dot{A}^T| = |d/dt\, A^T| = -|\dot{A}|$. Therefore, $|\dot{A}| = 0$.

Finally, from Equation (7.23),

$$\sum_{i=1}^{3} \left(\dot{a}_{ij}\, a_{ik} + a_{ij}\, \dot{a}_{ik}\right) = 0 \qquad k, j = 1, 2, 3 \ , \tag{7.23'}$$

which, when written out, yields

$$\begin{aligned} {}'11\ a_{11} + \dot{a}_{21} a_{21} + {}'31\ {}'31 &= 0 \\ {}'12\ a_{12} + \dot{a}_{22} a_{22} + \dot{a}_{32}\, {}'32 &= 0 \\ \dot{a}_{13} a_{13} + {}'23'23 + {}'33'33 &= 0 \end{aligned} \tag{7.25a}$$

$$\begin{aligned} \dot{a}_{11} a_{12} + \dot{a}_{21} a_{22} + {}'31\ a_{32} + a_{11}\, {}'12 + a_{21}\, {}'22 + a_{31} \dot{a}_{32} &= 0 \\ \dot{a}_{11} a_{13} + \dot{a}_{21} a_{23} + \dot{a}_{31} a_{33} + a_{11} \dot{a}_{13} + a_{21} \dot{a}_{23} + a_{31} \dot{a}_{33} &= 0 \\ {}'12\ a_{13} + \dot{a}_{22} a_{23} + {}'32\ a_{33} + a_{12}\, {}'13 + a_{22}\, {}'23 + a_{32}\, {}'33 &= 0 \ . \end{aligned} \tag{7.25b}$$

The main point is, as noted in Chapter 6, that there are only three independent generalized coordinates required for relating the rotation of one reference frame to another. By using direction cosines, there are nine elements introduced. Hence, out of all the foregoing relationships from Equation (7.12) on, there are only 6 independent constraining scalar relationships, but any of the algebraic or differential ones may be used for conveniently simplifying expressions.

The dynamics and kinematics are now developed, and the general equations of motion derived. To begin with,

$$w = \omega_1 \hat{x}_1 + \omega_2 \hat{x}_2 + \omega_3 \hat{x}_3 \tag{7.26}$$

is defined as the vector representing the rate of rotation of the spacecraft about its principal axes of inertia with respect to the orbital reference frame $\bar{y}$. Since the orbital frame $\bar{y}$ rotates inertially about the $\hat{y}_2$ axis at a rate $-\Omega_0$,

$$\bar{W} = \bar{w} - \Omega_0 \hat{y}_2 \tag{7.27}$$

where $\bar{W}$ is the inertial rotation of the body frame. From Equation (7.5),

$$\bar{y} = [A]^T \bar{x} \ . \tag{7.28}$$

Thus,

$$\hat{y}_2 = a_{12} \hat{x}_1 + a_{22} \hat{x}_2 + a_{32} \hat{x}_3 \ ;$$

hence,

$$\bar{W} = (\omega_1 - \Omega_0 a_{12})\hat{x}_1 + (w, - \Omega_0 a_{22})\hat{x}_2 + (\omega_3 - \Omega_0 a_{32})\hat{x}_3$$

$$= W_1 1, + W_2 \hat{x}_2 + W_3 \hat{x}_3 \quad . \tag{7.29}$$

Of course, if the orbital reference frame to which the attitude control system aligns the spacecraft is inertial rather than earth-oriented, then $\Omega_0 = 0$ and $\bar{\omega} = \bar{W}$. Or, for attitude motion during a time interval that is small with respect to an orbital period $2\pi/\Omega_0$, so that $|\omega_i| >> \Omega_0$, orbital rate is neglected and $\bar{\omega} \approx \bar{W}$. (Remember, $|a_{ij}| \leq 1$, i, j = 1, 2, 3.)

The total angular momentum, $\bar{H}$, of the spacecraft consists of two parts. One is $\bar{H}_{s/c}$* that is due to the rigid body rotating in inertial space, i.e.,

$$\bar{H}_{s/c} = \bar{\bar{\Phi}} \cdot \bar{W} = \begin{bmatrix} I_1 \hat{x}_1 \hat{x}_1^T & 0 & 0 \\ 0 & I_2 \hat{x}_2 \hat{x}_2^T & 0 \\ 0 & 0 & I_3 \hat{x}_3 \hat{x}_3^T \end{bmatrix} \begin{bmatrix} W_1 \hat{x}_1 \\ W_2 \hat{x}_2 \\ W_3 \hat{x}_3 \end{bmatrix}$$

$$= I_1 W_1 \hat{x}_1 + I_2 W_2 \hat{x}_2 + I_3 W_3 \hat{x}_3 \ , \tag{7.30}$$

where $\bar{\bar{\Phi}}$ is the previously mentioned inertia tensor in dyadic matrix form. The second is $\bar{h}$ due to the momentum of internal rotating parts such as reaction flywheels, rotating solar array paddles, tape recorders, etc. That is,

$$\bar{H} = \bar{H}_{s/c} \ t \ \bar{h} = H, \hat{x}_1 \ t \ H_2 \hat{x}_2 + H_3 \hat{x}_3 \quad . \tag{7.31}$$

Calling $\bar{N}$ the total external torque on the spacecraft, one can write

$$\bar{N} = N_1 \hat{x}_1 + N_2 \hat{x}_2 + N_3 \hat{x}_3 \quad . \tag{7.32}$$

*s/c is an abbreviation for spacecraft.

$\bar{H}$ and $\bar{N}$ can also be resolved into inertial coordinates via [A] and [α] . That is, if $\bar{H}$ and $\bar{N}$ are expressed as column matrices in the body frame,

$$(\bar{H}) = \begin{pmatrix} H_1 \\ H_2 \\ H_3 \end{pmatrix}$$
$$(\bar{N}) = \begin{pmatrix} N_1 \\ N_2 \\ N_3 \end{pmatrix} \tag{7.33a}$$

and as column matrices in the inertial frame,

$$(\bar{H})^I = \begin{pmatrix} H_1^I \\ H_2^I \\ H_3^I \end{pmatrix}$$
$$(\bar{N})^I = \begin{pmatrix} N_1^I \\ N_2^I \\ N_3^I \end{pmatrix} , \tag{7.33b}$$

then they are related by

$$(\bar{H}) = [A]\,[\alpha]\,(\bar{H})^I = [B]\,(\bar{H})^I$$
$$(\bar{N}) = [A]\,[\alpha]\,(\bar{N})^I = [B]\,(\bar{N})^I , \tag{7.34}$$

where $[B] = [A]\,[\alpha]$. The elements of [B], b_{ij}, all have the same properties as a_{ij}, since [B], like [A], is an orthogonal unitary transformation matrix.

Just as Newton's inertial law equating force and time-rate change of translational momentum is basic to linear motion, so is the fundamental equation of rigid-body motion. It is simply written in matrix notation as

$$\frac{d}{dt}(\bar{H})^I = (\bar{N})^I , \tag{7.35}$$

and is basic to all rotational motion. Equation (7.35) is written with respect to body coordinates (Reference 21) as

$$\frac{d}{dt}\bar{H} + \bar{W} \times \bar{H} = \bar{N} , \tag{7.36}$$

where

$$(\bar{W}) = \begin{pmatrix} W_1 \\ W_2 \\ W_3 \end{pmatrix} . \tag{7.37}$$

Equation (7.36) is equivalent to

$$\frac{d}{dt}(\bar{H}) + [P_W](\bar{H}) = (\bar{N}) , \tag{7.38}$$

where

$$[P_W] = \begin{bmatrix} 0 & -W_3 & W_2 \\ W_3 & 0 & -W_1 \\ -W_2 & W_1 & 0 \end{bmatrix} . \tag{7.39}$$

Note that $|P_W| = 0$. Hence, $[P_W]$ is a singular matrix and, as such, possesses no inverse. Also note that

$$[P_W]^T = -[P_W] . \tag{7.40}$$

Now from Equation (7.35) and (7.34),

$$\frac{d}{dt}(\bar{H})^I = (\bar{N})^I = [B]^{-1}(\bar{N}) . \tag{7.41}$$

Also

$$\frac{d}{dt}(\bar{H})^I = \frac{d}{dt}\left\{[B]^{-1}(\bar{H})\right\}$$

$$= \frac{d}{dt}\left\{[B]^{-1}\right\}(\bar{H}) + [B]^{-1}\frac{d}{dt}(\bar{H}) . \tag{7.42}$$

Equating the right-hand sides of Equations (7.41) and (7.42), premultiplying both by $[B]$, and realizing $[B]^{-1} = [B]^T$, yields:

$$\frac{d}{dt}(\bar{H}) + [B]\frac{d}{dt}\left\{[B]^T\right\}(\bar{H}) = (\bar{N}) . \tag{7.43}$$

Equations (7.36), (7.38) and (7.43) are all equivalent ways of stating the well-known three scalar Euler equations where

$$(\bar{H}) = \begin{pmatrix} I_1 W_1 + h_1 \\ I_2 W_2 + h_2 \\ I_3 W_3 + h_3 \end{pmatrix} \tag{7.44}$$

Written out, their familiar form is

$$\begin{aligned} N_1 &= I_1 \dot{W}_1 + (I_3 - I_2) W_2 W_3 + \dot{h}_1 + h_3 W_2 - h_2 W_3 \\ N_2 &= I_2 \dot{W}_2 + (I_1 - I_3) W_3 W_1 + \dot{h}_2 + h_1 W_3 - h_3 W_1 \\ N_3 &= \underbrace{I_3 \dot{W}_3 + (I_2 - I_1) W_1 W_2}_{\text{Rigid body}} + \underbrace{\dot{h}_3 + h_2 W_1 - h_1 W_2}_{\text{Internal rotating parts}} \end{aligned} \tag{7.45}$$

It is clear from Equations (7.38) and (7.43) that

$$[B] \frac{d}{dt} [B]^T = [P_W] \tag{7.46}$$

Premultiplying both sides by $[B]^{-1}$ yields

$$\frac{d}{dt} [B]^T = [B]^{-1} [P_W]$$

Taking the transpose of both sides and using the identities

$$[B]^{-1} = [B]^T$$

$$[P_W]^T = -[P_W]$$

$$\left[\frac{d}{dt} \{[B]^T\}\right]^T = \frac{d}{dt} [B]$$

$$\{[X] [Y]\}^T = [Y]^T [X]^T$$

yields

$$\frac{d}{dt} [B] = -[P_W] [B] .* \tag{7.47}$$

*Thus $|d/dt\ [B]| = -|P_W||B| = -|P_W|$, and both $[\dot{B}]$ and $[P_W]$ are singular matrices, as previously stated.

The equivalent vector form of (7.47) is

$$\dot{\bar{b}}_i = \bar{b}_i \times \bar{W}, \qquad i = 1, 2, 3 \tag{7.48}$$

where

$$\bar{b}_i = b_{1i}\,\hat{x}_1 + b_{2i}\,\hat{x}_2 + b_{3i}\,\hat{x}_3 \tag{7.49}$$

Equation (7.47) or (7.48) represents nine scalar first-order differential equations. These nine, along with the three Euler equations, plus all necessary constraints, comprise the dynamics and kinematics of the spacecraft. They must now be put in the form used in Chapter 8. Firstly, it is assumed that for all practical purposes, any significant motion takes place in a sufficiently short time with large $\bar{\omega}$, so that [A] = [B] and Ω_0 is ignored. Hence $\bar{W} = \bar{\omega}$. Also, it is assumed that any external torque generator, such as a pneumatic or mass-explusion system, is much larger in torque than the torques produced by the internal rotating elements. Hence, $\dot{\bar{h}} = \bar{h} = 0$. One must be careful with this assumption since even for small $\bar{h}$, $\bar{W} \times \bar{h}$ can be large if $\bar{W}$ is large. A detailed computer simulation is usually necessary to show that the $\bar{h}$ terms do indeed cause only small perturbations to the system motion. This is most often the case for active systems, but caution must be exercised for passive or semi-passive systems. An additional assumption is to consider 2-axis positional control that aligns a principal axis to an orbital (inertial) axis, and controls the spacecraft rate about this axis, but not the angle. Two-axis control of this nature is all that is necessary for most spacecrafts during initial acquisition. The orbiting vehicle leaves the last stage of the booster, and is left with some initial rates at an arbitrary 3-axis attitude. The satellite is then stabilized to the sun line, or the local vertical connecting the spacecraft's center of gravity and the center of the earth. Only after the initial stabilization mode is accomplished does a sensor take over and establish the third positional axis of control. This dissertation is concerned with this first mode, i.e., initial acquisition, (or large angle control, or restabilization mode); and for purposes of the next chapter the local vertical is assumed as the reference axis. Thus, interest lies only in the three components of rate and in the three direction cosines, a_{13}, a_{23} and a_{33}, that are formed by the $\hat{z}_3$ axis and the spacecraft's principal axes. Hence, a five-dimensional problem exists (the three rates ω_1, ω_2 and ω_3, and any two of the three a_{i3}), with six state variables involved. The governing equations are

$$\begin{aligned}
\dot{\omega}_1 &= \left(\frac{I_2 - I_3}{I_1}\right) \omega_2 \omega_3 + \frac{N_1}{I_1}\left(\omega_1, \omega_2, \omega_3, a_{13}, a_{23}, a_{33}\right) \\
\dot{\omega}_2 &= \left(\frac{I_3 - I_1}{I_2}\right) \omega_3 \omega_1 + \frac{N_2}{I_2}\left(\omega_1, \omega_2, \omega_3, a_{13}, a_{23}, a_{33}\right) \\
\dot{\omega}_3 &= \left(\frac{I_1 - I_2}{I_3}\right) \omega_1 \omega_2 + \frac{N_3}{I_3}\left(\omega_1, \omega_2, \omega_3, a_{13}, a_{23}, a_{33}\right)
\end{aligned} \tag{7.50a}$$

$$\dot{a}_{13} = \omega_3 a_{23} - \omega_2 a_{33}$$

$$\dot{a}_{23} = \omega_1 a_{33} - \omega_3 a_{13}$$

$$\dot{a}_{33} = \omega_2 a_{13} - \omega_1 a_{23} \ , \tag{7.50b}$$

which come from Equations (7.45) and (7.47) with the above-stated assumptions. The constraint equation used is from Equation (7.24a),

$$a_{13}^2 + a_{23}^2 + a_{33}^2 = 1 \ . \tag{7.51}$$

Equations (7.50) are in the general form considered in Part I of this dissertation, and only the control laws

$$N_i = N_i(\bar{\omega}, \bar{a}_3) \qquad i = 1, 2, 3 \tag{7.52}$$

need be specified to describe the system completely.

One additional comment is in order here. Henceforth, cyclical indexed notation is used extensively for the sake of brevity. That is, three equations

$$x_1 = y_2 + z_3$$

$$x_2 = y_3 + z_1$$

$$x_3 = y_1 + z_2$$

are written as

$$x_i = y_j + z_k \ ,$$

where the i, j, k take on the values of 1, 2, 3 in a cyclic fashion.

Also, the sign function is defined as

$$\text{sgn}(x) = \begin{cases} -1 \\ \text{undefined} \\ +1 \end{cases} \text{ when } x \text{ is } \begin{cases} < 0 \\ = 0 \\ > 0 \end{cases} . \tag{7.53}$$

A graph of the sgn function is shown in Figure 7.2

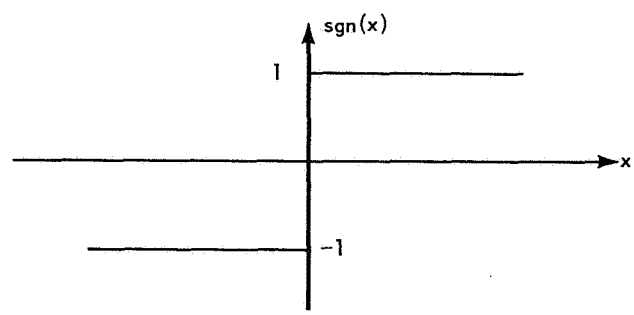

Figure 7.2—sgn(x) Function.

8. INVESTIGATION OF EQUILIBRIUM POINTS

In this chapter, some characteristic properties of attitude control systems are shown and the equilibrium point stability question is investigated. The relationship between potential troublesome dynamic behavior and equilibrium point stability is demonstrated.

One method commonly used for general nonlinear systems' stability investigations, is to approximate the system near an equilibrium point linearly, and apply well-defined stability criteria. However, for attitude control equations, the linear procedure is usually fruitfully pursued for only small regions about the one desired equilibrium state (which of course is forced by design to be stable), and at any other points one usually is forced to make invalid assumptions (with respect to sensors and cross-coupling) in order to obtain practical answers. That is, for anything but raw first cuts these methods are unyielding. Perturbation techniques of the type

$$\dot{\bar{x}} = A\bar{x} + \lambda\bar{f}(\bar{x}) ,$$

where one tries to extend $A = 0$ results to the nonlinear case by stretching the parameter λ, have also not been successful for these highly nonlinear systems that the attitude control engineer encounters in practice. New techniques are being developed, but at present none can be practically utilized. To date, to meet with success one utilizes a computer simulation, and is usually forced to make as many Monte Carlo runs as economically feasible. As already pointed out, this process is more efficient when the system equilibrium points are all known.

The equilibrium points for satellite attitude control systems of interest are now determined. First the Euler Equations, (7.50a),

$$\begin{aligned} N_1 &= I_1 \dot{\omega}_1 - (I_2 - I_3)\,\omega_2\,\omega_3 \\ N_2 &= I_2 \dot{\omega}_2 - (I_3 - I_1)\,\omega_3\,\omega_1 \\ N_3 &= I_3 \dot{\omega}_3 - (I_1 - I_2)\,\omega_1\,\omega_2 \end{aligned} \tag{8.1}$$

as developed in the previous chapter, are examined. With $R_{jk} = I_j - I_k$, Equation (8.1) yields

$$N_i = I_i \dot{\omega}_i - R_{jk}\,\omega_j\,\omega_k , \tag{8.2}$$

where $i, j, k = 1, 2, 3$ in cyclic order. For the system to be in equilibrium, the rates ω_i and torques N_i are time-invariant, thus the rate state variables at equilibrium points are the

algebraic solutions to

$$N_i + R_{jk}\,\omega_j\,\omega_k = 0 \tag{8.3}$$

or

$$w. = \frac{-N_k}{R_{ij}\,\omega_j} = \left(\frac{-N_k}{R_{ij}}\right)\left(\frac{R_{jk}\,\omega_k}{-N_i}\right) = \left(\frac{-N_k}{R_{ij}}\right)\left(\frac{R_{jk}}{-N_i}\right)\left(\frac{-N_j}{R_{ki}\,\omega_i}\right) .$$

That is,

$$\omega_i^2 = -\frac{N_j N_k}{N_i}\frac{R_{jk}}{R_{ij} R_{ki}} . \tag{8.4}$$

This relationship furnishes much information. For any given rigid body, the polarities of R_{12}, R_{23}, and R_{31} are fixed. Hence, the sign combination of N_1, N_2, and N_3 must yield a positive quantity for ω_i^2. This polarity constraint given by Equation **(8.4)** immediately reduces the number of possible combinations that yield real equilibrium points. (If the control torques depended upon only the rates, e.g., all sensors are rate gyros, then the three Equations (8.3) or **(8.4),** along with the three equations

$$N_i = N_i\left(\omega_1, \omega_2, \omega_3\right) ,$$

completely define the locations of equilibrium states and simplify the problem, since the positions do not enter the picture.)

Further analysis of the ω_i components of the equilibrium points is now made. The direction cosine Equations (7.50b) which are defined with respect to the local vertical, that is, the a_{i3}'s, are

$$\begin{aligned} \dot{a}_{13} &= \omega_3 a_{23} - \omega_2 a_{33} \\ \dot{a}_{23} &= \omega_1 a_{33} - \omega_3 a_{13} \\ a_{33} &= \omega_2 a_{13} - \omega_1 a_{23} \end{aligned} \tag{8.5}$$

There are only two-independent a_{i3} in (8.5) via the

$$\sum_{i=1}^{3} a_{i3}^2 = 1$$

constraint. That is, by multiplying $\dot{a}_{i3}$ by ω_i and adding the three equations, one obtains

$$a_{13}\,\omega_1 + \dot{a}_{23}\,\omega_2 + \dot{a}_{33}\,\omega_3 = 0 .$$

In the cyclic i, j, k indexed notation, (8.5) is

$$\dot{a}_{i3} = \omega_k\, a_{j3} - \omega_j\, a_{k3} \tag{8.6}$$

or

$$\omega_k = \frac{\dot{a}_{i3} + \omega_j\, a_{k3}}{a_{j3}} \tag{8.7}$$

Substituting (8.7) in the Euler Equation (8.2),

$$N_i = I_i\,\dot{\omega}_i - R_{jk}\, w.\, \omega_k , \tag{8.2}$$

yields

$$N_i = I_i\,\dot{\omega}_i - R_{jk}\left(\frac{\dot{a}_{k3} + \omega_i\, a_{j3}}{a_{i3}}\right)\left(\frac{\dot{a}_{i3} + \omega_j\, a_{k3}}{a_{j3}}\right)$$

$$\dot{\omega}_i - R_{jk}\left(\frac{\dot{a}_{k3} + \omega_i\, a_{j3}}{a_{i3}}\right)\left(\frac{\dot{a}_{i3}\;\Big|\;a_{k3} + \omega_i\, a_{i3}\;\Big|\;a_{k3}}{}\right)$$

The above expression, after some algebraic manipulation and use of

$$\sum_{i=1}^{3} a_{i3}^2 = 1 ,$$

reduces to

$$\dot{w}. = \frac{N_i}{I_i}\; t\; \frac{R_{jk}\, a_{j3}\, a_{k3}}{I_i\, a_{i3}^2}\;\omega_i^2 + \left[\frac{R_{jk}\,\frac{d}{dt}\left(a_{k3}^2 - a_{j3}^2\right)}{2I_i\, a_{i3}^2}\; w. - \frac{R_{jk}\,\dot{a}_{k3}\,\dot{a}_{j3}}{I_i\, a_{i3}^2}\right] . \tag{8.8}$$

Equation (8.8) represents three general equations of motion where the position and velocity variables, purposely intertwined, are changing with time. It is shown later that close to an

equilibrium point $\dot{a}_{i3}$ remains arbitrarily small. (Obviously $\dot{a}_{i3} = 0$ at the equilibrium point.) Thus, if the a_{i3}'s are approximately constant, the bracketed terms in **(8.8)** are small; hence

$$\dot{\omega}_i \approx \frac{N_i}{I_i} t \frac{R_{jk}\, a_{j3}\, a_{k3}}{I_i\, a_{i3}^2}\, \omega_i^2 \,. \tag{8.9}$$

During the time interval for which (8.9) holds, the phase-space trajectories' projection onto the three now *uncoupled* phase planes $\dot{\omega}_i$ vs. ω_i are vertical parabolas. The parabolas are stationary with time if the N_i's are constant. Which way the parabolas open depends on the sign of $R_{jk}\, a_{j3}\, a_{k3}$ (since $I_i\, a_{i3}^2$ is positive). The polarity of $\dot{\omega}_i$ where the parabolas cross the ordinate is the polarity of N_i.

Now several observations are made. The above three uncoupled phase-plane plots represent the system's motion if the N_i and a_{i3} are sufficiently constant for a long enough interval of time. When these conditions are exactly met, i.e., $\dot{a}_{i3} = N_i = 0$, then the ω_i-axis crossings of the parabolas yield the values of ω_i that are the equilibrium points of the entire system (i.e., compatible solutions of Equations (7.50) with all derivative terms zero). Thus, for these conditions it is evident that for positive N_i, positive ω_i equilibrium points are stable, and negative ω_i equilibrium points are unstable. These are shown in the first two diagrams of Figure 8.1. For negative N_i the opposite is true, as shown in the last diagram of the same figure. (Arrows indicate direction with time, so that if $\dot{\omega}_i > 0$, then ω_i increases with time.) That is, if $\mathbf{sgn}(N_i\, \omega_{i\,equib}) = -\mathbf{sgn}(R_{jk}\, a_{j3}\, a_{k3}\, \omega_{i\,equib}) = +1\,(-1)$, then the equilibrium point is stable (unstable). (Later on, a torque bang-bang system is discussed in which two unstable equilibrium points trap a phase trajectory between them, and around a third point, such that a limit cycle is generated.) Even though each parabola may contain two equilibrium points, one of these points is usually eliminated by the control laws. If a parabola opens up (down) and N_i is positive (negative), then no equilibrium points exist, and the algebraic system will yield only non-real solutions. This occurs when $\mathbf{sgn}(R_{jk}\, a_{j3}\, a_{k3}\, N_i) = +1$. Thus, $\mathbf{sgn}(R_{jk}\, a_{j3}\, a_{k3}\, N_i) = -1$ is a necessary condition for $\omega_{i\,equib}$ to exist. If N_i is zero, then there exists only the one quasi-stable equilibrium point.

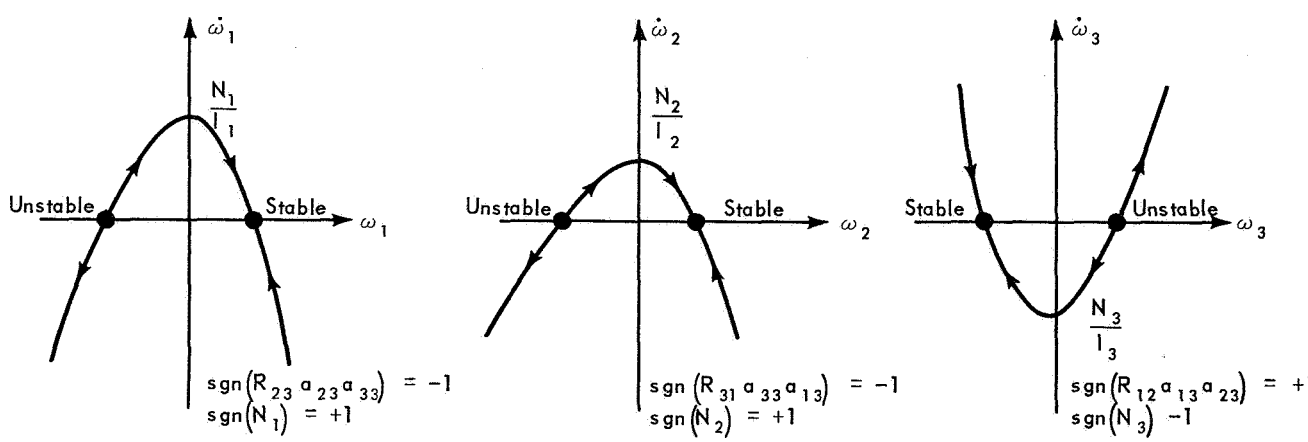

Figure 8.1 — Stability Parabolas.

(Note: Many more polarity constraints can be derived for a_{i3}, ω_i, and N_i to help locate equilibrium points. These are treated later, and tabulated in Table 8.2.)

The assumption that $\dot{a}_{i3}$ remains sufficiently small around an equilibrium point is now investigated. The three equations

$$a_{i3} = \omega_k a_{j3} - \omega_j a_{k3} \qquad (8.10)$$

$$i, j, k, = 1, 2, 3 \text{ cyclic indices}$$

lead to a single uncoupled third-order equation for each a_{i3}. As previously noted, the above three equations are not independent; the algebraic relationship

$$\sum_{i=1}^{3} a_{i3}^2 = 1 \qquad (8.11)$$

must be satisfied. After multiplying each a_{i3} in Equations (8.10) by ω_i and adding, one obtains

$$\dot{a}_{13}\,\omega_1 + \dot{a}_{23}\,\omega_2 + \dot{a}_{33}\,\omega_3 = 0 \; . \qquad (8.12)$$

Taking the second derivative of Equations (8.10) with respect to time yields, after some algebraic manipulation,

$$\ddot{a}_{i3} + \left(\omega_i^2 + \omega_j^2 + \omega_k^2\right)\dot{a}_{i3} = -\frac{3}{2}\, a_{i3}\, \frac{d}{dt}\left(\omega_j^2 + \omega_k^2\right)$$

$$+ a_{j3}\left[\frac{d}{dt}\left(\dot{\omega}_k + \omega_i\,\omega_j\right) + \omega_i\,\dot{\omega}_j\right] - a_{k3}\left[\frac{d}{dt}\left(\dot{\omega}_j - \omega_i\,\omega_k\right) - \omega_i\,\dot{\omega}_k\right] \; . \qquad (8.13)$$

Like Equation (8.8), the above equation represents purposely intertwined general equations of motion in which the state variables are changing with time. However, the equations are uncoupled when the ω_i's are assumed constant (which they are at an equilibrium point); in this case, the entire right-hand side of Equations (8.13) is zero. That is,

$$\ddot{a}_{i3} + \omega^2\,\dot{a}_{i3} = 0 \; , \qquad i = 1, 2, 3 \qquad (8.14)$$

where

$$\omega = \sqrt{\omega_1^2 + \omega_2^2 + \omega_3^2} = \text{constant} \qquad (8.15)$$

is the magnitude of the system's angular velocity vector. The three simple third-order linear Equations (8.14) are solved to yield the behavior of a_{i3} when $\dot{\omega}_i = \dot{\omega}_j = \dot{\omega}_k = 0$. That is,

$$a_{i3}(t) = A_i + B_i \sin\omega t + C_i \cos\omega t \; . \qquad (8.16)$$

Here, the A_i, B_i, and C_i are constants, but not arbitrary constants. They are determined by the initial conditions and the constraint **(8.11).** The relationship of the nine constants is investigated in the Appendix. The important point here is that by letting all acceleration terms vanish, the three a_{i3}'s are decoupled and can now each be examined independently, using, as an aid, phase plane plots. In each phase plane,

$$(a_{i3} - A_i)^2 + \frac{\dot{a}_{i3}^2}{\omega^2} = \text{constant} = K^2 , \qquad \textbf{(8.17)}$$

and the phase portrait consists of a family of periodic trajectories that are concentric ellipses centered at the equilibrium point, $a_{i3} = A_i$. Hence, it is clear from **(8.17)** and Figure **8.2,** that starting arbitrarily close to the centroid at A_i, the trajectory hovers around it, with the maximum $\dot{a}_{i3} = K\omega$ occuring at $a_{i3} = A_i$. Thus, for sufficiently small K, $\dot{a}_{i3}$ stays arbitrarily small.

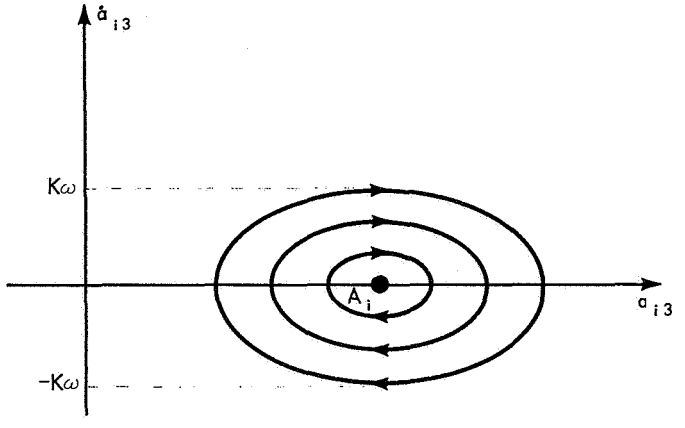

Figure 8.2—Direction Cosine Phase Plane Portrait for $\dot{\omega}_i = 0$.

The above discussion is now summarized. At an equilibrium point, all dynamic quantities remain constant with respect to time. When it is assumed that near an equilibrium point the $\dot{a}_{i3} = 0$ but not the $\dot{\omega}_i$, then, depending on certain polarity considerations, one concludes that the state of the system moves either toward or away from the equilibrium state. When it is assumed that the $\dot{\omega}_i = 0$ but not the $\dot{a}_{i3}$, and when the system is started near an $\dot{a}_{i3} = 0$ system equilibrium state, then the system state remains near the equilibrium state. Hence, if the system state is very close to an equilibrium point at $t = 0$, then it is the $\dot{\omega}_i$-vs.-ω_i parabola polarity that determines stability in some neighborhood of the equilibrium point. This conclusion is fortified by the fact that usually most main torque generators used in attitude control systems are used in an on-off fashion. Therefore, unless a torquer is duty-cycling (as discussed in the next chapter), its bang-bang characteristic gives it a digitized constant level in a neighborhood of of sensor signals such that N_i is constant, thereby keeping the $\dot{\omega}_i$-vs.-ω_i parabolas almost stationary with time. For example, an ideal pneumatic loop, consisting of voltage from a rate gyroscope feeding into a double-ended threshold detector that drives pneumatic thruster solenoids, is shown in block diagram form in Figure **8.3.**

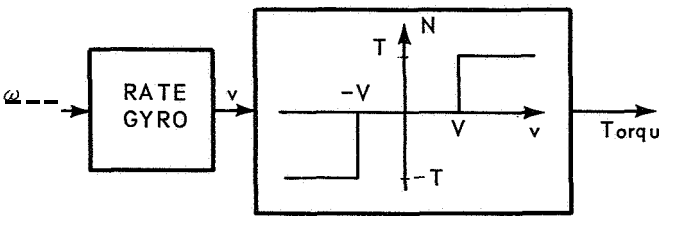

Figure 8.3—Ideal Pneumatic Loop.

From Equation (8.4), it is seen that if the N_i's take on only discrete levels, then

out"the system so that it correlates with the mathematical system described in Part I of this dissertation, the bang-off-bang pneumatic controller is roundedout to that shown in Figure 8.4. This continuous characteristic is:

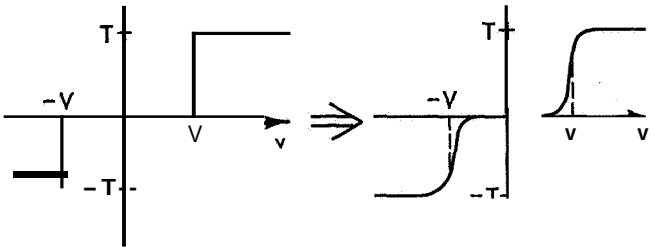

Further strengthening of the conclusion that the values of ω_i (and the control laws which yield N_i) at an equilibrium point completely determine the stability of the equilibrium point is obtained by an approximate linear expansion of the equations of motion about that equilibrium point. Defining the values of the state variables at the equilibrium point as ω_{1e}, ω_{2e}, ω_{3e}, a_{13e}, a_{23e}, a_{33e}, the transformation,

$$\begin{aligned} \omega_1 &= u_1 + \omega_{1e} \\ \omega_2 &= u_2 + \omega_{2e} \\ \omega_3 &= u_3 + \omega_{3e} \\ a_{13} &= u_4 + a_{13e} \\ a_{23} &= u_5 + a_{23e} \\ a_{33} &= u_6 + a_{33e} \end{aligned} \tag{8.18}$$

converts Equations (8.1) and (8.5), for u_i near equilibrium, into

$$N_i \approx I_i \dot{u}_i - (I_j - I_k)(\omega_{je} u_k + \omega_{ke} u_j + \omega_{je} \omega_{ke}) \tag{8.19}$$

for cyclic i, j, k = 1, 2, 3, and

$$\begin{aligned} \dot{u}_\ell &= (u_k + \omega_{ke})(u_m + a_{j3e}) - (u_j + \omega_{je})(u_n + a_{k3e}) \\ &\sim \omega_{ke} u_m + a_{j3e} u_k + \omega_{ke} a_{13e} - a_{k3e} u_j - \omega_{je} u_n - \omega_{je} a_{k3e} , \end{aligned} \tag{8.20}$$

for cyclic ℓ, m, n = 4, 5, 6, where all higher order nonlinear terms in **u** are neglected.

Equations **(8.19)** and **(8.20)** are equivalent to the linear matrix equation

$$\begin{pmatrix} \dot{u}_1 \\ \dot{u}_2 \\ \dot{u}_3 \\ \dot{u}_4 \\ \dot{u}_5 \\ \dot{u}_6 \end{pmatrix} = \left[\begin{array}{ccc|ccc} 0 & \sigma_{23}\omega_{3e} & \sigma_{23}\omega_{2e} & 0 & 0 & 0 \\ \sigma_{31}\omega_{3e} & 0 & \sigma_{31}\omega_{1e} & 0 & 0 & 0 \\ \sigma_{12}\omega_{2e} & \sigma_{12}\omega_{1e} & 0 & 0 & 0 & 0 \\ \hline 0 & -a_{33e} & a_{23e} & 0 & \omega_{3e} & -\omega_{2e} \\ a_{33e} & 0 & -a_{13e} & -\omega_{3e} & 0 & \omega_{1e} \\ -a_{23e} & a_{13e} & 0 & \omega_{2e} & -\omega_{1e} & 0 \end{array}\right] \begin{pmatrix} u_1 \\ u_2 \\ u_3 \\ u_4 \\ u_5 \\ u_6 \end{pmatrix} + \left[\begin{array}{c} N_1 + \sigma_{23}\omega_{2e}\omega_{3e} \\ N_2 + \sigma_{31}\omega_{3e}\omega_{1e} \\ N_3 + \sigma_{12}\omega_{1e}\omega_{2e} \\ \hline \omega_{3e}a_{23e} - \omega_{2e}a_{33e} \\ \omega_{1e}a_{33e} - \omega_{3e}a_{13e} \\ \omega_{2e}a_{13e} - \omega_{1e}a_{23e} \end{array}\right], \tag{8.21}$$

where $\sigma_{ij} = (I_i - I_j)/I_k$. When the matrices are partitioned as indicated in **(8.21)**, the roles of Equations **(7.37)** through **(7.39)**, **(7.44)** and **(7.47)** are clear and **(8.21)** is derivable from these equations with the proper assumptions. The linear Equation **(8.21)** has the form

$$\frac{d}{dt}(\bar{u}) = [D](\bar{u}) + (E), \tag{8.22}$$

where $(\bar{u})$ is the variable-column matrix, and $[D]$ and (E) are constants. It is important to note that

$$\det [D] = |D| \equiv 0. \tag{8.23}$$

From a stability viewpoint, if the eigenvalue problem is attacked by solving

$$|[D] - \lambda[U]| = 0, \tag{8.24}$$

where $[U]$ is the six-by-six identity matrix, the following sixth-order polynomial in λ is obtained:

$$-\lambda\left(\omega_{1e}^2 + \omega_{2e}^2 + \omega_{3e}^2 + \lambda^2\right)\begin{vmatrix} -\lambda & \sigma_{23}\omega_{3e} & \sigma_{23}\omega_{2e} \\ \sigma_{31}\omega_{3e} & -\lambda & \sigma_{31}\omega_{1e} \\ \sigma_{12}\omega_{2e} & \sigma_{12}\omega_{1e} & -\lambda \end{vmatrix} = 0, \tag{8.25}$$

or

$$\lambda\left[\lambda^2 + \left(\omega_{1e}^2 + \omega_{2e}^2 + \omega_{3e}^2\right)\right]\left[\lambda^3 - \lambda\left(\sigma_{12}\sigma_{31}\omega_{1e}^2 + \sigma_{12}\sigma_{23}\omega_{2e}^2 + \sigma_{23}\sigma_{31}\omega_{3e}^2\right) - 2\sigma_{12}\sigma_{23}\sigma_{31}\omega_{1e}^2\omega_{2e}^2\omega_{3e}^2\right] = 0. \tag{8.26}$$

Several observations are now made concerning the characteristic Equation **(8.26).** Firstly, nowhere do the direction cosines a_{i3e} appear. That is, all six eigenvalues (λ-roots) are *independent of the spacecraft attitude* near the equilibrium point. (A constant value of N_i is of course assumed. That is, N_i is not a function of $\bar{u}$ (or time) and hence does not enter into [D] but only into (E) in Equation **(8.22).** Thus, by letting $(\bar{v}) = (\bar{u}) + [D]^{-1}(E)$, Equation **(8.22)** becomes $(+) = [D](\bar{v})$ and the eigenvalues are the same.) Another interesting observation is that three of the characteristic roots of Equation **(8.26)** are

$$\lambda_1 = 0 , \qquad \lambda_2 = \sqrt{-1}\,\omega_e , \qquad \lambda_3 = -\sqrt{-1}\,\omega_e ,$$

where

$$\omega_e = \sqrt{\omega_{1e}^2 + \omega_{2e}^2 + \omega_{3e}^2}$$

is a real number (and the same frequency as in Equation **(8.16)** where $\omega_i = \omega_{ie}$ was held constant). These are the three eigenvalues obtained from $\left| \square \quad -\lambda[U] \right| = 0$, where $\left[P_{W_e}\right]$ is as in Equation (7.39). Thus, the linear analysis does not yield the complete stability picture and the nonlinear terms must be accounted for. It is also interesting to note that the remaining three roots, λ_4, λ_5, and λ_6, depend on the spacecraft moments of inertia as well as the ω_{ie}'s for their realness as well as for their polarity.

Another aspect of the attitude control system's equilibrium points is that of polarity combinations mentioned earlier in this chapter. For the sake of definitiveness, it is assumed that the spacecraft has the following inertia relationships:

$$I_1 > I_2 > I_3 > 0 . \tag{8.27}$$

(No loss in generality results from this assumption since similar results are obtained for any inertia magnitude order.) Hence,

$$\begin{aligned} R_{12} &> 0 \\ R_{23} &> 0 \\ R_{31} &< 0 \end{aligned} \tag{8.28}$$

and Equations **(8.3)** become

$$\begin{aligned} N_1 &= -K_1 \omega_2 \omega_3 \\ N_2 &= K_2 \omega_1 \omega_3 \\ N_3 &= -K_3 \omega_1 \omega_2 . \end{aligned} \tag{8.29}$$

where K_i $(i = 1, 2, 3)$ is positive. The above three equations, plus Equations (8.5) with no derivative terms, i.e.,

$$\begin{aligned} \omega_3 a_{23} &= \omega_2 a_{33} \\ \omega_1 a_{33} &= \omega_3 a_{13} \\ \omega_2 a_{13} &= \omega_1 a_{23} \end{aligned} \tag{8.30}$$

are satisfied at any equilibrium point. In addition,

$$a_{13}^2 + a_{23}^2 + a_{33}^2 = 1 \tag{8.31}$$

must be true. There are eight possible polarity combinations for the three ω_i, and from Equations (8.29) each of these combinations yields a specific polarity for N_i. They are shown in Table 8.1.

Table 8.1

Combination	ω_1	ω_2	ω_3	N_1	N_2	N_3
1	+	+	+	-	+	-
2	+	+	-	+	-	-
3	+	-	+	+	+	+
4	+	-	-	-	-	+
5	-	+	+	-	-	+
6	-	+	-	+	+	+
7	-	-	+	+	-	-
8	-	-	-	-	+	-

Table 8.2

Case	ω_1	ω_2	ω_3	a_{13}	a_{23}	a_{33}	N_1	N_2	N_3
1	+	-	+	+	-	+	+	+	+
2	-	+	-			-			
3	+	-	+	-	+	-			
4	-	+	-						
5	+	+	-	+	+	-	+	-	-
6	-	-	+						
7	+	+	-	-	-	+			
8	-	-	+						
9	+	+	+	+	+	+	-	+	-
10	-	-	-						
11	+	+	+	-	-	-			
12	-	-	-						
13	+	-	-	+	-	-	-	-	+
14	-	+	+						
15	+	-	-	-	+	+			
16	-	+	+						

From Equations (8.4),

$$\operatorname{sgn}\left(N_1 N_2 N_3\right) = +1 \tag{8.32}$$

for ω_i^2 positive (and thus ω_i real). (Note that

$$\operatorname{sgn}\left(N_j N_k / N_i\right) = \operatorname{sgn}\left(N_1 N_2 N_3\right) ,$$

and

$$\operatorname{sgn}\left(R_{jk} / R_{ij} R_{ki}\right) = -1$$

from Equation (8.28).) Equation (8.32) is, of course, true for all combinations in Table 8.1. In total, there are 64 polarity combinations of all the variables, that is eight direction cosine (a_{13}, a_{23}, a_{33}) combinations for every combination of rates in Table 8.1. However, Equations (8.30) reduce the number of cases to 16 as given in Table 8.2.

Table 8.2 shows all possible combinations of parameters for arbitrary control laws (assuming a spacecraft with inertias as in Equation (8.27)) for any real equilibrium points. It is evident from the table that there

are only four permissible control torque polarity combinations. Each one exists in only two octants that are mirror images* of each other on the direction cosine unity sphere. The unity sphere is a useful geometric device for displaying attitude, and is defined as a sphere in a_{13}, a_{23}, a_{33} space of unit radius and center at the origin. (See Figure 8.5). Allattitudes of the spacecraft lie on the surface of this sphere since

$$\sum_{i=1}^{3} a_{i3}^2 = 1 .$$

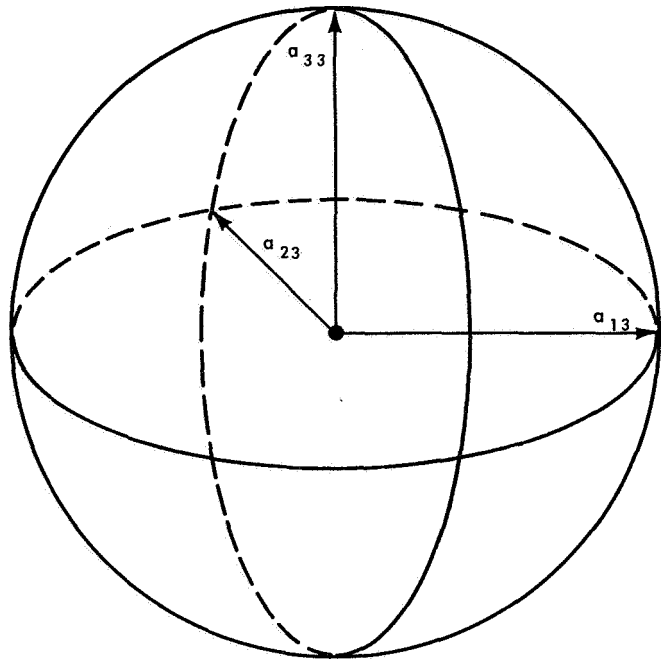

Figure 8.5— Direction Cosine Unity Sphere.

Each surface quadrant of the direction cosine unity sphere allows equilibrium points to exist only in two (mirror image) octants of three-dimensional $\omega_1, \omega_2, \omega_3$ rate space. The two mirror image points fall out from the two roots of Equation **(8.4).** Table 8.2 and its interpretation (which comes with practice) is an extremely useful analytical tool in locating equilibrium points in a system.

The above results are independent of any specific attitude control system with explicit control laws. This chapter has been an attempt at understanding equilibrium points that exist in an attitude control system. This analysis, coupled with the mathematical development of Part I that puts equilibrium points inside limit cycles, establishes a basis for finding potentially troublesome regions of the system. In the following chapter, examples of practical application are given in the hope of demonstrating the power behind this type of an approach when utilized with a computer simulation.

***Mirror image points in 3-dimensional space is where the polarity of each component of one point is the negative of its respective component of the other point, i.e., the position vector to both points are equal and opposite.**

9. PRACTICAL APPLICATIONS

The equilibrium analysis technique developed in the previous chapters has been successfully applied to actual complex attitude control systems. The power of this approach is demonstrated by the resulting usefulness from these practical applications. Thus, in this chapter, the method is illustrated by considering the following systems:

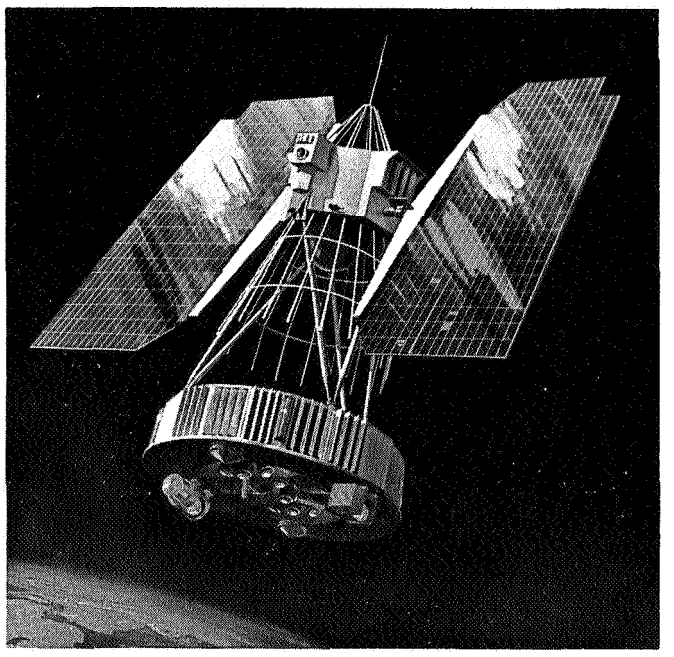

Figure 9.1 —Nimbus Spacecraft.

I) The NASA* advanced meteorological satellite, Nimbus I, (Figure 9.1), an earth-oriented spacecraft. The analysis shows the shortcomings of the attitude control system for large perturbations (such as those which would necessitate reacquisition of the earth's local vertical) or large initial conditions at the time of separation from the launch vehicle. Nimbus I was launched August 28, 1964, and had a fairly successful active life until September 23, 1964. Its solar array drive mechanism then locked up, preventing efficient energy conversion from the sun. As a result, the spacecraft experienced intermittent power outages. This, in turn, led to erroneous signals in the pneumatic torquing system. The erroneous error signals caused the vehicle to spin at such a high angular velocity that even if the power situation had corrected itself, the spacecraft could not be restabilized (Reference 26).

11) The follow-on Nimbus weather satellites II and 111 which have progressive modifications in the attitude control systems. Although improved, due to cost limitations involved in change, they still have similar stability-in-the-large potential dangers. Nimbus 11 was launched May 15, 1966. The initial. conditions for earth acquisition were small and the spacecraft stabilized successfully. The control system is still performing satisfactorily. Nimbus 111 will be launched in the late part of 1967. It is interesting to note that several easily implemented schemes were proposed for remedying certain non-stable characteristics of the system and at first, after several hundred thousand computer runs, these schemes appeared attractive. However, after a thorough equilibrium analysis (Reference 27), it was shown that in several cases the original equilibrium points are moved to different locations in state space, bringing their unstable behavior with them. Also, new equilibrium points are introduced. The large number

*National Aeronautics & Space Administration.

of computer runs never located these isolated trouble areas. As an example, runs are made where the initial attitude and the roll and pitch rates are held constant, while the yaw initial rate is varied as a parameter for each simulated run. Later, when equilibrium points are calculated, one is found to lie in between two of these yaw-rate runs. When the computer is initialized at the equilibrium point, the system is unstable; it "meanders" so to speak (in almost periodic fashion), ejecting gas, and then finally takes off. Here is a "hole" in a region of state space declared a stable region because of the results from a grid of computer runs in the region. This example illustrates that unless the initial condition grid is infinitesimally small (which takes an infinitely large number of runs, especially for high-dimensional systems), a brute-force coverage pattern or a Monte-Carlo random approach does not yield a high degree of confidence that the computer will find all the "holes" of a complex nonlinear system. The equilibrium analysis is designed to substantially boost this confidence factor.

III) The advanced Nimbus satellite (Nimbus D) which has a completely new set of attitude control laws and sensors. This vehicle is scheduled for launch in 1969. The equilibrium point approach was used in the original design (which is now being completed) to eliminate all equilibrium points in a reasonably bounded region of interest of state space. This application is described in more detail later in this chapter.

The equilibrium approach is to be attempted for other major scientific NASA spacecraft, such as the Orbiting Astronomical Observatory (OAO), which is an inertially-oriented satellite to study the stars; the Orbiting Geophysical Observatory (OGO), which is earth-oriented and studies many physical phenomena in a region of space around the earth; the Aerobee Sounding Rocket 350, which is a short-lived economical inertially-oriented spacecraft that is flexible so as to study many items of interest; the Applied Technology Satellite (ATS-F) whose design has just commenced and will be used to demonstrate space technologyin many areas; and possibly many others (Orbiting Solar Observatory, Deep Space and Galactic Probes, Apollo Application Missions, etc.).

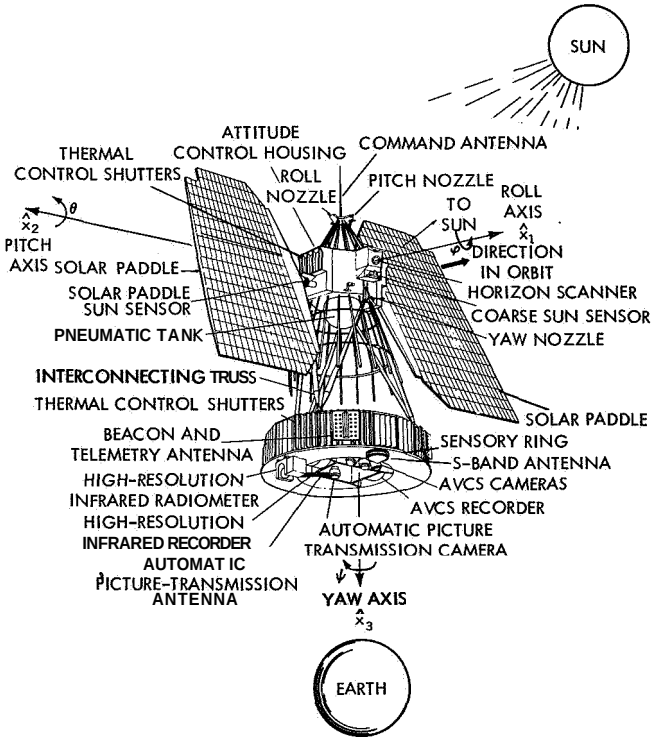

Figure 9.2— Nimbus I.

A brief background description of the Nimbus weather satellite is now presented. How the equilibrium approach is utilized, and the results, are given. (For more detailed description of Nimbus, see Reference 28, 29.) Nimbus I is shown in Figure 9.2. The spacecraft stands 9-1/2 feet tall, weighs 850 pounds, and has moments of inertia

approximately equal to:

$$I_1 = 222 \text{ slug-ft}^2{}^*, \qquad I_2 = 196 \text{ slug-ft}^2, \qquad I_3 = 90 \text{ slug-ft}^2, \tag{9.1}$$

and peak-power capability of approximately 470 watts generated from a solar-cell array. (It is noted that many simplifying assumptions are made for the sake of brevity. However, the actual detailed analysis includes the entire physical system as well as it can be determined; all assumptions are looked at qualitatively if not quantitatively to see their effects on the final results. One such assumption, aside from taking the structure as a rigid body, is to ignore the small time-varying property of the moments of inertia due to the large solar-array paddles rotating to follow the sun.) The spacecraft is broken down into three major physical sections:

1) The sensory ring on the bottom which houses all the meteorological equipment that looks down at the earth, (such as T.V. cameras, infrared energy sensors for obtaining three-dimensional pictures of clouds, etc.), and the associated subsystems such as batteries and power supply, communications and antennas, spacecraft clock, etc.

2) Two 3-1/4 x 8 feet solar array paddles that are driven via a closed control loop to follow the sun for maximum energy input (Figure 9.3). The orbit is a nominal 500-nautical-mile-altitude, circular, "high-noon," nearly polar orbit. That is, launch time is local midnight, and the inclination angle of the orbit (≈98.7 degrees to the equator) is such that the orbital plane precesses one revolution per year, at the same rate as the earth moving around the sun† (Figure 9.5). Thus, the sun remains nominally in the orbital plane (i.e., the orbital plane is sun-synchronous), and, if the attitude control system aligns the vehicle in the orbital plane, then the solar array drive needs only one degree of freedom (about the orbital pitch axis). The solar array drive control system is a straightforward feedback loop and is functionally designed and analyzed in a simple classical manner, but the mechanical hardware problems, as demonstrated by the first Nimbus flight failure, are not so simple.

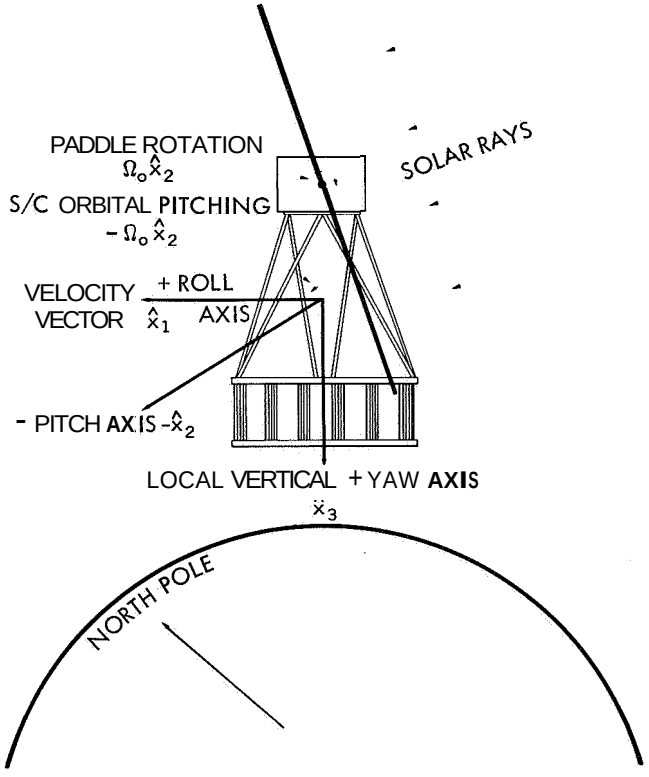

Figure 9.3—Nimbus Spacecraft Body Axes.

*1 slug-ft^2 = 1 ft-lb-sec^2.

†This orbit also affords the spacecraft cameras complete earth coverage twice a day, during local noon and midnight, as shown in Figure 9.4.

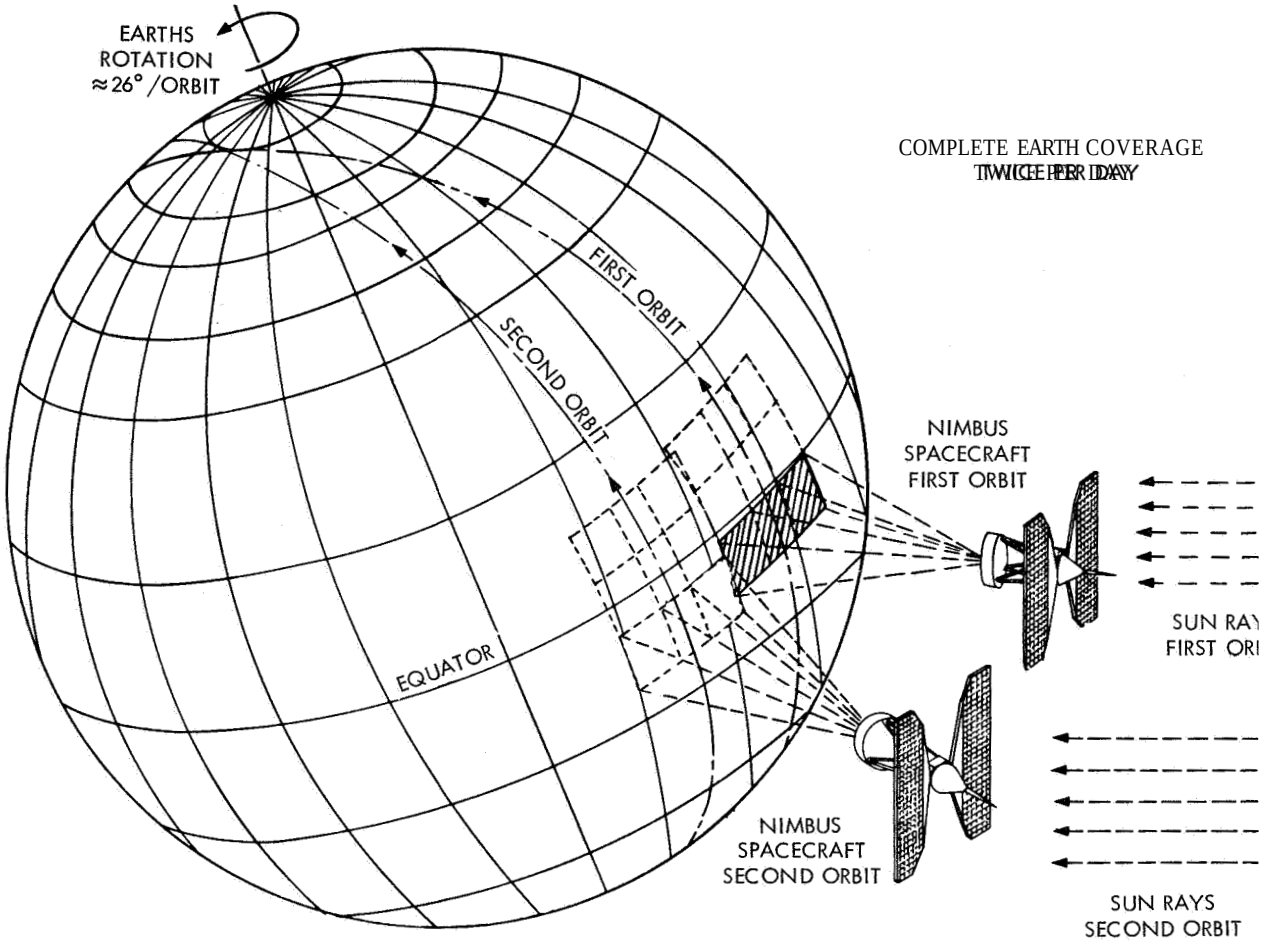

Figure 9.4—Nimbus Picture Coverage.

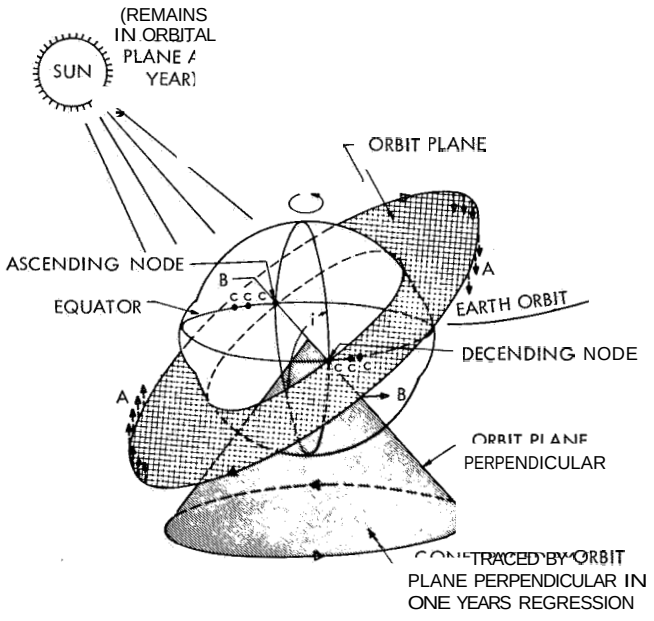

Figure 9.5—Orbit-Plane Regression (Autumnal Equinox).

3) The attitude control system and all its associated subsystems which, of course, are the parts of the satellite of most concern for this dissertation. After a Thor-Agena combination boosts and injects Nimbus into orbit, the satellite separates from the Agena at approximately a vertical position with angular rates (hopefully) less than 1 degree/sec in all three axes. The solar paddles are unfolded, and the control system is initiated. It brings the spacecraft from its initial conditions to within a small neighborhood of the desired equilibrium point in a short time, and with a small percentage of available control gas. The desired equilibrium point expressed in the notation of Chapter 7 is:

$$W_1 = W_3 = 0 , \qquad W_2 = -\Omega_0$$

$$[A] = \begin{bmatrix} 1 & 0 & 0 \\ 0 & 1 & 0 \\ 0 & 0 & 1 \end{bmatrix} = [U] , \tag{9.2}$$

where $(X) = [A]\,(\bar{y})$ and $(\bar{y}) = [\alpha]\,(\bar{z})$. If the acquisition and control response times are small (on the order of seconds) compared to the orbital period ($\tau = 2\pi/\Omega_0$ for a 500 nautical mile altitude -103.5 minutes) as they are in this case, orbital rate may be neglected compared to attitude rates, so that

$$[\alpha] = [0] , \tag{9.3}$$

and the system is as described in Chapter 8. Equation (9.2) then describes a satellite whose vertical (yaw) axis is aligned to the earth's local vertical as the satellite orbits round the earth, and whose body-roll and yaw axes lie in the orbital plane. That is, the satellite is inertially rotating at one revolution per orbit about an axis normal to the orbital plane. The accuracy and rate specifications for the control system are that the angular errors (in an Euler small-angle sense) be less than one degree, and the angular error rates be less than 0.05 degrees per second with respect to the orbital reference axes.

To meet these requirements, Nimbus I has as control system sensors:

A) Two infrared horizon scanners which ideally provide sufficient information to determine the location of the earth's local vertical.

B) A rate gyroscope used as a gyro-compass to furnish yaw control.

C) Sun sensors for backup yaw control to the sun line.

For control actuators (muscles), there are:

D) A pneumatic cold gas mass expulsion system capable of changing the system momentum.

E) Reaction flywheels, which are two-phase linearly wound inside-out motors (heavy pancake rotor revolves around inside stator), capable of storing momentum.

Before the control laws that connect the sensors and muscles are defined, a brief description is stated for each. One must realize that volumes could be (and have been) written (e.g. References 30, 31) on any one particular area of an attitude control system, such as a specific scanner, but here the intent is to oversimplify for background familiarity. First the sensors are discussed.

Sensors:

A) Each horizon scanner has an optical prism that is motor-driven to sweep out a conical field of view, with the cone axis along the body-roll axis ($\hat{x}_1$). There is one scanner fore and

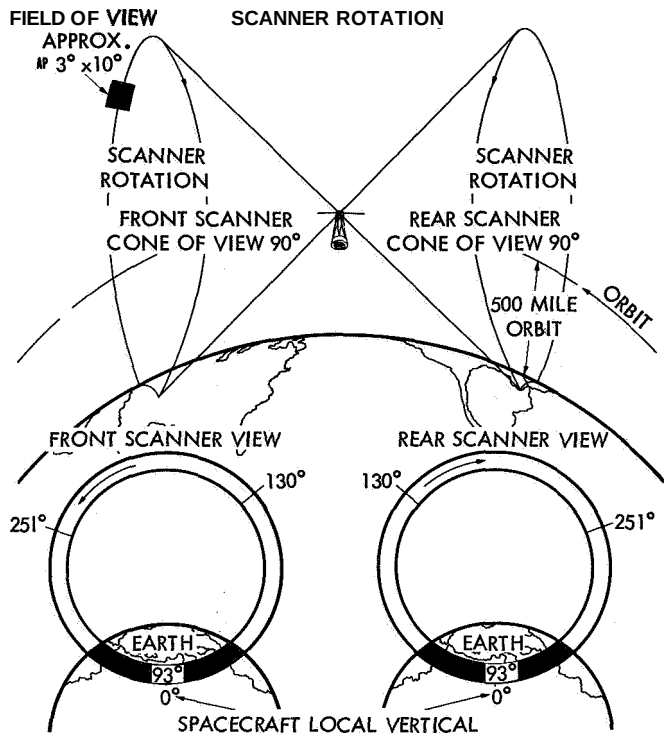

Figure 9.6a—Earth as Seen by Scanners in Stabilized Nimbus.

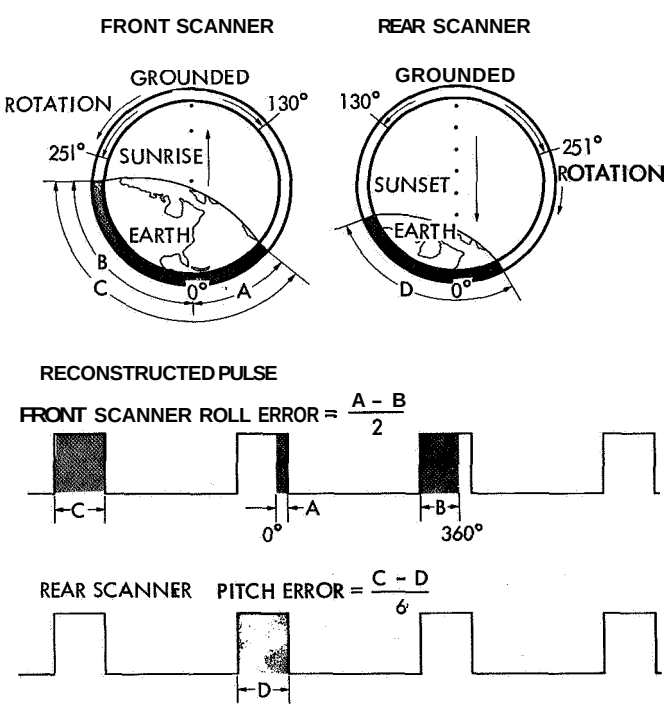

Figure 9.6b—Roll and Pitch Error Computation.

another aft of the spacecraft (Figure 9.6a). Incident infrared (IR) energy is detected by an immersed thermistor bolometer, and a voltage pulse is obtained as the *scan* path moves through cold space to hot earth and back to cold space again. If the spacecraft has a roll error, then a vertical reference pulse generated at the bottom of the scan cone (fixed with respect to the spacecraft), is displaced from the center of the earth IR pulse, and this displacement is a measure of the roll error. To obtain pitch information, a scanner cannot be used along the pitch axis, since the solar paddles block the field of view; therefore, two roll scanners are used back-to-back. A pitch error angle means that one scanner apparently sees a larger earth than the other. Hence, the difference in the two IR earth pulse widths is a measure of the pitch error (Figure 9.6b). The scanners are extremely nonlinear roll-pitch cross-coupled error detectors for all but very small angles. This is due to **(1)** the geometry of the situation—for instance, if the spacecraft pitches far enough one scanner leaves the earth. Pitching still further until the spacecraft is almost horizontal, the other scanner cone sees only earth; **(2)** the digital error processing must be severely constrained—for example, not only are sunshades used, but the bolometer output signal is electrically clamped to zero at the top of the scan cone; this ensures that if the sun comes into the field of view (the sun is a very hot IR source) it is not processed as is the earth (which is actually down below); **(3)** the earth is not an ideal homogeneous spherical IR source—for example, high cold clouds next to a warm patch on earth may lead the sensor to suppose that a cold-space/hot-earth horizon is falsely within the earth disc, thus

producing significant sensing errors; (4) the scanners and processors are non-ideal pieces of hardware in many physical respects. Thus, it is a formidable task to mathematically represent realistic roll and pitch control errors as

$$V_1 = V_1(a_{13}, a_{23}, a_{33})$$
$$V_2 = V_2(a_{13}, a_{23}, a_{33}) \quad , \tag{9.4}$$

and one is compelled to use a graphical representation (Reference 32, also page 9.11 and Figures 9.10 through 9.13 later in this chapter). The graphs consist of a family of parametric curves on the a_{i3} ($i = 1, 2, 3$) direction-cosine unity sphere that are projected on the a_{13}, a_{23} plane for positive and negative a_{33}. A highly complex hardware simulation that includes the actual geometry can also be used statically to find the errors needed in the equilibrium point search. Note that for an assumed spherical earth, V_1 and V_2 do not depend on yaw, and hence are only functions of a_{i3} ($i = 1, 2, 3$).

B) To understand the gyro-compass error detector, assume that the spacecraft is perfectly aligned with the orbital reference axes with zero relative rate. Then, the only rate a gyro measures is the inertial rate, perpendicular to the orbital plane, of the reference axes going around the earth, i.e., $-\Omega_0 \hat{y}_2$. Hence, if the input axis of the gyro is along the body-roll axis $\hat{x}_1$, any misalignment of $\hat{x}_1$ out of the orbital plane causes the gyro to sense a component of orbital rate proportional to the sine of the misalignment yaw angle. Thus, the gyro rate output is a measure of the yaw error and is used as such. The input axis of the gyro is tilted up toward the $-\hat{x}_3$ axis by a small angle γ so that the gyro output voltage also contains a small component of yaw error rate, ω_3, for damping of the yaw control loop. The yaw error voltage is

$$V_1 = W_1 \cos\gamma - W_3 \sin\gamma \tag{9.5}$$

in the notation of Chapter 7. If $\Omega_0 = 0$ is assumed, then V_1 no longer contains yaw angle information, but only undesired roll rate and desired yaw rate. That is,

$$V_1 = \omega_1 \cos\gamma - \omega_3 \sin\gamma \quad , \tag{9.6}$$

and the system exhibits no yaw positional control. The gyro-compass operation is illustrated in Figure 9.7 for zero roll and pitch errors.

C) The sun sensor is used in a backup failure mode and is not considered in this chapter.

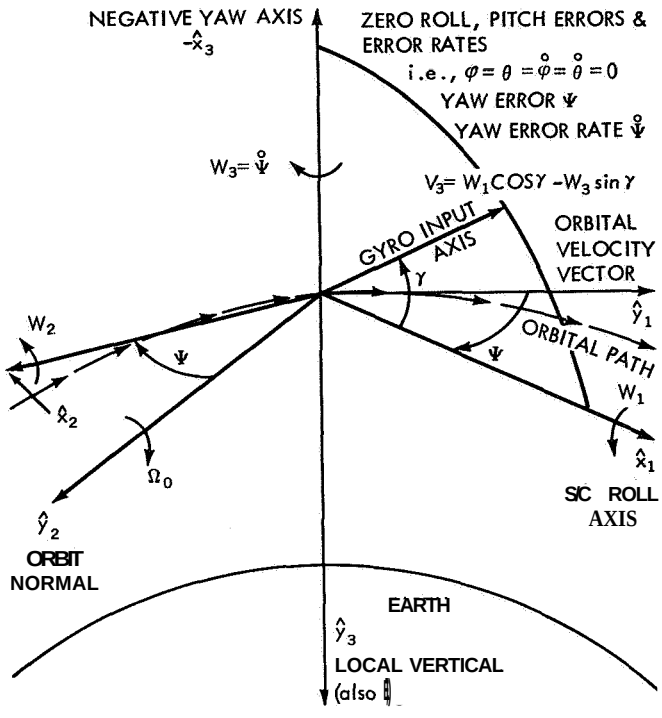

$$\bar{W} = -\Omega_0 \hat{y}_2 \text{ t } \overbrace{\dot{\psi}\hat{y}_3}^{\bar{\omega}} = -\Omega_0 \left(\sin\psi\hat{x}_1 + \cos\psi\hat{x}_2\right) + \dot{\psi}\hat{x}_3$$

$$\therefore W_1 = -\Omega_0 \sin\psi\,, \quad W_2 = -\Omega_0 \cos\psi\,, \quad W_3 = \dot{\psi}$$

thus, $V_3 = -\left(\Omega_0 \cos\gamma\right)\sin\psi - (\sin\gamma)\dot{\psi}$ and, if $\Omega_0 = 0$ (i.e. $\% = \bar{\omega}$), then V_3 contains no yaw position information

Figure 9.7—Gyro-Compass Operation.

Muscles:

D) In Nimbus, bang-off-bang controllers for the pneumatics are used. Current from a power stage of a double-ended threshold detector with hysteresis is fed to the proper gas solenoid valve which, when open, produces a thrust. This thrust is collinear with the spacecraft center of mass; hence, an external torque is produced. A simplified schematic representation is shown in Figure 9.8(a). In Figure 9.8(b), the system is further simplified by ignoring hysteresis, valve transport delays, pressure buildup lags, etc., and combining everything in a smooth pseudo-bang-off-bang curve with sufficiently sharp slopes to be realistic enough for present purposes. One of these torque generators exists for each of the three axes: roll, pitch, and yaw.

E) Flywheels are used primarily for fine pointing control for small and cyclic-type disturbances. (For cumulative disturbances, the flywheels saturate and become ineffectual; thus, gas is fired to unload momentum when the wheels reach a certain speed). The wheel torque levels are much smaller than the gas system; therefore the wheels are neglected for present purposes.

The system is connected together by electronic implementation of control laws, involving loop compensation networks designed to give the loops proper response. When searching for equilibrium points, one looks for time-invariant behavior; therefore noise filters, lead-lag networks, etc., need not be considered dynamically. Only the DC steady-state gains are at issue. Limiting, and physical saturation are also considered. The control laws of Nimbus I reduce to those statically shown in Figure 9.9. However, early in the design it was realized, and vividly dramatized by computer runs, that the system does not work well for all reasonable rates. The reason is the yaw loop responds to five times more roll rate than yaw rate, so that the yaw gas produces still higher yaw rates. These rates couple back through the dynamics as roll and pitch torques, as evidenced by Equation 8.1. The loop is designed for fine performance as well as coarse; so the V_3 control law is needed to obtain yaw-angle information which is only contained in the ω_1 term.) The yaw gas is throttled down by allowing it to pulse for at most one half second out of every thirty seconds. Thus, N_3 (compared to N_1 and N_2) is small for the first few important seconds of action. Hence, for present purposes, $N_3 = 0$ is assumed.

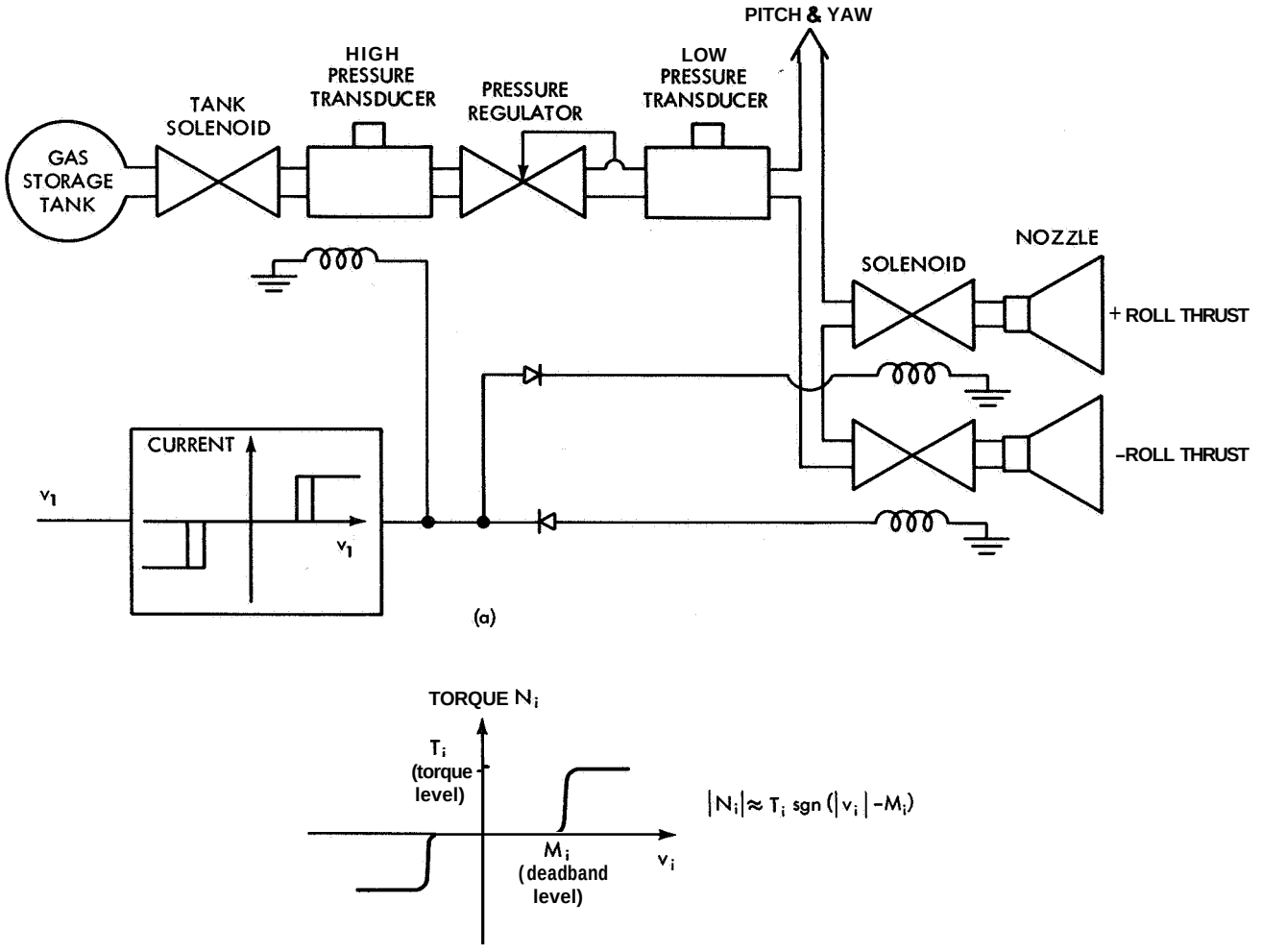

Figure 9.8—Simp1ified Pneumatic System.

The work is now made simple by the groundwork already laid by this and previous chapters. All equilibrium points are solutions to the following set of relationships:

$$N_1\left(K_1\left(V_1\left(a_{13}, a_{23}, a_{33}\right)\right)\right) = -\left(I_2 - I_3\right)\omega_2\,\omega_3 \qquad (9.7a\text{-}1)$$

$$N_2\left(K_2\left(V_2\left(a_{13}, a_{23}, a_{33}\right)\right)\right) = -\left(I_3 - I_1\right)\omega_3\,\omega_1 \qquad (9.7a\text{-}2)$$

$$N_3 = 0 = -\left(I_1 - I_2\right)\omega_1\,\omega_2 \qquad (9.7a\text{-}3)$$

$$\omega_3\, a_{23} = \omega_2\, a_{33} \qquad (9.7b\text{-}1)$$

$$\omega_1\, a_{33} = \omega_3\, a_{13} \qquad (9.7b\text{-}2)$$

$$\omega_2\, a_{13} = \omega_1\, a_{23} \qquad (9.7b\text{-}3)$$

$$a_{13}^2 + a_{23}^2 + a_{33}^2 = 1\,. \qquad (9.7c)$$

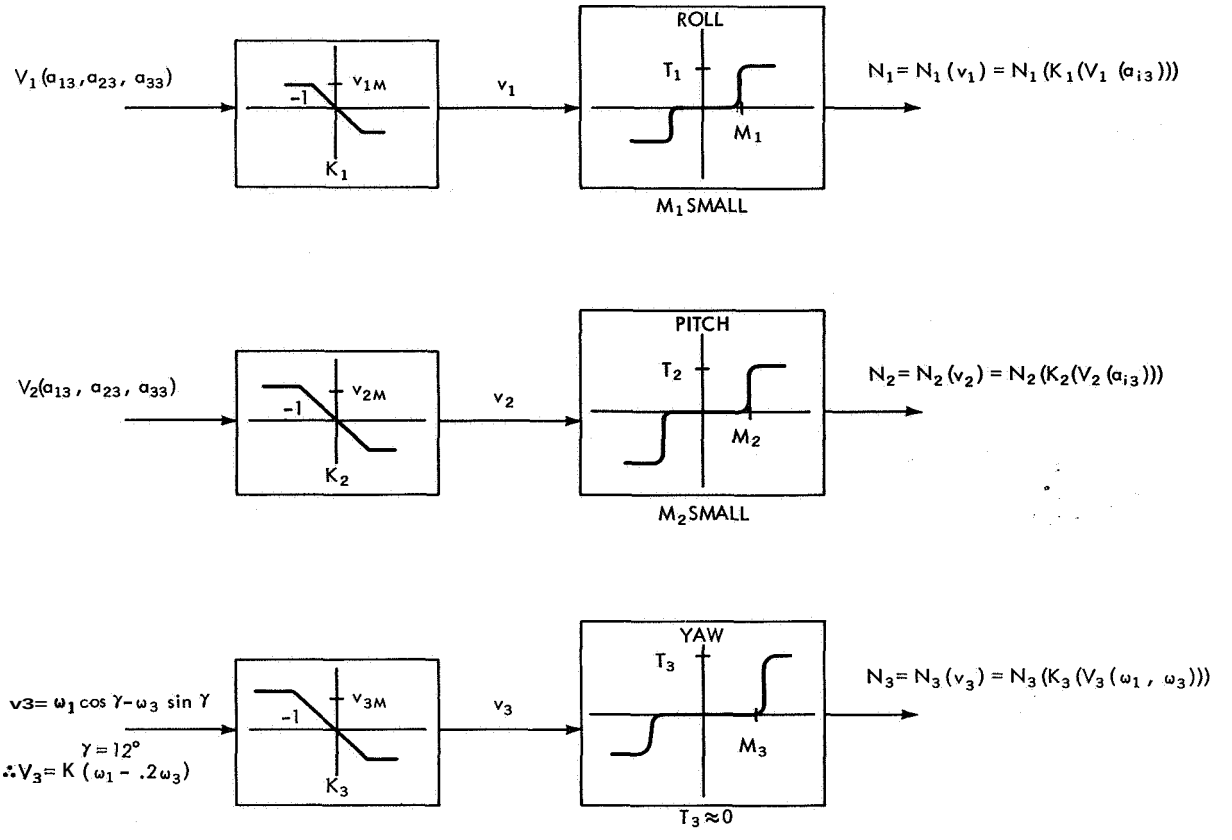

TORQUE ERROR SIGNALS, $v_i = K_i(V_i)$, $i = 1, 2, 3$,
$v_{1M} = v_{2M} = 12°$ SATURATION FOR NIMBUS I

Figure 9.9—Simplified Static Control Laws.

$V_1(a_{13}, a_{23}, a_{33})$ and $V_2(a_{13}, a_{23}, a_{33})$ are given graphically in Figure 9.10 through 9.13. ($V_1(0, 0, 1) = V_2(0, 0, 1) = 0$ by design, to make the origin, $\omega_1 = \omega_2 = \omega_3 = a_{13} = a_{23} = 0$, $a_{33} = 1$ an equilibrium point.) On these curves, $v_1 = K_1(V_1)$ and $v_2 = K_2(V_2)$ (which include all saturations) are indicated by crossed-hatched regions. Thus, N_1 and N_2 are defined. Since a_{33} is redundant via Equation (9.7c), the curves are presented as two projections within the a_{13}-versus-a_{23}-plane unity circles, one for positive a_{33} and one for negative a_{33}. Therefore, only four sets of curves in total are necessary. How they are generated (Reference **32**) is incidental to the discussion. The curves are used as follows: for any (a_{13}, a_{23}), the family of curves (interpolation is needed between curves) have numbers which are in units of degrees, representing the signals fed to the gas bang-off-bang controllers, i.e., $v_i = K_i(V_i(a_{13}, a_{23}, a_3))$ with the crossed-hatched regions representing saturated signals. There are shaded clamped and indeterminant regions that, for example, represent a scan cone completely on the earth so that the error signal depends on a random cold-cloud distribution over the earth at that particular time. Hence, in these regions, the signals are anywhere from minus saturation to plus saturation.

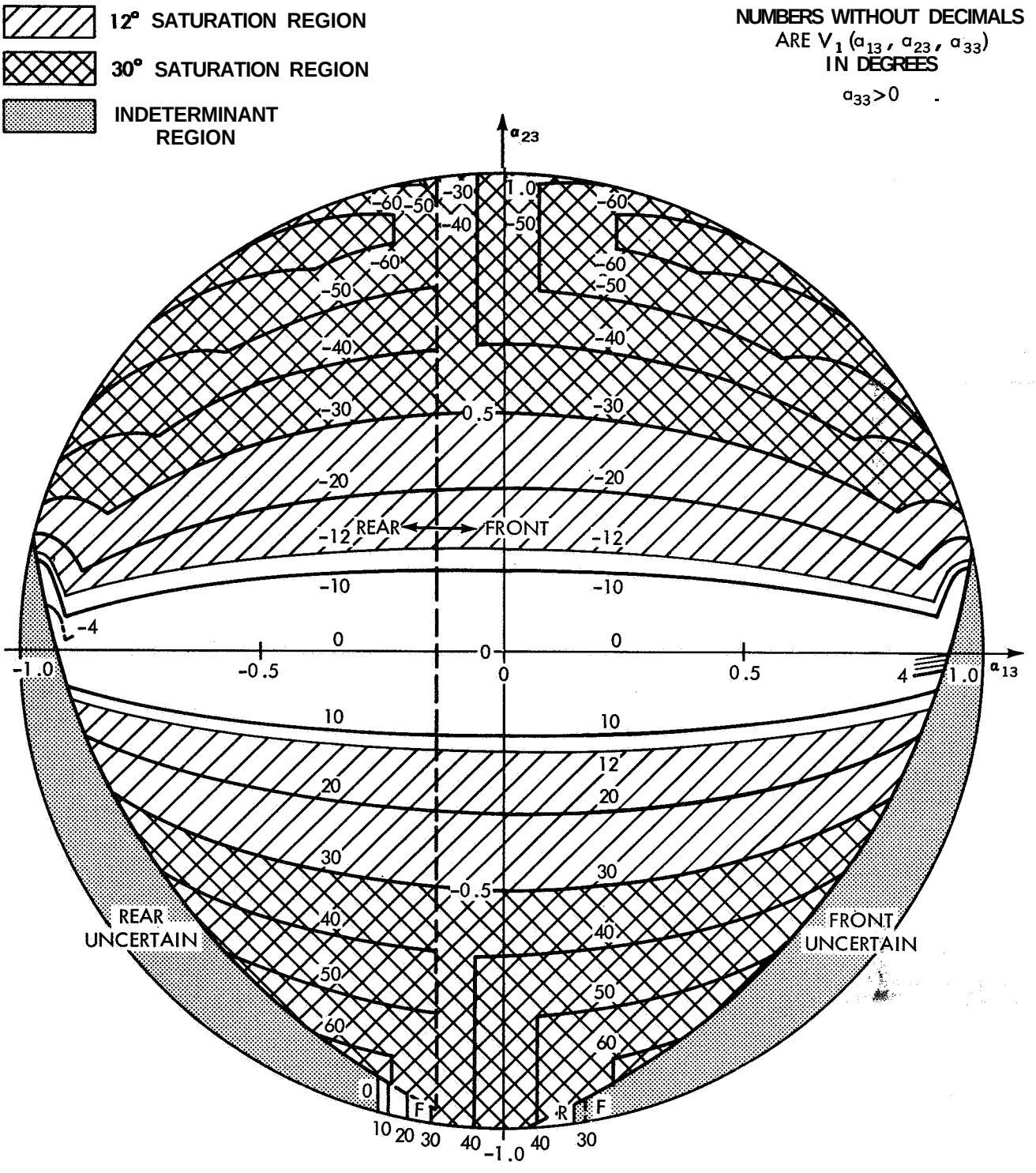

Figure 9.10—Roll Error Versus Attitude, $a_{33} > 0$.

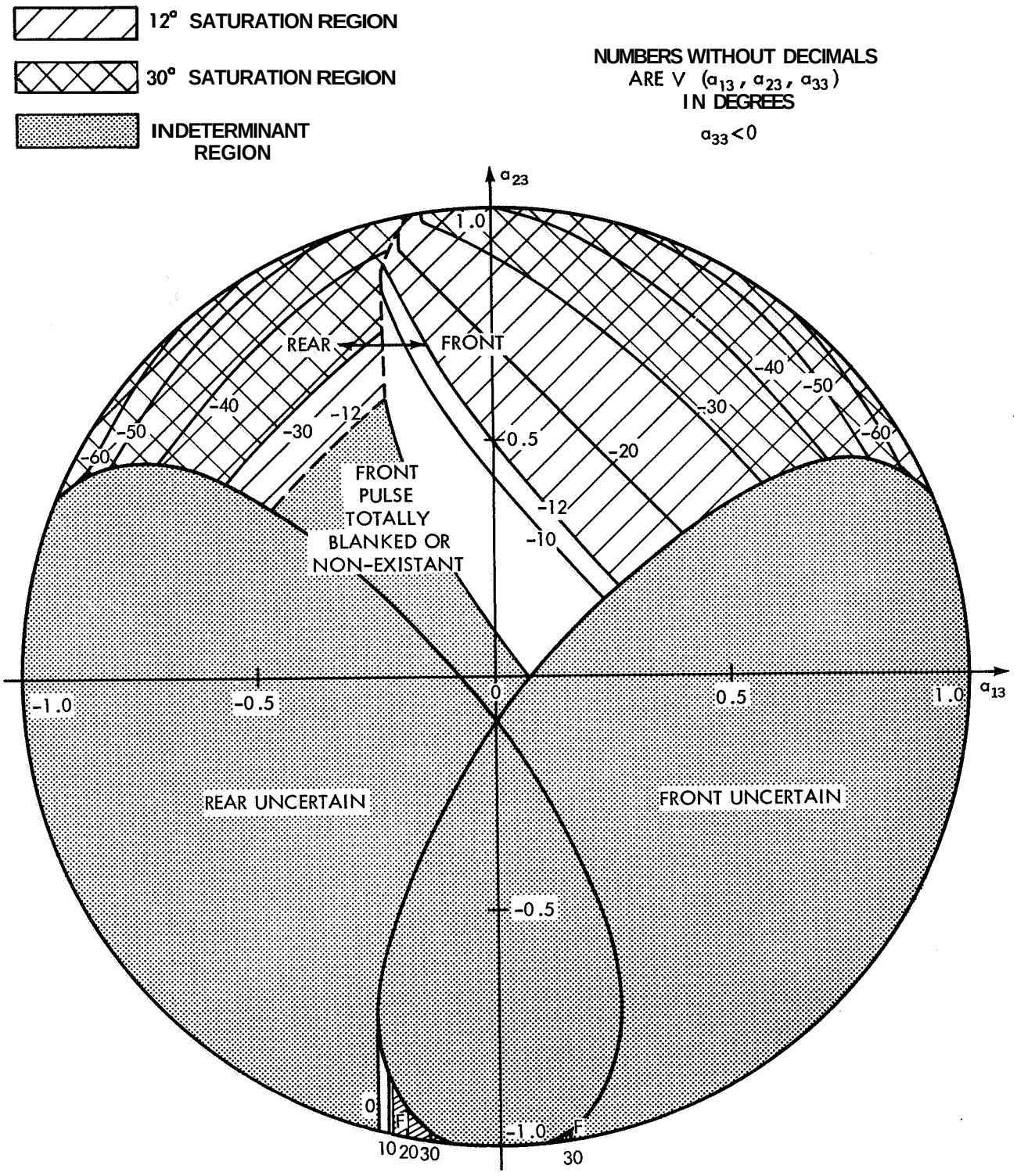

Figure 9.11—Roll Error Versus Attitude, $a_{33} < 0$.

12° SATURATION REGIONS ARE NOT SHOWN

30° SATURATION REGION

INDETERMINANT REGION

NUMBERS WITHOUT DECIMALS
ARE $V_2(a_{13}, a_{23}, a_{33})$
IN DEGREES

$a_{33} > 0$

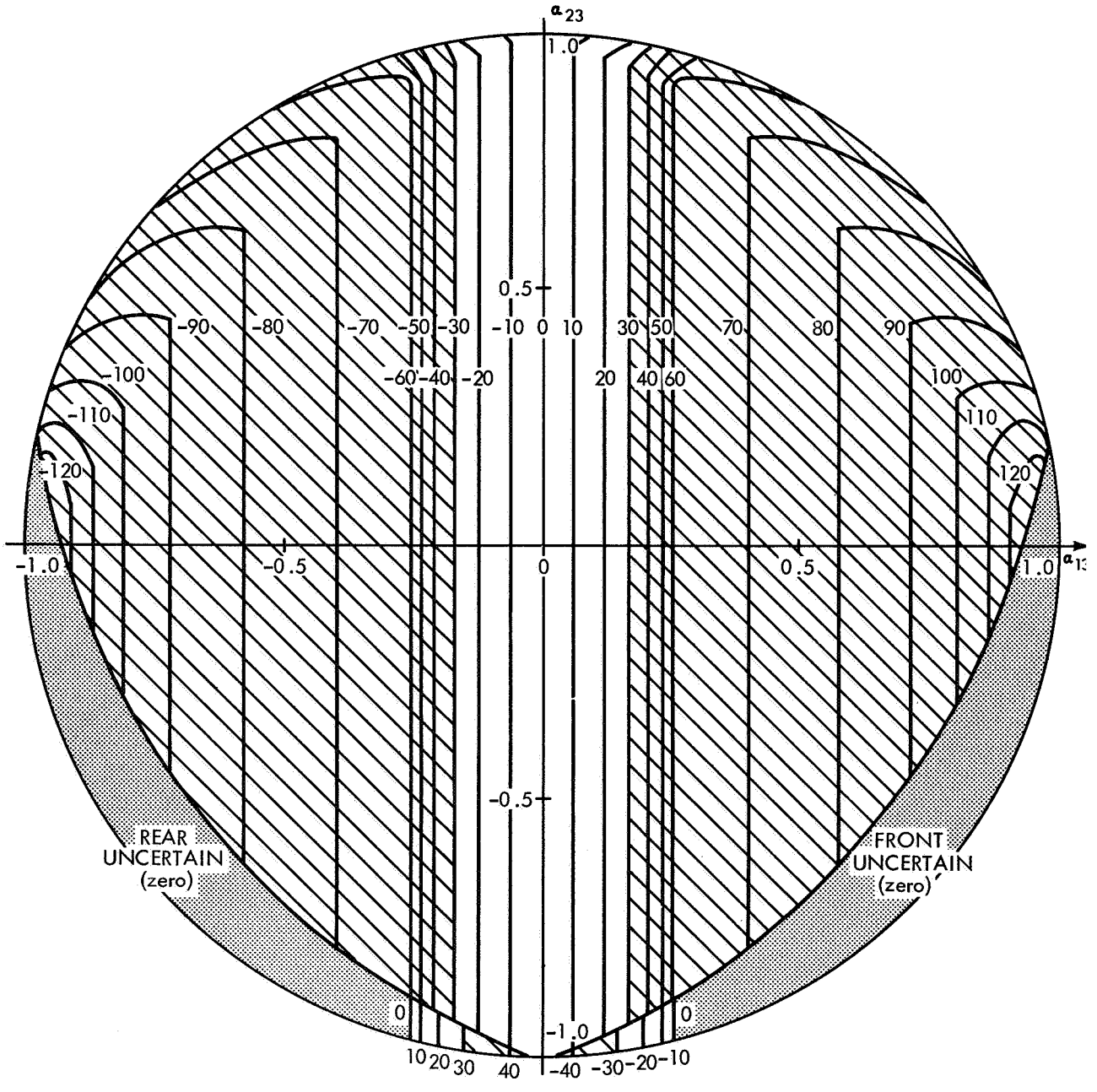

Figure 9.12—Pitch Error Versus Attitude, $a_{33} > 0$.

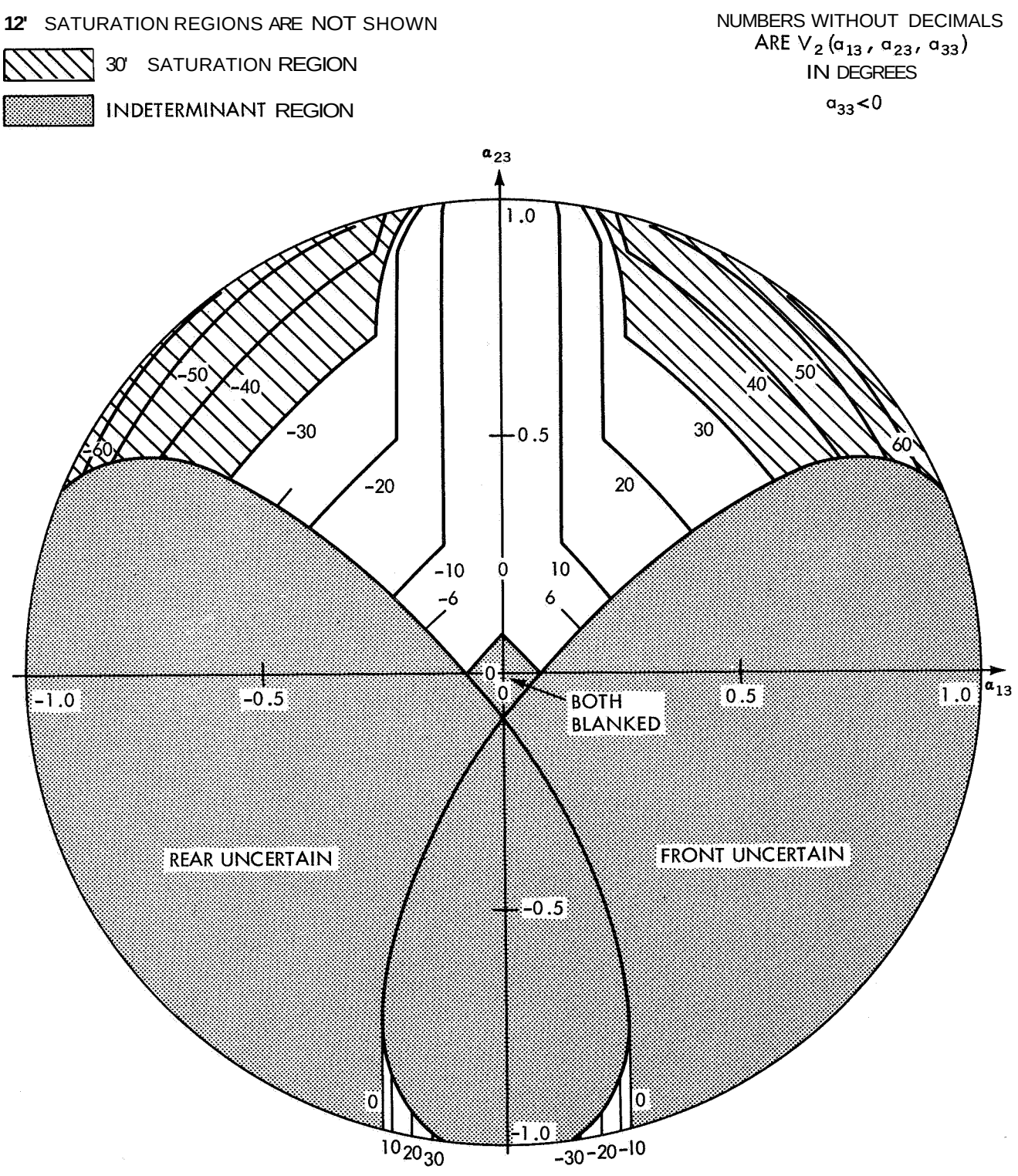

Figure 9.13—Pitch Error Versus Attitude, $\alpha_{33} < 0$.

Equations (9.7) are now solved. From (9.7a-3), either ω_1 or ω_2 (or both) are zero. If $\omega_1 = 0$, then $N_2 = 0$ (therefore $|K_2(V_2)| < M_2$) from (9.7a-2). From Equations (9.7b) either $\omega_2 = \omega_3 = 0$ (therefore $N_1 = 0$), or $\omega_2 = a_{13} = 0$ (therefore $N_1 = 0$), or $\omega_3 = a_{13} = 0$ (therefore $N_1 = 0$), or only a_{13} is zero. The various cases are traced out in Figure 9.14. There are only six distinct categories, as tabulated in Figure 9.15.

Case I, which includes the origin, indicates that if all the rates are zero, any attitude for which the scanners have near-zero output are equilibrium points. From the $K_i(V_i)$ curves, there are many regions where this is true. The only way to eliminate these cases, is to change the sensors and make the deadbands zero. Cases II, III and IV allow ω_i to have any value when

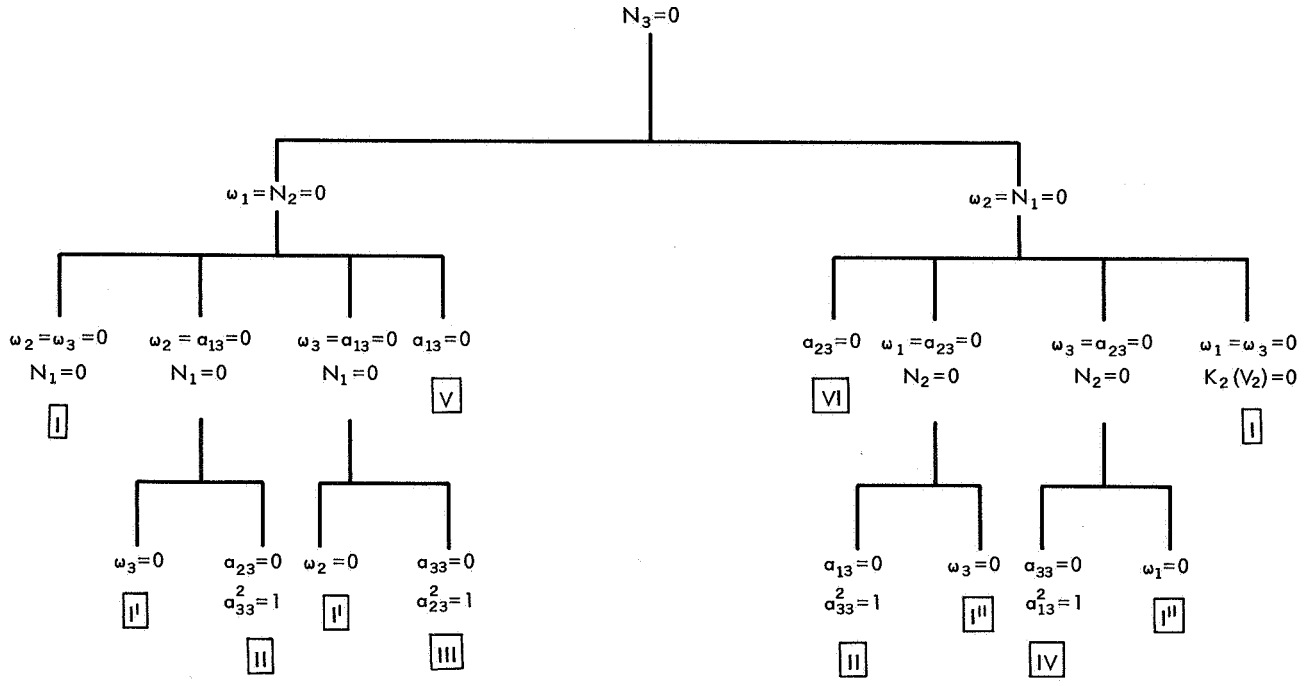

Figure 9.14—Equilibrium Cases.

Case	ω_1	ω_2	ω_3	$a_{33}^2 = 1 - a_{23}^2 - a_{13}^2$		$\lvert K_1(V_1)\rvert$	$\lvert K_2(V_2)\rvert$	$N_3 = 0$		No. of equib. Attitudes
				a_{13}^2	a_{23}^2			N_1	N_2	
I	0	0	0	?	?	$<M_1$	$<M_2$	0	0	Many
II	0	0	?	0	0	$<M_1$	$<M_2$	0	0	2
III	0	?	0	0	1	$<M_1$	$<M_2$	0	0	1
IV	?	0	0	1	0	$<M_1$	$<M_2$	0	0	2
V	0	?	?	0	?	?	$<M_2$	?	0	Many
VI	?	0	?	?	0	$<M_1$	?	0	?	Many

Figure 9.15—Table of Equilibrium Cases.

$a_{i3} = \pm 1$ $(i = 1, 2, 3)$, as long as the sensors have near-zero outputs. Therefore, Case II admits a right-side-up or upside-down spacecraft which is spinning about the yaw $(\hat{x}_3)$ body axis. Case III cannot exist at $a_{23} = \pm 1$, since $K_1(V_1(0, +1, 0)) < -M_1$. However, owing to nonsymmetrical scanners, the $a_{23} = -1$ point can exist. In case IV, the vehicle is pitched 90 degrees and rolling at an arbitrary rate about its plus or minus roll axis which is vertical.

Cases I through IV arise from false nulls of the sensors, that is, near-zero outputs at attitudes other than the origin. This is a sensor problem that is not easy to eliminate. However, in all four cases, no gas is used (i.e., $N_i = 0$, $i = 1, 2, 3$). Hence, there is the comforting fact that the spacecraft is not lost (i.e., gas is not expended) while the long-term effects (gyrocompass, flywheels and other small effects which have been neglected) pull the system away from these points even if they turn out to be stable. These are easy points to put into the full-blown computer simulation, and the behavior can be observed. In fact, these are the obvious points associated with any physical system with non-ideal sensors, and the points are usually easily found. If these points produce instabilities, then there exists the constraint of non-all-attitude stabilization, even from zero rates. Such turns out to be the case for Nimbus I.

It is the more subtle and interesting cases V and VI that are easily overlooked. Here the sensors do not have to have zero outputs; yet the vehicle is in equilibrium and using up gas. These are the "nasty" points that cause trouble in a system design. For illustrative purposes, only Case V is examined, since Case VI is analogous. First, $K_1(V_1)$ curves are used, and only the regions of a_{13}, a_{23} where the $|K_2(V_2)|$ curves are $< M_2$ are considered. These regions are the a_{23} axes and the three shaded areas shown in Figures 9.12 and 9.13. In these regions, if $\omega_1 = 0$, which it does as seen from Equation (8.4), then Equations (9.7a-2 and -3) are satisfied. But for Case V, $a_{13} = 0$ is necessary to satisfy Equations (9.7b-2 and -3) as indicated in Figure 9.15. Thus in Figures 9.12 and 9.13 only the a_{23} axes need be considered, The remaining relationships from Equations (9.7) are

$$a_{33}^2 = 1 - a_{23}^2 \tag{9.8a}$$

$$\dot{\omega}_3 a_{23} = \omega_2 a_{33} \tag{9.8b}$$

$$N_1\left(K_1\left(V_1\left(0, a_{23}, \pm\sqrt{1 - a_{23}^2}\right)\right)\right) = -(I_2 - I_3)\,\omega_2\,\omega_3 \,. \tag{9.8c}$$

The control laws approximately yield

$$\begin{aligned}
N_1 &= 0 && \text{for } |K_1(V_1)| < M_1 \\
N_1 &= T_1 && \text{for } K_1(V_1) > M_1 \\
N_1 &= -T_1 && \text{for } K_1(V_1) < -M_1 \\
0 \le N_1 &\le T_1 && \text{for } K_1(V_1) = M_1 \\
-T_1 \le N_1 &\le 0 && \text{for } K_1(V_1) = -M_1 \,,
\end{aligned} \tag{9.9}$$

as shown in Figure 9.9. Now an entire set of equilibrium points is obtained. First, plotting $K_1(V_1)$ from the $K_1(V_1)$ curves with $a_{13} = 0$, and then applying Equation (9.9), yields the $N_1 = N_1(a_{23})$ shown in Figure 9.16. Clearly,

$$\operatorname{sgn}(N_1 a_{23}) = -1 \tag{9.10}$$

for all but the indeterminant region. Combining Equations (9.8) yields

$$\omega_2^2 = -N_1(a_{23})\, a_{23}/R_{23}\, a_{33} \quad , \tag{9.11}$$

where $R_{23} = I_1 - I_3 > 0$ for Nimbus. Therefore, aside from the indeterminant region, real values of ω_2 exist when $a_{33} > 0$, that is, the vehicle is right-side-up. In the indeterminant region, $\operatorname{sgn}(a_{23} a_{33}) = +1$; hence, $N_1 \leq 0$ for an equilibrium to exist. Therefore, a large set of equilibrium points are found in the deterministic right-side-up region. They are:

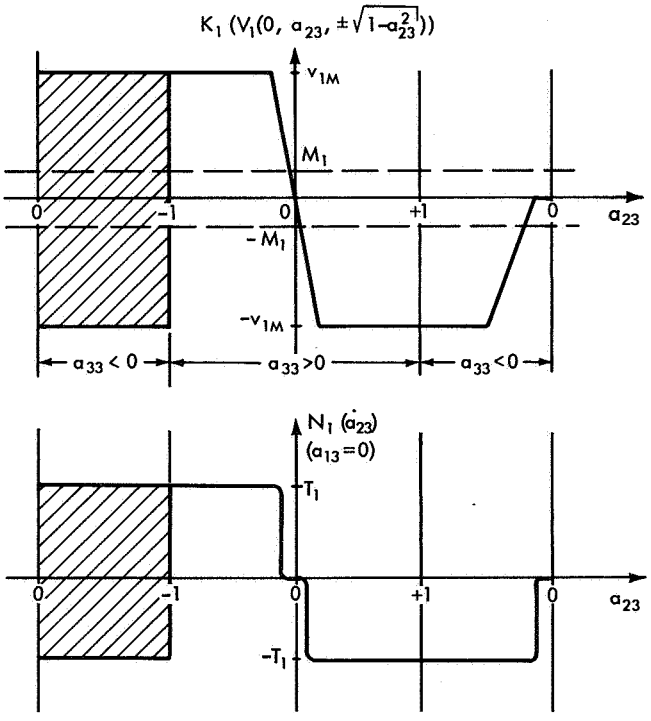

Figure 9.16—N_1 and K_1 versus a_{23}.

$$\begin{aligned}
a_{13} &= 0 \\
a_{23} &= \text{arbitrary} \\
a_{33} &= +\sqrt{1 - a_{23}^2} \\
\omega_1 &= 0 \\
\omega_2 &= \omega_2(a_{23}) \\
\omega_3 &= (a_{33}/a_{23})\,\omega_2 \\
N_1 &= N_1(a_{23}) \\
N_2 &= 0 \\
N_3 &= 0 \quad ,
\end{aligned} \tag{9.12}$$

where $N_1(a_{23})$ is given in Figure 9.16 and

$$\omega_2(a_{23}) = \pm\sqrt{\frac{-a_{23} N_1(a_{23})}{\sqrt{1 - a_{23}^2}\, R_{23}}} \quad , \tag{9.13}$$

which is plotted in Figure 9.17 with Nimbus I numbers. Physically interpreting this equilibrium point, one concludes for $a_{13} = 0$ that the body-roll axis $\hat{x}_1$ remains perpendicular to the local vertical $\hat{y}_3$. Hence, as a_{23} varies while $a_{13} = 0$, the spacecraft is rolled about the body-roll axis. In fact, for the yaw, roll, pitch Euler angle sequence such as described in Chapter 6, the a_{23} direction cosine is expressed as

$$a_{23} = \sin\phi \quad , \tag{9.14}$$

where ϕ is the roll angle. Thus, rolling the spacecraft by an angle ϕ generates a signal to fire roll gas, and the roll torque is just enough to counteract the pitch-yaw coupling torque so that ω_1 remains zero and all state variables are constant.

The stability of this equilibrium point (actually set of points in state space) described by Equation **(9.12)** for the case of $a_{23} > 0$ and $N_1 < 0$ is examined by the methods developed in Chapter **8.** In Figure **9.18,** there are plots of the three $\dot{\omega}_i$-vs-ω_i parabolas as in Figure **8.1,** but with the polarities and numbers of the present equilibrium point.

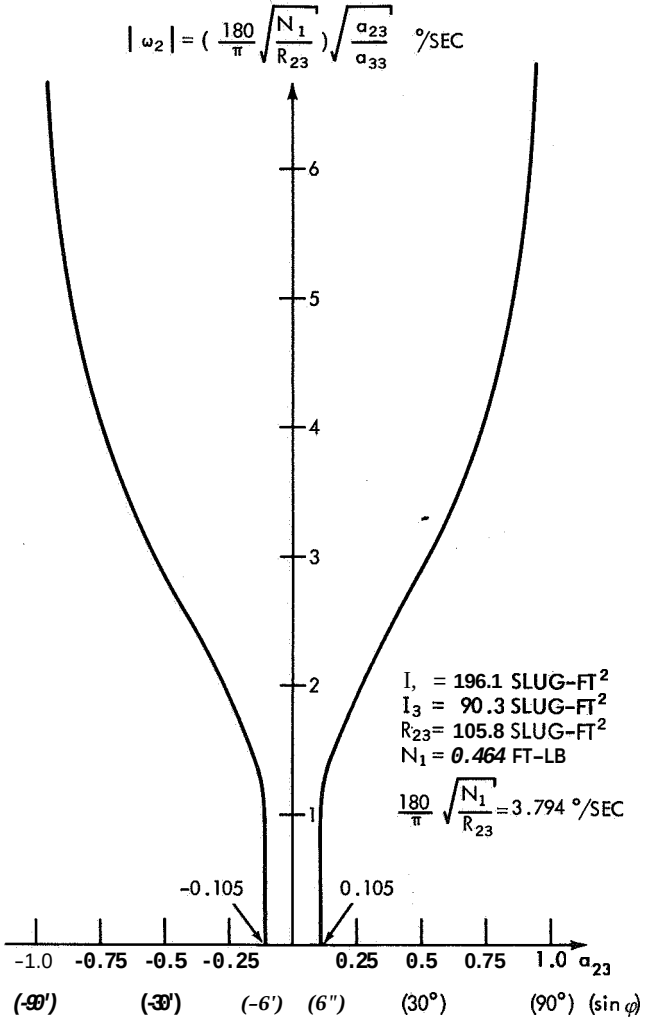

Figure 9.17— $|\omega_2|$ versus a_{23}.

The parabolas in Figure **9.18** are degenerate, as is always true whenever an $a_{i3} = 0$ $(i = 1, 2, 3)$ at the equilibrium point. For this vehicle, five cases fit this degenerate category with only Case I an exception (as seen from the table in Figure **9.15).** No real stability information is obtained from the straight line parabolas other than that (assuming ω_2 and ω_3 are both positive) a negative perturbation of N_1 and N_2 drives the system slowly away from equilibrium (as in the first 2 parabolas of Figure 8.1), and a positive N_2 and N_3 perturbation drives the system back (as in the last parabola in Figure **8.1).** The important point is that all possible locations of equilibrium points have been determined and the computer is used efficiently. For Nimbus, the computer responses, starting at many of the equilibrium points, meandered around in almost

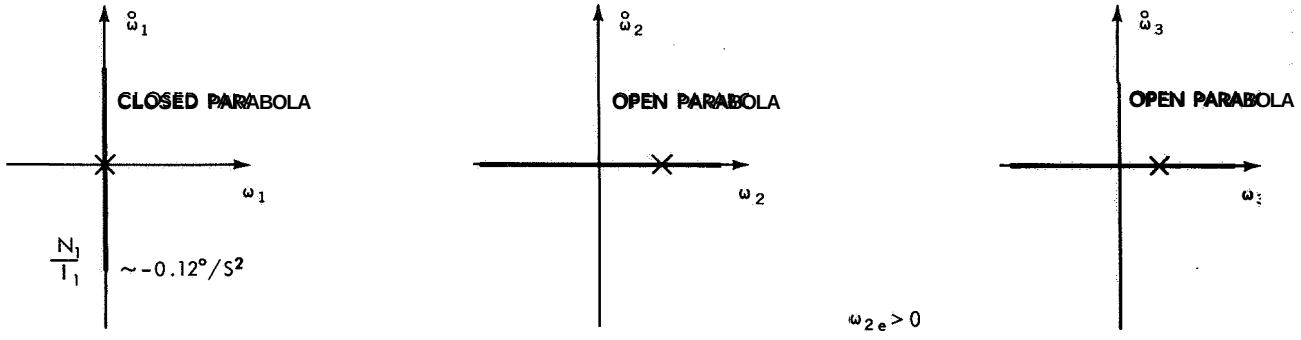

Figure 9.18—Degenerate Stability Parabolas.

closed limit cycles, and then converged or diverged. It is apparent that these are marginal cases, and second-order effects such as the initial momentum stored in a flywheel (completely neglected in this analysis) determine stability. It is emphasized that the only undesirable responses that occurred in the hundreds of thousands examined, were associated with equilibrium points! This lends much engineering credence to the ***power*** and ***usefulness*** of a ***thorough equilibrium approach.***

It is mentioned in the beginning of this chapter how proposed new computer verified control laws for Nimbus II and III were discarded because of equilibrium points. One of these schemes is essentially to raise the yaw torque level N_3 back up to the same level as N_1 and N_2. Because of the problem mentioned on page 91 of yaw torque firing mainly due to roll rate, it is attempted to cancel out the roll rate information from the gyro compass. This is accomplished by taking the roll horizon scanner signal ϕ, putting it through a lead network to get approximately $\phi + K\dot{\phi}$, subtracting the original roll signal ϕ, and feeding the result ($\approx -\dot{\phi}$) into the yaw channel. That is working with ***small*** Euler angles,

$$\omega_1 \approx \dot{\phi} - \Omega_0 \psi \quad , \tag{9.15}$$

where the yaw error term ψ is wanted and the roll-rate term $\dot{\phi}$ is the unwanted coupling. Therefore, $\dot{\phi}$ is generated so that it can be subtracted from Equation (9.15). At the same time, since the gyro-compass signal couples the roll and yaw channels, and since this signal contains five times more roll rate than yaw rate, why not feed its output signal into the roll loop? These new control laws logically sound good, and they are very good for small angles. As it turned out, the computer results via many runs also indicated that the system seemed good, or at least better than the original system for large angles. However, the same initial conditions were used to compare both systems. This new system is now viewed through an equilibrium approach.

The simplified control laws are given in Figure 9.19. The steady-state control-law equations are

$$\begin{aligned} \epsilon_1 &= v_1' - v_3 \\ \epsilon_2 &= v_2 \\ \epsilon_3 &= v_1 + v_3 \quad , \end{aligned} \tag{9.16}$$

where v_1, v_1', and v_2 are statically shown in Figures 9.10 to 9.13. v_1' is the same as v_1 except that the saturation level is 30 degrees rather than 12 degrees,

$$v_3 = \begin{cases} -9\omega_1 + 1.9\omega_3 & \text{for } |-9\omega_1 + 1.9\omega_3| < 27.6 \text{ deg} \\ 27.6\,\mathrm{sgn}(-9\omega_1 + 1.9\omega_3) & \text{for } |-9\omega_1 + 1.9\omega_3| \geq 27.6 \text{ deg} \quad , \end{cases} \tag{9.17}$$

(all ω's are in degrees/sec), and the N_i's ($i = 1, 2, 3$) are bang-off-bang functions of the ϵ_i as shown in Figure 9.8b.

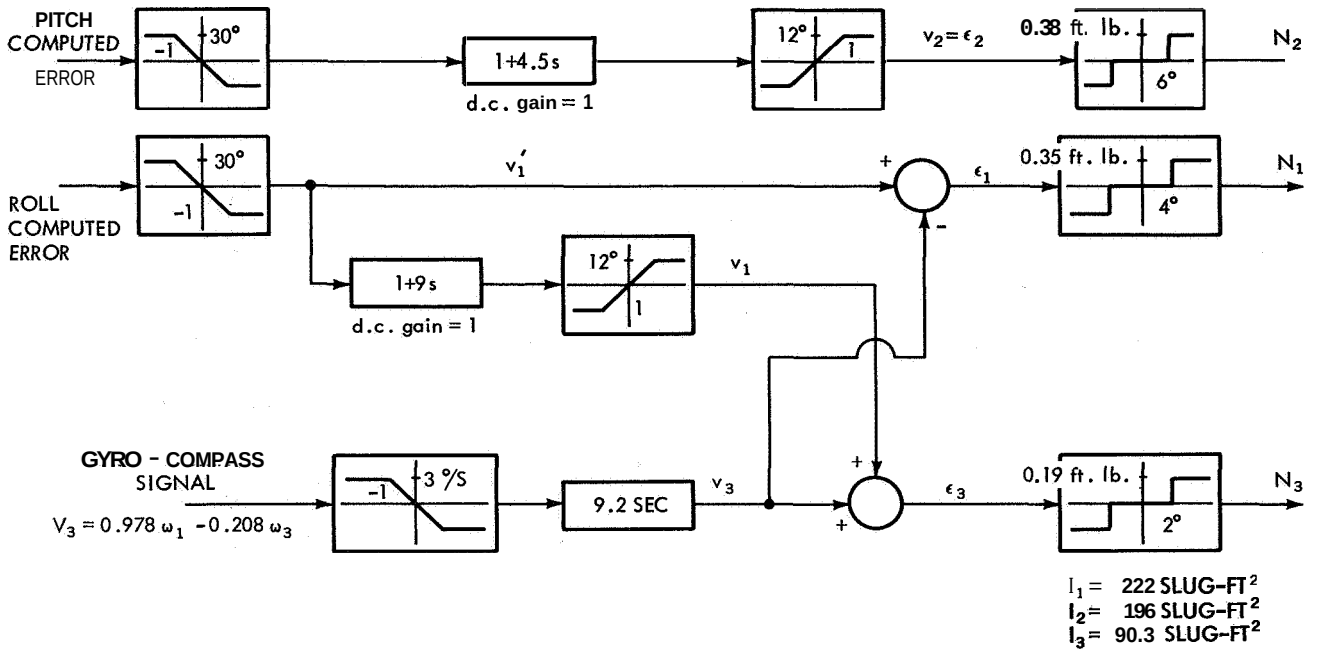

Figure 9.19—Proposed Control Laws.

This system has **42** distinct cases which are equilibrium points (Reference **27).** The cases are established by taking all **27** combinations of the following torque laws:

$$
\begin{array}{lll}
N_1 = 0, \quad |\epsilon_1| < 4 \text{ deg} & N_2 = 0, \quad |\epsilon_2| < 6 \text{ deg} & N_3 = 0, \quad |\epsilon_3| < 2 \text{ deg} \\
N_1 = 0.35, \quad \epsilon_1 \geq 4 \text{ deg} & N_2 = 0.38, \quad \epsilon_2 \geq 6 \text{ deg} & N_3 = 0.19, \quad \epsilon_3 \geq 2 \text{ deg} \\
N_1 = -0.35, \quad \epsilon_1 \leq -4 \text{ deg} & N_2 = -0.38, \quad \epsilon_2 \leq -6 \text{ deg} & N_3 = -0.19, \quad \epsilon_3 \leq -2 \text{ deg} \\
0 \leq N_1 \leq 0.35, \quad \epsilon_1 = 4 \text{ deg} & 0 \leq N_2 \leq 0.38, \quad \epsilon_2 = 6 \text{ deg} & 0 \leq N_3 \leq 0.19, \quad \epsilon_3 = 2 \text{ deg} \\
-0.35 \leq N_1 \leq 0, \quad \epsilon_1 = -4 \text{ deg} & -0.38 \leq N_2 \leq 0, \quad \epsilon_2 = -6 \text{ deg} & -0.19 \leq N_3 \leq 0, \quad \epsilon_3 = -2 \text{ deg}.
\end{array}
\tag{9.18}
$$

Sometimes graphical techniques are required to solve the algebraic system of relationships unless **a** computer is used for the tedious **task.** Instead of all of the points, for illustrative purposes only one point is investigated. This point is categorized under Case 111 in Reference **27,** and is one of the "holes" in a computer-derived "stable region" mentioned in the beginning of this chapter. It is a case for which

$$
\begin{array}{lll}
N_1 = 0.35 \text{ ft-lb} & \epsilon_1 > 4 \text{ deg} & \text{(full On)} \\
N_2 = 0.38 \text{ ft-lb} & \epsilon_2 > 6 \text{ deg} & \text{(full on)} \\
0 \leq N_3 \leq 0.19 \text{ ft-lb} & \epsilon_3 = 2 \text{ deg} & \text{(duty-Cycling)}.
\end{array}
\tag{9.19}
$$

Equations (9.7), (9.16), (9.17), and (9.19) are all simultaneously satisfied, and they reduce to:

$$\omega_2 \omega_3 = -10.9(\text{deg/s})^2 \tag{9.20a-1}$$

$$\omega_3 \omega_1 = +9.52(\text{deg/s})^2 \tag{9.20a-2}$$

$$\omega_1 \omega_2 = -130N_3(\text{deg/s})^2, \qquad 0 \leq N_3 \leq 0.19 \text{ ft-lb} \tag{9.20a-3}$$

$$\omega_3 a_{23} = \omega_2 a_{33} \tag{9.20b-1}$$

$$\omega_1 a_{33} = \omega_3 a_{13} \tag{9.20b-2}$$

$$\omega_2 a_{13} = \omega_1 a_{23} \tag{9.20b-3}$$

$$a_{13}^2 + a_{23}^2 + a_{33}^2 = 1 \tag{9.20c}$$

$$\epsilon_1 = v_1'(a_{13}, a_{23}) - v_3(\omega_1, \omega_3) > 4 \text{ deg} \tag{9.20d-1}$$

$$\epsilon_2 = v_2(a_{13}, a_{23}) > 6 \text{ deg} \tag{9.20d-2}$$

$$\epsilon_3 = v_1(a_{13}, a_{23}) + v_3(\omega_1, \omega_3) = 2 \text{ deg}, \tag{9.20d-3}$$

where v_1', v_1 and v_2 are given graphically, and v_3 is given in Equation (9.17).

Equations (9.20a-1, 2) combine with (9.20b-3) to yield

$$\frac{a_{23}}{a_{13}} = \frac{\omega_2}{\omega_1} = \frac{-10.9}{9.52} = -1.145, \tag{9.21}$$

which plots as a straight line in the a_{13}-a_{23} plane.

Equations (9.20a-2, 3) are combined with (9.20b-1) and (9.20c) to yield

$$\left(\frac{\omega_3}{\omega_2}\right)^2 = \left(\frac{9.52}{-130N_3}\right)^2 = \left(\frac{a_{33}}{a_{23}}\right)^2 = \frac{1 - a_{13}^2 - a_{23}^2}{a_{23}^2}$$

or

$$a_{13}^2 + \left(1 + \frac{0.00536}{N_3^2}\right) a_{23}^2 = 1, \tag{9.22}$$

which is a family of ellipses ($0 \leq N_3 \leq 0.19$) in the a_{13}-a_{23} plane.

For the case where N_3 is full-on positive, negative, or completely off, Equation (9.22) represents a single (possible degenerate) ellipse, and has in general eight common solutions with Equation (9.21), four each for positive and negative a_{33}. Four of these cases are eliminated by the polarity table, Table 8.2. For the remaining four, Equations (9.20a) are solved explicitly for the three ω's, v_3 is computed, and the control-law inequalities (9.20d) are checked. This procedure yields all the equilibrium points. When none of the N's are duty-cycling, the procedure is simple and straightforward, since the ω's can be determined. It is when one or

more of the N's have any value (within bounds) such as this illustrative case, that the procedure is more involved.

The constraint Equation (9.20d-2) permits one to plot the straight line of Equation (9.21) on the graphs of Figures 9.12 and 9.13. The only valid regions are approximately

$$\begin{aligned} 0.11 \le a_{13} \le 0.66, \qquad & a_{33} > 0 \\ 0.04 \le a_{13} \le 0.66, \qquad & a_{33} < 0 \end{aligned} \tag{9.23}$$

such that ϵ_2 is greater than 6 degrees. Using Equation (9.21) again as a straight line, but this time plotted on Figures 9.10 and 9.11, one can graph v_1 and v_1' as a function of a_{13}. These are shown in Figure 9.20, but only for a_{13} positive because of (9.23). The shaded regions are the indeterminate regions. No value is defined for $a_{13} > 0.66$, in order not to violate Equation (9.21), or (9.23).

Since the set of Equations (9.20a, b, c) has one more variable than independent relationship, it is possible to express all the rates and direction cosines in terms of N_3. Manipulating Equations (9.20a) yields

$$\begin{aligned} \omega_1^2 &= \frac{(9.52)(-130)}{(-10.9)} N_3 \\ \omega_2^2 &= \frac{(-10.9)(-130)}{(9.52)} N_3 \\ \omega_3^2 &= \frac{(-10.9)(9.52)}{(-130) N_3} . \end{aligned} \tag{9.24}$$

Using these relationships in conjunction with Equations (9.20b, c) one obtains

$$\begin{aligned} a_{13}^2 &= \frac{(9.52)^2 (-130)^2 N_3^2}{D(N_3)} \\ a_{23}^2 &= \frac{(-10.9)^2 (-130)^2 N_3^2}{D(N_3)} \qquad (9.25a) \\ a_{33}^2 &= \frac{(-10.9)' (9.52)'}{D(N_3)} , \qquad (9.25a) \end{aligned}$$

where

$$D(N_3) = (-10.9)^2 (9.52)^2 + \left[(-10.9)^2 + (9.52)^2\right] (-130)^2 N_3^2 . \tag{9.25b}$$

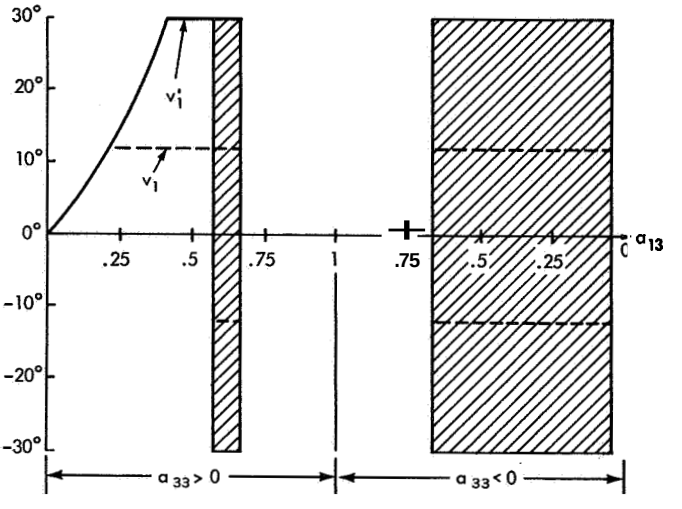

Figure 9.20—v_1, v_1' versus a_{13}.

Hence, once N_3 is known, the equilibrium point is defined. To obtain the values of N_3, the deadband Equation (9.20d-3) is used in a graphical solution. That is,

$$v_1\left(a_{13}, a_{23}(a_{13})\right) = 2 - v_3\left(\omega_1\left(N_3(a_{13})\right), \omega_3\left(N_3(a_{13})\right)\right) . \tag{9.26}$$

From Equations (9.20a-2) and (9.24),

$$v_3' = -9\omega_1 + 1.9\omega_3 = \omega_3\left[1.9 - \frac{}{}\right]$$

$$= \left[\operatorname{sgn}(\omega_3)\right]\sqrt{\frac{(-10.9)(9.52)}{(-130)N_3}}\left[1.9 - \frac{(9)(-130)}{(-10.9)}N_3\right] . \tag{9.27}$$

But, from Equation (9.25), realizing $N_3 \geq 0$, then

$$N_3 = \sqrt{\frac{(-10.9)^2/(-130)^2}{1/a_{13}^2 - \left[1 + (-10.9)^2/(9.52)^2\right]}} . \tag{9.28}$$

Hence, Equation (9.27) becomes

$$v_3' = \sqrt{9.52}\left[1.9\, f(a_{13}) - 9/f(a_{13})\right]\left[\operatorname{sgn}(\omega_3)\right] , \tag{9.29a}$$

where

$$f(a_{13}) = \left[1/a_{13}^2 - 1 - (-10.9)^2/(9.52)^2\right]^{1/4} . \tag{9.29b}$$

From Equation (9.17),

$$v_3 = \begin{cases} v_3' & \text{for } |v_3'| < 27.6 \\ 27.6\ \operatorname{sgn}(v_3') & \text{for } |v_3'| \geq 27.6 \end{cases} , \tag{9.30}$$

and $(2 - v_3)$ is plotted in Figure 9.21 for positive a_{13}. Also, $v_1(a_{13})$ from Figure 9.20 is plotted in Figure 9.21, and Equation (9.26) indicates that the intersections of the two curves are the desired equilibrium points. Thus, there are two determinate-region equilibrium points for $a_{33} > 0$, and a range of indeterminate-region points for $a_{33} < 0$. All these points satisfy Equation (9.23), which ensure satisfaction of (9.20d-2). Equation (9.20d-1) is clearly satisfied by v_1' being sufficiently large. Hence, all the equilibrium points corresponding to (9.19) are determined. Summarizing the values for the two right-side-up (i.e., positive a_{33}) points,

Equations (9.28), (9.24) and (9.25) yield, for the first point,

$$a_{13} = 0.122$$

$$a_{23} = -0.139 \qquad \textbf{(9.31a)}$$

$$a_{33} = 0.983 \qquad \textbf{(9.31a)}$$

$$\omega_1 = -1.08 \text{ deg/sec}$$

$$\omega_2 = 1.24 \text{ deg/sec} \qquad \textbf{(9.31b)}$$

$$\omega_3 = -8.79 \text{ deg/sec} \qquad \textbf{(9.31b)}$$

$$N_1 = 0.35 \text{ ft-lb}$$

$$N_2 = 0.38 \text{ ft-lb} \qquad \textbf{(9.31c)}$$

$$N_3 = 0.0103 \text{ ft-lb} \qquad \textbf{(9.31c)}$$

(i.e., N_3 has a 5.4 percent duty cycle)

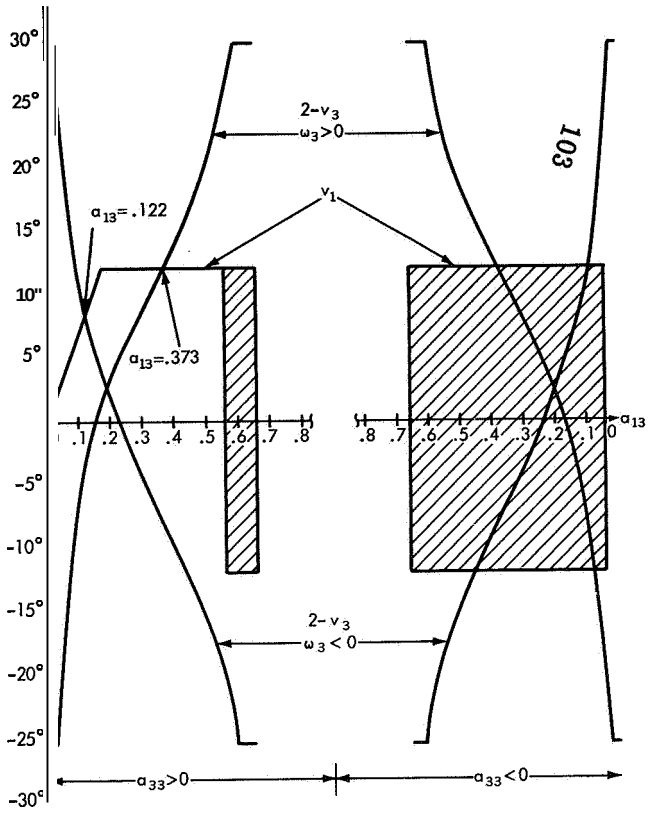

Figure 9.21—v_1 and $2 - v_3$ versus a_{13}.

$$v_1 = 8.9 \text{ deg}$$

$$v_1' = 8.9 \text{ deg}$$

$$v_2 = 7 \text{ deg} \qquad \textbf{(9.31d)}$$

$$v_3 = -6.9 \text{ deg}$$

$$\epsilon_1 = 15.8 \text{ deg} > 4 \text{ deg}$$

$$\epsilon_2 = 7 \text{ deg} > 6 \text{ deg} \qquad \textbf{(9.31e)}$$

$$\epsilon_3 = 2 \text{ deg},$$

and for the second point,

$$a_{13} = 0.373$$

$$a_{23} = -0.428 \qquad \textbf{(9.32a)}$$

$$a_{33} = 0.823$$

$$\omega_1 = 2.08 \text{ deg/sec}$$
$$\omega_2 = -2.38 \text{ deg/sec} \qquad (9.32b)$$
$$\omega_3 = 4.58 \text{ deg/sec}$$

$$N_1 = 0.35 \text{ ft-lb}$$
$$N_2 = 0.38 \text{ ft-lb} \qquad (9.32c)$$
$$N_3 = 0.0380 \text{ ft-lb}$$

(i.e., N_3 has a 20 percent duty cycle)

$$v_1 = 12 \text{ deg}$$
$$v_1' = 27.5 \text{ deg} \qquad (9.32d)$$
$$v_2 = 12 \text{ deg}$$
$$v_3 = -10 \text{ deg}$$

$$\epsilon_1 = 37.5 \text{ deg} > 4 \text{ deg}$$
$$\epsilon_2 = 12 \text{ deg} > 6 \text{ deg} \qquad (9.32e)$$
$$\epsilon_3 = 2 \text{ deg} .$$

The first equilibrium point, which is described by Equations (9.31), has a relatively high yaw rate, $\omega_3 = -8.8$ degrees/sec. The design goal was a three-dimensional rate envelope of 6 degrees/sec, within which all initial attitudes produced stable responses. Hence, this point is not of much concern. However, the second point, which is described by Equation (9.32), is definitely of much concern, since the three rates are in the region of interest. Also, the attitude of the spacecraft is such that the yaw axis $\hat{x}_3$ is only about 35 degrees from the local vertical $\hat{y}_3$, that is, $a_{33} = 0.823$. Previous to the calculation of this point, the region in six-dimensional state space around the point appeared to be a stable region as a result of many computer runs. For instance, initial conditions of

$$\omega_1 = 2 \text{ deg/sec}$$
$$\omega_2 = -2.5 \text{ deg/sec} \qquad (9.33)$$
$$\omega_3 = 4.5 \text{ deg/sec}$$

were run for 22 strategically located positions on the direction-cosine unity sphere. All the responses were well-behaved. The initial rates were varied in ± 0.25 degrees/sec step

increments such that almost all combinations within the 6 degrees/sec rate envelope were tried, each with 22 starting positions, resulting in hundreds of thousands of computer runs. All those near the rates of (9.33) were stable. However, when the initial conditions of (9.32a, b) were used (after the equilibrium analysis was performed), the system meandered in an almost periodic fashion. The numbers read from the computer were

$$\begin{aligned} a_{13} &\approx 0.36 \pm 0.07 \\ a_{23} &\approx -0.41 \pm 0.03 \\ a_{33} &\approx 0.84 \pm 0.02 \end{aligned} \tag{9.33a}$$

$$\begin{aligned} \omega_1 &\approx 1.95 \pm 0.15 \text{ deg/sec} \\ \omega_2 &\approx -2.4 \pm 0.2 \text{ deg/sec} \\ \omega_3 &\approx 4.9 \pm 0.7 \text{ deg/sec} \end{aligned} \tag{9.33b}$$

and

N_1 full-on positive

N_2 full-on positive

N_3 on positive with about 25-percent duty cycle. (9.33c)

This continued for a long time, using up much precious gas; then finally diverged unstably when the secondary effects (neglected in any paper analysis) grew sufficiently large. (A typical run is Number 181 in Reference 33.) Thus, here is an unstable "hole" in a "stable region." It corresponds to an equilibrium point which is not at all obvious, since the sensors have non-zero (in fact saturated) outputs, and the gas is firing. As evidenced in this chapter, it is not easy to locate these types of points for a highly nonlinear system.

To conclude this chapter, an advanced Nimbus control system design (Nimbus D whose design is just being completed and implementation commenced) is briefly discussed. Emphasis is on the equilibrium approach as a design tool. At the outset, the design goal was a system, stable in the large, for rates up to 6 degrees/sec in all axes for any attitude. The system was to be as simple (hardware-wise) as possible. The previous Nimbus systems all contain only one rate gyroscope as a sensor. However, no control scheme could be devised (and some proposed were quite ingenious) for which no equilibrium points exist in the state-space regions of interest. On the other hand, it is very easy to design a system with three ideal rate gyros for which complete rate stability can be mathematically demonstrated. For example, if one uses variable linear thrusters, the well-known control laws are

$$N_i = -K_i \omega_i \qquad i = 1, 2, 3, \tag{9.34}$$

where $K_i > 0$, and ω_i are the sensed rates. To prove stability, one of many possible suitable Liapunov functions that is chosen is the rotational kinetic energy

$$V = \frac{1}{2} I_1 \omega_1^2 + \frac{1}{2} I_2 \omega_2^2 + \frac{1}{2} I_3 \omega_3^2 \ , \tag{9.35}$$

which, of course, is positive-definite in ω_i. The time-derivative is

$$\dot{V} = I_1 \dot{\omega}_1 \omega_1 + I_2 \dot{\omega}_2 \omega_2 + I_3 \dot{\omega}_3 \omega_3 \ , \tag{9.36}$$

which, when Equations (7.50a) and (9.34) are substituted in, is

$$\begin{aligned} \dot{V} &= N_1 \omega_1 + N_2 \omega_2 + N_3 \omega_3 \\ &= -K_1 \omega_1^2 - K_2 \omega_2^2 - K_3 \omega_3^2 \ . \end{aligned} \tag{9.37}$$

Equation (9.37) is obviously negative-definite. That is, the control laws of (9.34) insure that rotational kinetic energy is always removed from the rigid body until it comes to rest; but it comes to rest at any arbitrary attitude. If one defines ideal position sensors that measure a_{13} and a_{23}, then it is possible to evolve control laws which lend themselves to a mathematical proof of assymptotic stability in the large, for both rates and positions, via Liapunov functions. As an example, from Reference 24, Section 4.3, the following control laws are used:

$$\begin{aligned} N_1 &= -K_1 \omega_1 - C_2 a_{23} \\ N_2 &= -K_2 \omega_2 + C_1 a_{13} \\ N_3 &= -K_3 \omega_3 \ . \end{aligned} \tag{9.38}$$

A suitable Liapunov function is

$$V = \frac{1}{2} \left[I_1 (\omega_1 + A_1 a_{23})^2 + I_2 (\omega_2 - A_2 a_{13})^2 + I_3 \omega_3^2 + B(1 - a_{33})^2 + (B - I_2 A_2^2) a_{13}^2 + (B - I_1 A_1^2) a_{23}^2 \right] , \tag{9.39}$$

where

$$\begin{aligned} &B = A_1 K_1 + C_2 = A_2 K_2 + C_1 \\ &K_1 > A_1 I_1 > 0 \\ &K_2 > A_2 I_2 > 0 \\ &C_1 > 0 \\ &C_2 > 0 \\ &K_3 \geq \frac{\left[A_1 I_1 + A_2 (I_3 - I_1)\right]^2}{4(K_1 - A_1 I_1)} + \frac{\left[A_2 I_2 + A_1 (I_3 - I_2)\right]^2}{4(K_2 - A_2 I_2)} \ , \end{aligned} \tag{9.40}$$

since V is then positive-definite and $\dot{V}$ (proof in Reference 24, Section 4.33) is negative-semi-definite in ω_1, ω_2, ω_3, a_{13}, a_{23}, and $1 - a_{33}$. But as demonstrated earlier in this chapter, sensors are far from ideal and do not yield such things as direction cosines. Also it is more efficient to build nonlinear controllers such as on-off thrusters. Hence, a Liapunov or similar approach, even with the aid of large-capacity digital computers, has not been fruitful up to this time.

For Nimbus D, it was decided that the approach should be a design that eliminates all (but the desired null) equilibrium points from the state-space region of interest using a minimum number of reliable components. This was accomplished with a low-cost, non-inertial quality, spring-restrained gyro (in addition to the high-accuracy gyro-compass used for yaw position information in the fine-accuracy pointing mode). For damping, electronic lead networks are employed. The thrusters are driven by pulse-frequency, pulse-width modulators as shown in Figure 9.22. These are implemented by placing a passive lag network in a feedback path around the usual threshold detector. For a DC input signal x, the output y settles down into a pulse train with the width and frequency of the pulses functions of x. The steady-state duty cycle of Y, defined as on-time divided by on-time plus off-time, is plotted in Figure 9.22 as a function of x. If y is thought of as the driving signal to a solenoid for an idealizedpneumatic system, then the graph in Figure 9.22 is one of normalized torque versus x. The advantages of this control circuit are many. The deadband and full-on characteristics still exist as in a pure bang-bang controller (i.e., K = 0) for small and large error signals. In addition, a linear range exists, since $t_{on} + t_{off}$ is small compared to the time constants of the overall system loops. That is, the steady-state duty cycle acts like a constant torque. The loop provides damping, since a lag in the feedback path is in effect similar to a lead in the feedforward path. (Another point of view is that for large T the integral of torque, i.e., rate damping information, is fed back.) The circuit is analog, simple, reliable, and low-power-consuming. (For a flywheel controller, the pulse modulator allows the use of a very efficiently wound 2-phase servo motor, with an essentially flat torque-speed curve. It is used in an on-off fashion, so that the power efficiency is significantly increased and a linear drive amplifier is not needed. For analysis purposes,

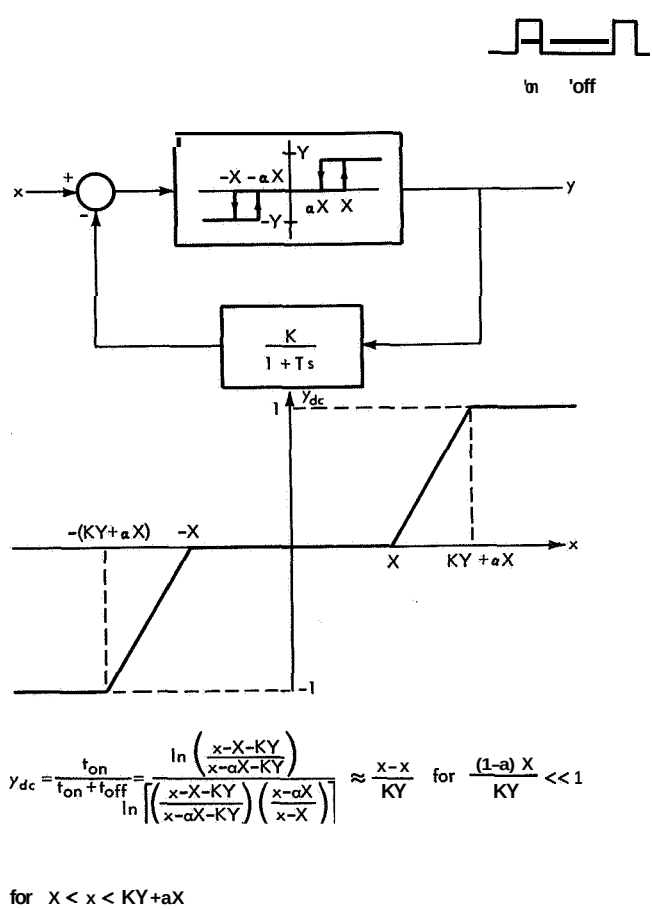

Figure 9.22—Pulse-Frequency, Pulse-Width Modulation Control.

the system acts as if it is linear for fine control.) The dynamic operating range of the torquer is greatly increased. For initial stabilization a large torque is available for quick energy removal, and yet, for fine unloading of the flywheels, extremely small torques are also available. That is, the minimum on-time for a single pulse can be made arbitrarily small, down to the limitations of the hardware,

$$\text{minimum pulse width time} = T \ln \left[\frac{(1-\alpha)X}{KY} - 1 \right] \tag{9.41}$$

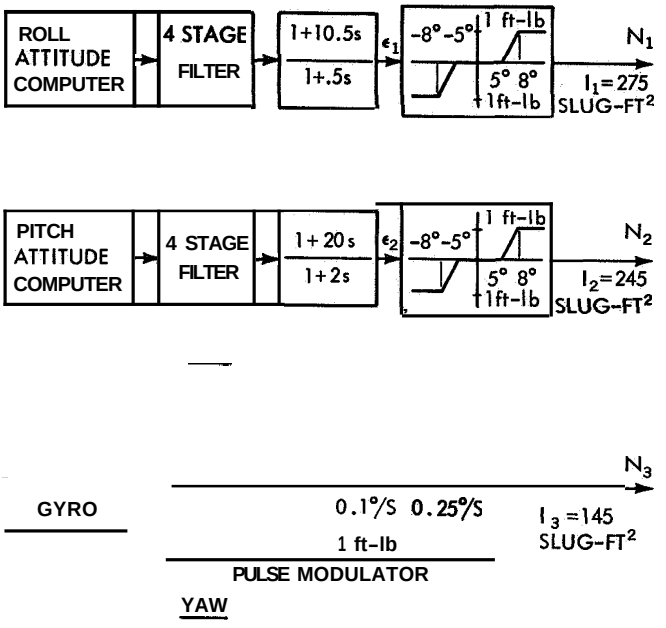

Figure 9.23—Nimbus-D Control Laws.

The small pulse time allows the system to obtain a final limit cycle that has extremely small pulses and long coast periods. The control laws that are designed for Nimbus D are simplified to only essentials shown in Figure 9.23. The yaw torque is as large as roll and pitch, but is controlled by a rate gyro down to 0.1 degree/sec. (The gyro-compass still feeds the fine-loop flywheel which is not shown.) The pulse modulators are represented statically. The roll and pitch information is displayed graphitally. However, this time the horizon sensors and attitude processing is such that no electrical clamping is necessary, thus making the error information symmetrical and determinate, yielding all attitude control. Saturation limits of all the electronics and processing are above the full-on levels of the pulse modulators, and thus do not affect the analysis.

If the assumption is made that the deadband in the yaw loop of Figure 9.23 is zero rather than 0.1 degree/sec, then the yaw torque drives ω_3 to zero. This eliminates the cross-coupling torque terms in the roll and pitch Euler dynamic Equations (7.50a). Hence, at all equilibrium points, N_1 and N_2 are zero. Referring again to the control laws in Figure 9.23, ϵ_1 and ϵ_2 (and thus the roll and pitch computed error signals) lie within the ±5 degree deadbands. For the Nimbus D scanners, this occurs only around the desired equilibrium point and at $a_{13} \approx \pm 1$. Hence, aside from the designed null point, the only equilibrium regions that exist are two mirror images at approximately:

$$\begin{aligned} a_{13} &= \pm 1 & \omega_1 &= \omega_1 & N_1 &= 0 \\ a_{23} &= 0 & \omega_2 &= 0 & N_2 &= 0 \\ a_{33} &= 0 & \omega_3 &= 0 & N_3 &= 0 . \end{aligned} \tag{9.42}$$

There are no others. These are trivial ones, in that they do not use any gas and the sensors have near-zero outputs. They occur when the spacecraft is rotating with an arbitrary rate about its roll axis, $\hat{x}_1$, which is aligned to within about 20 degrees of the local vertical, $\hat{y}_3$. Thus one scanner views only the earth and no sky, and the other scanner views only the sky and no earth. The earth horizons cannot be distinguished and zero errors are developed. (In this attitude the yaw gyro-compass still measures the misalignment between the spacecraft and orbit pitch axes. If there is any error, the yaw wheel speeds up and drives the roll spin axis off the earth. Thus, (9.42) represents unstable equilibrium points and the system does not long remain at the points.) In these attitudes, the solar paddles still fully track the sun, thus not depriving the satellite of any power. If the system gets into these equilibrium conditions, they are safe, short lived, and acceptable.

Much confidence was gained for the Nimbus D control system design by the elimination of equilibrium points via driving ω_3 to near zero. Many computer runs have been successfully made which further solidify one's confidence. However, complete confidence is still out of reach, and much work has yet to be done. At present, one must wait for a flight to point out any remaining flaws in the attitude control system. Then, using actual telemetered performance data, the engineer updates his computer model, and if necessary, betters the system design for the next time (as well as figuring out what, if anything, went wrong in orbit).

10. SUMMARY AND CONCLUSIONS

It is shown in Part I, that if a finite bounded limit cycle exists for the general n^{th}-dimensional system

$$\dot{\bar{x}}(t) = \bar{f}(\bar{x}(t)) \quad , \tag{10.1}$$

then an equilibrium point lies inside the limit cycle. That is,

$$x_{im} < x_{ie} < x_{iM} \; ; \qquad i = 1, 2, \ldots, n \tag{10.2}$$

where $\bar{x}_e$ is an equilibrium point satisfying the relationship,

$$0 = \bar{f}(\bar{x}_e) \quad , \tag{10.3}$$

and x_{im}, x_{iM} are the minimum and maximum values of the $\bar{x}(t) = \bar{x}(t+\tau)$ limit cycle solution. If no equilibrium points exist, then no limit cycles exist. Equation (10.1) represents a physical system such that there exists a unique continuous solution $\bar{x}(t)$ for every initial condition $\bar{x}(0)$.

Furthermore, if Equation (10.1) is linear and admits periodic solutions, then one and only one equilibrium point exists, and it is at the centroid,

$$\bar{x}_e = \bar{x}_a \quad . \tag{10.4}$$

that is, for periodic solutions $\bar{x}(t) = \bar{x}(t+\tau)$, the equilibrium value of each state variable x_i is the average of the periodic function $x_i(t)$;

$$x_{ie} - x_{ia} = \int_t^{t+\tau} x_i(t)\,dt \qquad i = 1, 2, \ldots, n \tag{10.5}$$

In Part II, an equilibrium analysis technique is formulated and illustrated for complex attitude control systems encountered in practice. Since the stability of these systems cannot in general be determined by means of a theoretical analysis, a detailed computer simulation is employed. Various combinations of system parameters and initial conditions require a huge number of computer runs to gain sufficient confidence in the stability of the system throughout the state-space regions of interest. Using an equilibrium approach significantly raises the confidence level and lowers the number of required runs. Troublesome behavior in the physical system is linked to limit-cycle behavior in the mathematical formulation, which is shown to be associated with equilibrium points. Hence, instead of utilizing a uniform or random n-dimensional grid of computer initial conditions, a grid is concentrated around a few calculated points.

As discussed in Part II, completely general systems can be handled, but for illustrative detail, general two-axis stabilized attitude control systems are considered. They are designed to align and hold a spacecraft principle axis to a fixed axis with zero rotational rate (but at an arbitrary angle about the axis). The governing equations are

$$\dot{\omega}_i = \left(\frac{I_j - I_k}{I_i}\right) \omega_j \omega_k + \frac{N_i}{I_i} \left(\omega_i, \omega_j, \omega_k, a_{i3}, a_{j3}, a_{k3}\right) \tag{10.6a}$$

$$a_{i3} = \omega_k a_{j3} - \omega_j a_{k3} \tag{10.6b}$$

$$\sum_{m=1}^{3} a_{m3}^2 = 1 \tag{10.6c}$$

where i, j, k are the cyclic indices 1, 2, 3. The symbols are defined in Chapter 7; the N_i torque functions are defined by control laws for a particular attitude control system. Equilibrium points are the algebraic solutions of Equations (10.6) (with all the derivative terms zero) that simultaneously satisfy the control laws. The following Equations are derived from 10.6:

$$\omega_i^2 = -\frac{N_j N_k}{N_i} \frac{R_{jk}}{R_{ij} R_{ki}} \tag{10.7}$$

or

$$\omega_i^2 = -\frac{a_{i3}^2}{a_{j3} a_{k3}} \frac{N_i}{R_{jk}} \tag{10.8}$$

Table 10.1

$(I_1 > I_2 > I_3 > 0)$

Case	ω_1	ω_2	ω_3	a_{13}	a_{23}	a_{33}	N_1	N_2	N_3
1	+	−	+	+	−	+	+	+	+
2	−	+	−						
3	+	−	+	−	+	−			
4	−	+	−						
5	+	+	−	+	+	−	+	−	−
6	−	−	+						
7	+	+	−	−	−	+			
8	−	−	+						
9	+	+	+	+	+	3	−	+	−
10	−	−	−						
11	+	+	+	−	−				
12	−	−	−						
13	+	−	−	+	−	−	−	−	+
14	−	+	+						
15	+	−	−	−	+	+			
16	−	+	+						

where $R_{ij} = I_i - I_j$. If the moments of inertia of a rigid body are specified, polarity constraints are imposed on the torques and direction cosines, so that the right-hand sides of Equations (10.7) and (10.8) are positive. (These are illustrated by the last six columns of Table 8.2 in Chapter 8, and repeated here as Table 10.1, where $I_1 > I_2 > I_3 > 0$ is assumed for definiteness.) Equation (10.6b), with $\dot{a}_{i3} = 0$, provides the polarity constraints on the rates (with respect to the direction cosines). Hence, all equilibrium points satisfy the polarity relationships given in Table 10.1. The table is a useful tool to help determine equilibrium points.

From Equations (10.6), the following equations of motion are derived

$$\ddot{a}_{i3} + \left(\omega_1^2 + \omega_2^2 + \omega_3^2\right) \dot{a}_{i3} = \left\{ -\frac{3}{2} a_{i3} \frac{d}{dt}\left(\omega_j^2 + \omega_k^2\right) + a_{j3}\left[\frac{d}{dt}\left(\dot{\omega}_k + \omega_i \omega_j\right) + \omega_i \dot{\omega}_j\right] - a_{k3}\left[\frac{d}{dt}\left(\dot{\omega}_j - \omega_i \omega_k\right) - \omega_i \dot{\omega}_k\right]\right\} \quad (10.9)$$

and

$$\dot{w}_i = \frac{N_i}{I_i} + \frac{R_{jk}\, a_{j3}\, a_{k3}}{I_i\, a_{i3}^2}\, \omega_i^2 + \left\{\frac{R_{jk}\, \frac{d}{dt}\left(a_{k3}^2 - a_{j3}^2\right)}{2 I_i\, a_{i3}^2}\, \omega_i - \frac{R_{jk}\, \dot{a}_{k3}\, \dot{a}_{j3}}{I_i\, a_{i3}^2}\right\} \quad (10.10)$$

If the state of the system is sufficiently near an equilibrium point such that the angular rate is slowly varying with time, then Equation (10.9) approximately reduces to the three uncoupled equations,

$$\ddot{a}_{i3} + \omega^2 \left(a_{i3} - a_{i3\,equib}\right) = 0 \quad (10.11)$$

where ω is the magnitude of the (assumed constant) angular rate vector. From the solution to Equation (10.11), it is clear that if a_{i3} is initially near its equilibrium value, then it tends to remain near that value. On the other hand, if the direction cosines are assumed constant near an equilibrium point, but the ω_i's are allowed to vary, then Equation (10.10) reduces to three uncoupled equations in ω_i,

$$\dot{\omega}_i = \frac{N_i}{I_i} + \frac{R_{jk}\, a_{j3}\, a_{k3}}{I_i\, a_{i3}^2}\, \omega_i^2 . \quad (10.12)$$

Thus, if ω_i is initially near an equilibrium value, it moves further or closer depending on the value of $\dot{\omega}_i$. Equation (10.12) is plotted in the 3 phase planes shown in Figure 10.1. The curves are parabolas that are stationary with respect to time for constant N_i. The intersections of the parabolas with the ω_i axis (i.e., $\dot{\omega}_i = 0$) are the equilibrium points of the system given by

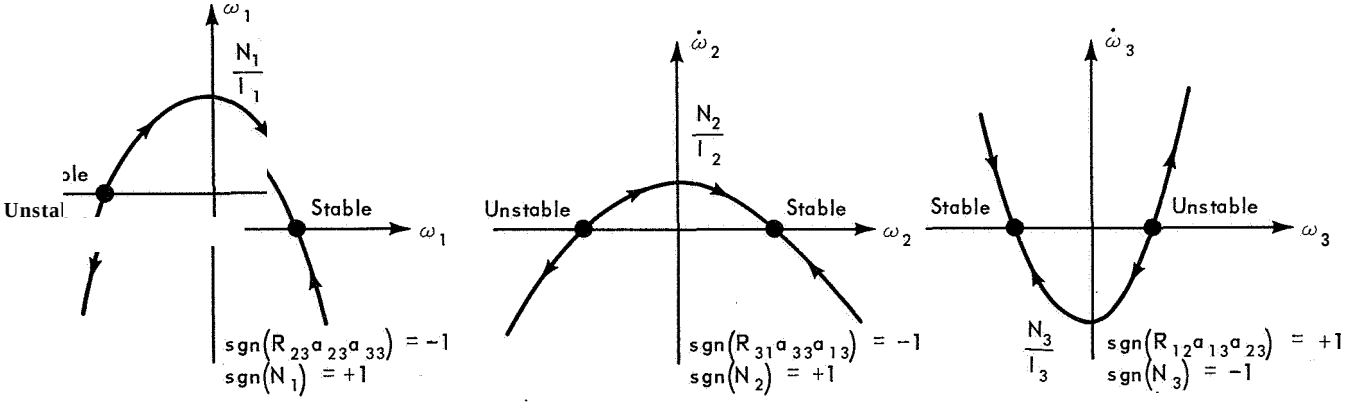

Figure 10.1 –Stability Parabolas.

Equation (10.8). The existence of these Points is determined by $\text{sgn}\left(N_i R_{jk} a_{j3} a_{k3}\right)$, and the stability by $\text{sgn}\left(N_i \omega_{i\,equib}\right) = -\text{sgn}\left(R_{jk} a_{j3} a_{k3} \omega_{i\,equib}\right)$ as is indicated in Figure 10.1.

Once the equilibrium points for an attitude control system are computed, the polarities of $N_i \omega_i$ non-rigorously determine the stability of the points. The stability parabolas shown in Figure 10.1 also yield a relative "feel" for the degree of stability or instability by the slopes of the parabolas at the equilibrium points. Also, in Chapter 8, a linear analysis is performed to show how stability does not directly depend on the equilibrium values of the direction cosines.

Much confidence is gained by a stability analysis of attitude control systems via this equilibrium approach as illustrated by some practical applications in Chapter 9. The design of the Nimbus D control system that eliminates equilibrium points by control laws which drive ω_3 to zero, is an example of how the technique is used as a design tool. However, many computer runs are needed, and complete confidence is still beyond reach. Much work remains to be done in this area. It is still the actual flight that is the best test for discovering any remaining flaws in an attitude control system. Then, using actual telemetered performance data, the engineer updates his computer model for the next flight system.

The attitude control system field is wide-open, interesting, and challenging. Each system is unique unto itself, since no general, powerful, analytical technique exists. Future designs may be based on nonlinear methods (such as a Liapunov approach as in Equation (9.39)), and these methods may be utilized to build optimum, adaptive, or learning attitude control systems via small airborne digital computers. That is, the engineer designs the desired system on paper and then solves a synthesis problem, as opposed to the present method of solving an analysis problem for a system designed mainly on the basis of engineering intuition and experience. However, in this author's opinion, the synthesis approach is a long way off. The fruitful direction for the immediate future is combining semi-analytical tools with the power of a computer simulation.

Goddard Space Flight Center
National Aeronautics and Space Administration
Greenbelt, Maryland, January 4, 1967
879-40-01-05-51

REFERENCES

1. Hochstadt, H., "Differential Equations, A Modern Approach," New York: Holt, Rinehart and Winston, 1965.

2. Ince, E. L., "Ordinary Differential Equations," New York: Dover Publications, 1956.

3. Stoker, J. J., "Nonlinear Vibrations in Mechanical and Electrical Systems," New York: Interscience Publishers, 1950.

4. Bogoliubov, N. N., and Mitropolsky, Y. A., "Assymptotic Methods in the Theory of Non-Linear Oscillations," (Translated from Russian), New York Gordon and Breach Science Publishers, 1961.

5. Minorsky, N., "Nonlinear Oscillations," Princeton, N. J.; D. Van Nostrand, 1962.

6. Hayashi, C., "Nonlinear Oscillations in Physical Systems," New York: McGraw-Hill, 1964.

7. Poincaré, H., Oeuvres. Volume I. "Sur les Courbes Definies par une Equation Differentelle," Paris: Gauthier-Villars, 1928.

8. Hahn, W., "Theory and Application of Liapunov's Direct Method," Englewood Cliffs, N. J.: Prentice-Hall, 1963.

9. Eisenhart, L. P., "A Treatise on the Differential Geometry of Curves and Surfaces," New York Dover Publications, 1960.

10. Taylor, A. E., "Advanced Calculus," Boston, Mass.: Ginn and Company, 1955.

11. Lefschetz, S., "Notes on Differential Equations." (Annals of Mathematical Studies, Number 29, Contributions to the Theory of Nonlinear Oscillations, S. Lefschetz, Volume 11), Princeton, N. J.: Princeton University Press, 1952.

12. Thomas, G. B., Jr., "Calculus and Analytic Geometry," Cambridge, Mass.: Addison-Wesley 1951.

13. Nemyckii, V. V., "Liapunov's Method of Rotating Functions for Finding Oscillatory Regimes," (In Russian). *Doklady Akademii Navk SSR*, 97:33-36, 1954.

14. Bendixson, I, "Sur les Courbes Definies par des Equations Differentielles," *Acta Math:* 24:1-88, 1901.

15. DeBaggis, H. F., "Dynamical Systems with Stable Structures." (Annals of Mathematical Studies, Number 29, Contributions to the Theory of Nonlinear Oscillations, S. Lefschetz, Volume 11), Princeton, N. J.: Princeton University Press, 1952.

16. Lefschetz, S., "Contributions to the Theory of Nonlinear Oscillations," Volumes I, II, III, IV, Princeton, N. J.: Princeton University Press, 1958.

17. Poincaré, H., Oeuvres. Volume I. "Sur les Courbes Definies par les Equations Differentielles, Paris: Gauthier-Villars, 1928.

18. Mendelson, P., "On Phase Portraits of Critical Points in n-Space." (Annals of Mathematical Studies, Number 41, Contributions to the Theory of Nonlinear Oscillations, S. Lefschetz, Volume N), Princeton, N. J.: Princeton University Press, 1958.

19. Haas, F., "On the Total Number of Singular Points and Limit Cycles of a Differential Equation." (Annals of Mathematical Studies, Number 36, Contribution to the Theory of Nonlinear Oscillations, S. Lefschetz, Volume III), Princeton, N. J.: Princeton University Press, 1956.

20. Synge, J. L., and Griffith, B. A., "Principles of Mechanics," New York: McGraw-Hill, 1959.

21. Goldstein, H., "Classical Mechanics." Reading, Mass. : Addison-Wesley Publishing Company, 1959.

22. Whittaker, E. T., "A Treatise on the Analytical Dynamics of Particles and Rigid Bodies," Cambridge, England: Cambridge University Press, 1960.

23. Hillman, A., "Euler Symmetric Parameters," *Israel* Journal of *Technology,* Number (1): 125-130, 1964.

24. Sabroff, A., Farrenhopf, R., Frew, A., and Gran, M., "Investigation of the Acquisition Problem in Satellite Attitude Control" (TRW/STL Technical Report AFFOL-TR-65-115), Wright-Patterson Air Force Base, Ohio: Air Force Flight Dynamics Laboratory, 1965.

25. Thrall, R. M. and Tornheim, L., "Vector Spaces and Matrices," New York Wiley, 1957,

26. Nimbus A Flight 1 Report. NASA/GSFC Document Number 65SD4259, Prepared by Nimbus Technical Control Center under Contract NAS5-3538, 1965.

27. Siegel, S. H., "Equilibrium Points in the STL System," (GE-PIR-9461-162, Rev. 1), Valley Forge, Pennsylvania: G. E. Missile and Space Division, 1964.

28. Barcus, R., "A Functional Description of the Stabilization and Control Subsystem for the Nimbus Satellite (Flight Vehicle)," Revision 1, NASA/GSFC GE Document 63SD4295, 1964.

29. Nimbus Handbook For Experimenters. Prepared by D. Beiber and R. Devlin, Greenbelt, Maryland: Goddard Space Flight Center, 1965.

30. Roberson, R. E., "Methods for the Control of Satellites and Space Vehicles. Volume I—Sensing and Actuating Methods, Volume II—Control System Mechanization and Analysis," Contract No. AF 33(616)-6674, Project No. 8219, Wright-Patterson Air Force Base, Ohio: Wright Air Development Division, 1960.

31. Singer, S. F., "Torques and Attitude Sensing in Earth Satellites," New York Academic Press, 1964.

32. Redisch, W. N., "Development of the Electrical Error Signals for the Nimbus Horizon Sensors," Unpublished Goddard Space Flight Center Report, Greenbelt, Md., 1964.

33. Redisch, W. N., "Computer Runs for the Proposed Nimbus Control Laws," Unpublished Goddard Space Flight Center Report, Greenbelt, Md., 1964.

34. Routh, E. J., "The Advanced Part of a Treatise on the Dynamics of a System of Rigid Bodies," New York: Dover Publications, 1905.

35. Hale, J. K., "Oscillations in Nonlinear Systems," New York: McGraw-Hill, 1963.

36. LaSalle, J. and Lefschetz, S., "Stability by Liapunov's Direct Method with Applications," New York Academic Press, 1961.

37. Truxal, J. G., "Automatic Feedback Control System Synthesis," New York: McGraw-Hill, 1955.

38. Malkin, I. G., "Some Problems in the Theory of Nonlinear Oscillations, 2 Volumes." (Translated from a publication of the State Publishing House of Technical and Theoretical Literature, Moscow, 1956.) United States Atomic Energy Commission, AEC-TR-3766, Physics and Mathematics, 1959.

Appendix A

Dynamic Direction Cosine Constraints

In Chapter 8, from Equations (8.10) and (8.11), that is,

$$\dot{a}_{i3} = \omega_k a_{j3} - \omega_j a_{k3} \tag{A.1}$$

and

$$\sum_{i=1}^{3} a_{i3}^2 = 1 , \tag{A.2}$$

the complex dynamic relationships of Equation (8.13) are derived. The i, j, k are the cyclic indices **1, 2, 3.** As in Chapter 7, the angular velocity vector is defined as

$$\begin{aligned} \bar{\omega} &= \omega_1 \hat{x}_1 + \omega_2 \hat{x}_2 + \omega_3 \hat{x}_3 \\ \omega &= \sqrt{\omega_1^2 + \omega_2^2 + \omega_3^2} , \end{aligned} \tag{A.3}$$

where $\hat{x}_1$, $\hat{x}_2$ and $\hat{x}_3$ are unit vectors along the body principle axes. $\hat{y}_3$ is the unit vector along the inertially fixed control reference axis such that,

$$a_{i3} = \hat{x}_i \cdot \hat{y}_3 . \tag{A.4}$$

When $\bar{\omega}$ is a constant vector with respect to time (i.e., $\dot{\bar{\omega}} = \bar{0}$), then Equation (8.13) reduces to (8.14), that is,

$$\ddot{a}_{i3} + \omega^2 \dot{a}_{i3} = 0 . \tag{A.5}$$

The solutions to (A.5) are stated in Equation (8.16), that is,

$$a_{i3}(t) = A_i + B_i \sin\omega t + C_i \cos\omega t . \tag{A.6}$$

It is also stated in Chapter 8 that the A_i, B_i and C_i are constants, but not arbitrary constants. That is, Equations (A.l) and (A.2) define only two first-order differential equations. In this Appendix, the relationships between the **A's**, B's, and C's are explored.

Differentiating (A.6) yields

$$\dot{a}_{i3} = \omega B_i \cos\omega t - \omega C_i \sin\omega_i t . \tag{A.7}$$

Equating like terms of (A.7) and (A.1) yields

$$\begin{aligned} 0 &= \omega_k A_j - w_j A, \\ \omega B_i &= \omega_k C_j - \omega_j C, \\ -\omega C_i &= \omega_k B_j - w_j B, \end{aligned} \qquad \text{(A.8)}$$

If the A's, B's, and C's are considered as nine variables, (A.8) is written in matrix form as,

$$\left[\begin{array}{ccc|ccc|ccc} 0 & \omega_3 & -\omega_2 & 0 & 0 & 0 & 0 & 0 & 0 \\ -\omega_3 & 0 & \omega_1 & 0 & 0 & 0 & 0 & 0 & 0 \\ \omega_2 & -\omega_1 & 0 & 0 & 0 & 0 & 0 & 0 & 0 \\ \hline 0 & 0 & 0 & \omega & 0 & 0 & 0 & -\omega_3 & \omega_2 \\ 0 & 0 & 0 & 0 & \omega & 0 & \omega_3 & 0 & -\omega_1 \\ 0 & 0 & 0 & 0 & 0 & \omega & -\omega_2 & \omega_1 & 0 \\ \hline 0 & 0 & 0 & 0 & \omega_3 & -\omega_2 & \omega & 0 & 0 \\ 0 & 0 & 0 & -\omega_3 & 0 & \omega_1 & 0 & \omega & 0 \\ 0 & 0 & 0 & \omega_2 & -\omega_1 & 0 & 0 & 0 & \omega \end{array}\right] \left|\begin{array}{c} A_1 \\ A_2 \\ A_3 \\ \hline B_1 \\ B_2 \\ B_3 \\ \hline C_1 \\ C_2 \\ C_3 \end{array}\right| = \left|\begin{array}{c} 0 \\ 0 \\ 0 \\ \hline 0 \\ 0 \\ 0 \\ \hline 0 \\ 0 \\ 0 \end{array}\right| . \qquad \text{(A.9)}$$

The coefficient matrix has a 9×9 determinant that is zero for any $\bar{\omega}$, as expected. Defining $[P_w]$ as in Chapter 7, Equation (7.39), Equation (A.9) is rewritten as

$$\begin{bmatrix} -[P_w] & [0] & [0] \\ [0] & \omega[U] & [P_w] \\ [0] & -[P_w] & \omega[U] \end{bmatrix} \begin{pmatrix} (A) \\ (B) \\ (C) \end{pmatrix} = \begin{pmatrix} (0) \\ (0) \\ (0) \end{pmatrix}, \qquad \text{(A.10)}$$

where [U] is the 3×3 identity matrix, and (A), (B), (C) are column matrices whose elements are A_i, B_i, C_i, respectively. Thus (A.8) is expressed by,

$$\begin{aligned} [P_w](A) &= 0 \\ \omega(B) + [P_w](C) &= 0 \\ \omega(C) - [P_w](B) &= 0 . \end{aligned} \qquad \text{(A.11)}$$

A good geometric picture is obtained by introducing the vector formalism,

$$\begin{aligned} \bar{A} &= A_1 \hat{x}_1 + A_2 \hat{x}_2 + A_3 \hat{x}_3 \\ \bar{B} &= B_1 \hat{x}_1 + B_2 \hat{x}_2 + B_3 \hat{x}_3 \\ \bar{C} &= C_1 \hat{x}_1 + C_2 \hat{x}_2 + C_3 \hat{x}_3 \ , \end{aligned} \tag{A.12}$$

as well as $\bar{\omega}$ defined in (A.3). Now (A.11) is expressed as,

$$\begin{aligned} \bar{A} \times \hat{\omega} &= 0 \\ \bar{B} \times \hat{\omega} &= -\bar{C} \\ \bar{C} \times \hat{\omega} &= \bar{B} \ , \end{aligned} \tag{A.13}$$

where $\hat{\omega}$ is the unit vector $\bar{\omega}/\omega$. ($\omega = 0$ gives rise to trivial equilibrium solutions, and is not considered here.) From (A.13), the following relationships are easily derived:

$$\begin{aligned} \bar{A} \times \hat{\omega} &= 0 \\ \bar{B} \cdot \hat{\omega} &= 0 \\ \bar{C} \cdot \hat{\omega} &= 0 \\ \bar{A} \cdot \bar{B} &= 0 \\ \bar{B} \cdot \bar{C} &= 0 \\ \bar{C} \cdot \bar{A} &= 0 \\ B &= C \ . \end{aligned} \tag{A.14}$$

Therefore, $\bar{A}$, $\bar{B}$, and $\bar{C}$ are orthogonal to each other with $|\bar{B}| = |\bar{C}|$, and $\bar{A}$ is parallel to $\bar{\omega}$. From the constraint Equation (A.2) and the solution Equations (A.6),

$$A^2 + B^2 \sin^2 \omega t + C^2 \cos^2 \omega t + 2(\bar{A} \cdot \bar{B}) \sin \omega t + 2(\bar{A} \cdot \bar{C}) \cos \omega t + 2(\bar{B} \cdot \bar{C}) \sin \omega t \cos \omega t = 1 \ . \tag{A.15}$$

Therefore, invoking (A.14),

$$A^2 + B^2 \sin^2 \omega t + C^2 \cos^2 \omega t = 1 \ . \tag{A.16}$$

Thus, the A, $\bar{B}$, and $\bar{C}$ vectors are confined within a unity sphere. That is,

$$B^2 = C^2 = 1 - A^2 \leq 1 ,$$

$$A^2 \leq 1 . \qquad \textbf{(A.17)}$$

Now,

$$\hat{\omega} \cdot \hat{y}_3 = \frac{\bar{A}}{A} \cdot \hat{y}_3 = \frac{1}{A}\left(A_1 a_{13} + A_2 a_{23} + A_3 a_{33}\right)$$

$$= \frac{1}{A}\left(A_1^2 + A, B, \sin wt + A, C, \cos wt + A_2^2 + A, B, \sin \omega t + A_2 C, \cos wt + A_3^2 + A_3 B, \sin wt + A, C_3 \cos \omega t\right)$$

$$= \frac{1}{A}\left(A^2 + (\bar{A} \cdot \bar{B}) \sin \omega t + (\bar{A} \cdot \bar{C}) \cos \omega t\right)$$

$$= A . \qquad \textbf{(A.18)}$$

That is, the angle between the $\bar{A}$ vector (or $\bar{\omega}$ vector) and the reference vector $\hat{y}_3$ is $\cos^{-1} A$. The geometry is shown in Figure A.1. Since the $\bar{\omega}$ was assumed constant, the body axes $\hat{x}_1$, $\hat{x}_2$, $\hat{x}_3$ are a set of orthogonal axes fixed with respect to $\bar{\omega}$ anywhere in the unity sphere. These axes are rotating at an angular rate w about the $\hat{\omega}$-axis with respect to $\hat{y}_3$. Thus, a clear geometrical picture is obtained by keeping $\bar{\omega}$, A, $\bar{B}$, $\bar{C}$, S_I, $\hat{x}_2$, $\hat{x}_3$ stationary in the unity sphere, and allowing the plane containing $\bar{A}$ and $\hat{y}_3$ to rotate around $\bar{A}$ at a rate ω.

To illustrate this dynamic geometry, assume $\bar{\omega} = \omega \hat{x}_1$, i.e., $\omega_2 = \omega_3 = 0$ and $\omega_1 = \omega$. Thus, from Equations (A.8), A, = A, = B, = C, = 0, and C, = - B, and C, = B, . That is,

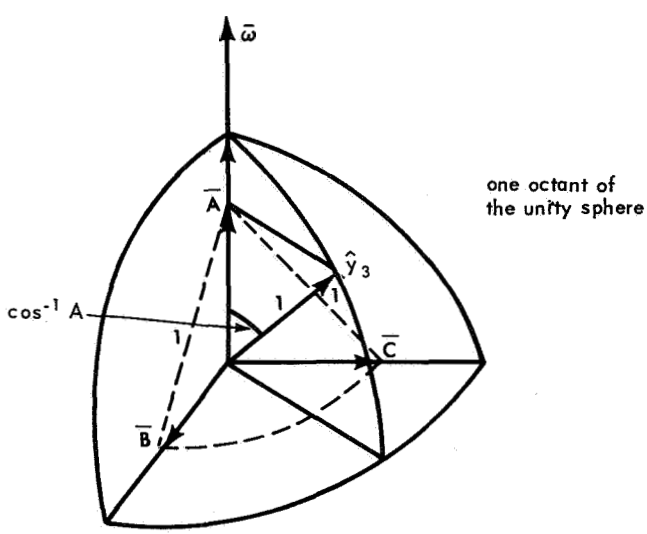

Figure A.1 —Unity-Sphere Geometry.

$$\bar{\omega} = \omega \hat{x}_1$$

$$\bar{A} = A, \hat{x}_1$$

$$\bar{B} = B, \hat{x}_2 + B_3 \hat{x}_3 \qquad \textbf{(A.19)}$$

$$\bar{C} = - B, \hat{x}_2 + B, \hat{x}_3 ,$$

where $A_1^2 + B_2^2 + B_3^2 = 1$. Therefore, from (A.6),

$$= A,$$

$$a_{23} = B, \sin wt - B_3 \cos wt \qquad \textbf{(A.20)}$$

$$a_{33} = B, \sin wt + B, \cos wt .$$

Or, letting $A_1 = A$, $B = \sqrt{B_2^2 + B_3^2}$, and $t_0 = 1/\omega \tan^{-1}(B_3/B_2)$, (A.20) becomes,

$$a_{13} = A$$

$$a_{23} = B \sin \omega (t - t_0) \qquad \text{(A.21)}$$

$$a_{33} = B \cos \omega (t - t_0) \ ,$$

where $A^2 + B^2 = 1$. The geometry is shown in Figure A.2. At $t = t_0$, $\hat{x}_3$ lies in the plane formed by $\hat{y}_3$ and $\hat{x}_1$. This plane is rotating about the $\hat{x}_1$-axis such that, at $t = t_0 + \pi/2\omega$, $\hat{x}_2$ lies in the plane. This example illustrates the behavior of a non-accelerating spacecraft rotating about one of its principle axes $(\hat{x}_1)$ with the fixed inertial reference vector at an arbitrary attitude, $\hat{y}_3$. The unity-sphere model is an especially useful visual aid for picturing attitude motion when $\bar{\omega}$ is at any arbitrary orientation with respect to the $\hat{x}_i$, and the ω_i are time-varying.

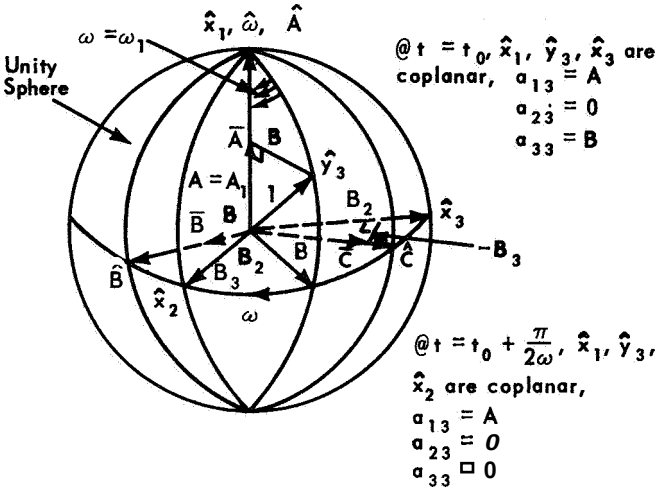

Figure A.2—Dynamics of Unity Sphere.

8/16/67

"The aeronautical and space activities of the United States shall be conducted so as to contribute . . . to the expansion of human knowledge of phenomena in the atmosphere and space. The Administration shall provide for the widest practicable and appropriate dissemination of information concerning its activities and the results thereof."

—NATIONAL AERONAUTICS AND SPACE ACT OF 1958

NASA SCIENTIFIC AND TECHNICAL PUBLICATIONS

TECHNICAL REPORTS: Scientific and technical information considered important, complete, and a lasting contribution to existing knowledge.

TECHNICAL NOTES: Information less broad in scope but nevertheless of importance as a contribution to existing knowledge.

TECHNICAL MEMORANDUMS: Information receiving limited distribution because of preliminary data, security classification, or other reasons.

CONTRACTOR REPORTS: Scientific and technical information generated under a NASA contract or grant and considered an important contribution to existing knowledge.

TECHNICAL TRANSLATIONS: Information published in a foreign language considered to merit NASA distribution in English.

SPECIAL PUBLICATIONS: Information derived from or of value to NASA activities. Publications include conference proceedings, monographs, data compilations, handbooks, sourcebooks, and special bibliographies.

TECHNOLOGY UTILIZATION PUBLICATIONS: Information on technology used by NASA that may be of particular interest in commercial and other non-aerospace applications. Publications include Tech Briefs, Technology Utilization Reports and Notes, and Technology Surveys.

Details on the availability of these publications may be obtained from:

SCIENTIFIC AND TECHNICAL INFORMATION DIVISION

NATIONAL AERONAUTICS AND SPACE ADMINISTRATION

Washington, D.C. 20546